L s z
9 000004 122365

OF 1915

# ANALELE UNIVERSITATII BUCURESTI

## fizica

Theoretical Physics • Plasma Physics •
Liquid State Physics • Solid State Physics
• Polymer Physics • Earth Physics

ANUL XXXIII — 1984

# FIZICĂ

**COMITETUL DE REDACȚIE**

Redactor responsabil : Prof. dr. *C. N. Plăvițu*
Redactor responsabil adj : Conf. dr. *I. Licea*
Membri : Prof. dr. *I. C. Petrea*
Prof. dr. *I. Iova*
Prof. dr. *V. Gheorghe*
Prof. dr. *V. Grecu*
Conf. dr. *C. Vrejoiu*
Secretar de redacție : Conf. dr. *L. Georgescu*

REDACȚIA

TIPOGRAFIA UNIVERSITĂȚII BUCUREȘTI
Șoseaua Panduri, nr. 90
Telefon 31.40.00/122

OF 1915

# ANALELE UNIVERSITĂȚII BUCUREȘTI

1989

BUDAPESTI MŰSZAKI ÉS GAZDASÁGTUDOMÁNYI EGYETEM
Országos Műszaki Információs Központ és Könyvtár
2001

## FIZICĂ

1984

### SUMAR • CONTENTS • SOMMAIRE

Pag.

*„1944—1984" — Une fructueuse periode de l'enseignement et de la recherche scientifique dans le domaine de la physique a l'Université de Bucarest* . . . 3

*THEORETICAL PHYSICS*

S. TURBATU : The Oscillating Semi-Infinite Rectangular Wing . . . . 7
D. ȘTEFĂNESCU : Effective Dependence of Multi-Instantons . . . . 13

*PLASMA PHYSICS*

G. G. BRĂTESCU, MAGDA CAZAN CORBASCA, LIVIA DOBOS : Potentiels explosifs dans les vapeurs de l'alcool isopropilique $CH_3$—CHOH—$CH_3$ dans des melanges de krypton et de vapeurs de l'alcool izopropilique . . . . . . . . . . . . . . . . 17
N. GHERBANOVSCHI, C. C. BORDEIANU : Lamb — Shift Polarised Ion Sources . . . . . . . . . . . . . . . . 21

*LIQUID STATE PHYSICS*

V. POPA-NIȚĂ, L. GEORGESCU : Pair Correlations in a Molecular Theory of Nematic Liquid Crystals . . . . . . . . . . 27
ST. LEVAI, S. LEVAI, M. CATRINESCU : Pulsed NMR Spectrometer . . . 33
V. DIMA, N. FLOREA : La propagation des ultra-sons dans les liquides $CCI_4$ et $CHCI_3$ dans le melange $CCI_4+CHCI_3$ . . . . . . . . 37

*SOLID STATE PHYSICS*

A. DAFINEI, I. LICEA : On the Thickness and Stoichiometry of Cuprous Sulphide for thin Film $Cu_2S$/CdS Electron—Voltaic Cells . . . . 43
I. SPÂNULESCU, I. SECĂREANU, TALAL KHALASS, N. BĂLȚĂȚEANU, IBRAHIM ZAKĂR ABDI : Photoconductivity of Evaporated CdSe Thin Films . . . . . . . . . . . . . . . . 51
I. CĂPLĂNUȘ, G. I. RUSU, C. H. BUDEANU : On the Electrical Properties of some Organic Semiconductors . . . . . . . . . . 57
C. CIUCU, S. GEORGESCU : The g Values of $Er^{3+}$ Ion in Yag . . . . 65

Pag.

## *POLYMER PHYSICS*

E. BARNA, LIVIA MARIA IONESCU, M. COJOCARU : La transmission de la lumière à travers des films de polyéthylène . . . . . . 71

LIVIA MARIA IONESCU, M. COJOCARU : Etude de la polydispersite des copolymeres polystyrene-polymethacrilate de methyle (PS—PMMA) . 77

## *EARTH PHYSICS*

ŞT. LASCU, ELENA DECU, M. CIOBANU : The Lateral Inhomogenity of the Mantle Beneath the Vrancea Zone . . . . . . . . . 85

ŞT. PĂTRAŞCU : The Study of Natural Remanent Magnetization of Some Neogene Volcanic Rocks from the Oaş—Gutîi—Ţibleş Mountains, Romania . . . . . . . . . . . . . . . . . . . 93

*Le Proesseur dr. ION C. PETREA* . . . . . . . . . . . . . . 105

BME KÖZPONTI KÖNYVTÁRA
F
8482
FOLYÓIRAT OSZTÁLY

Budapesti Műszaki Egyetem
Központi Könyvtára
Folyóiratleltár
P 84/1988

BUDAPESTI MŰSZAKI EGYETEM KÖZPONTI KÖNYVTÁRA 1848

ANALELE UNIVERSITĂŢII BUCUREŞTI, FIZICĂ, XXXIII, 1984, pag. 3—6

# *„1944 — 1984“*

# *UNE FRUCTUEUSE PERIODE DE L'ENSEIGNEMENT ET DE LA RECHERCHE SCIENTIFIQUE DANS LE DOMAINE DE LA PHYSIQUE A L'UNIVERSITÉ DE BUCAREST*

L'engagement constant de la Roumanie socialiste sur le chemin du progres et de la civilisation contemporaine a fait nécessaire l'élaboration d'une vraie stratégie du parti et de notre état dans le domaine de l'enseignement et de la recherche scientifique. La recherche scientifique est organisée ainsi en liaison étroite avec les nécessités de la production matérielle, tout en assurant le développement approprié de de recherche appliquée et de la recherche fondamentale en perspective. Le développement de la science, ainsi que de toutes les autres activités pratiques, notamment de la production matérielle, n'est pas possible sans un développement adéquat de l'enseignement à touts les niveaux. C'est pour cela que le principe de l'unité entre l'enseignement, la recherche et la production promu avec tant de fermeté par notre parti et l'état, de i'initiative du secrétaire général du Parti Communiste Roumaine, le président Nicolae Ceauşescu, a la valeur d'une idée unitaire sur la société, de la plus grande importance pour solutionner avec succès tous les problèmes théoriques et pratiques imposés par la construction de la société socialiste et du communisme en Roumanie.

En analysant l'évolution de l'enseignement et de la recherche scientifique de physique dans notre pays, on peut distinguer quelques étapes importantes.

Une première étape, lorsqu'il se précise l'enseignement supérieur en Roumaine dans les Universités de Bucarest, Jassy et Cluj, la formation dans le domaine de la physique ayant lieu dans les sections des sciences physico-chimiques, à une durée de quatre ans, plus un an de séminaire pédagogique, en vue du métier de professeur. L'activité de recherche scientifique de cette période a été effectuée dans le cadre des chaires de physique, les publications de ce temps étant une preuve de l'activité scientifique fébrile pour l'affirmation de la physique roumaine.

L'étape suivante 1948—1957, après la réforme de l'enseignement en Roumaine, représente la période lorsqu'ont été mises les bases nouvelles, modernes de l'éducation et de la recherche. De l'ancienne faculté des sciences se sont séparées ainsi quatre facultés, suivant les sciences fondamentales : Mathématiques-Physique, Chimie, Biologie et Géologie-Géographie. L'enseignement de physique s'est déroulé par la suite, naturellement, dans le cadre de la section de Physique de la Faculté de Mathématiques-Physique, étant organisé, dans les années supérieures d'étude, dans les spécialisations suivantes : Physique Théorique, Physique Atomique, Optique, Electro et Magnétophysique, et Météorologie. La durée des études était de quatre ans, et depuis 1952 elle est devenue de cinq ans.

L'apparition d'un grand nombre de facultés, sections et groupes de spécialisation a été une nécessité objective, étant donné le grand essor qu'ont connu dans cette période tous les domaines d'activité dans notre pays. Le développement sans précédent de l'industrie demandait des recherches fondamentales et appliquées de physique. Dans les nouveaux plans d'enseignement, le poids des activités pratiques, de séminaire et de laboratoire, dépassait de loin le poids des cours, et l'approfondissement du domaine de spécialisation dans l'enseignement universitaire se faisait dans la IV-ème année d'études, au cours d'un stage de pratique durant un mois dans un collectif de recherche.

Etant donné que les résultats de la recherche, dans le domaine de la physique, devaient stimuler le développement industriel, ont été organisés les premiers instituts de recherche de physique : I'Institut de Physique Atomique de Bucarest, avec des filiales à Jassy et Cluj, suivi par l'Institut de Physique Bucarest. Bien que les recherches dans le cadre de ces instituts étaient dirigées et même effectuées par de enseignants universitaires, est apparu pourtant le métier de „chercheur scientifique“. De cette manière l'enseignement se sépare de son support naturel, la recherche scientifique, avec des conséquences imédiates.

Un moment important dans l'évolution de l'enseignement de physique en Roumanie a eu lieu en 1962, lorsque la Faculté de Mathématiques-Physique de l'Université de Bucarest s'est divisée en deux facultés distinctes, la Faculté des Mathématiques et la Faculté de Physique, avec la durée des études de cinq ans. A cette occasion, les plans d'enseignement ont subi des changements importants, tels que :

— le développement de la formation dans les domaines modernes, fondamentaux de physique, concrétisé dans l'apparition de nouvelles sections de spécialisation telles l'Electrophysique, la Physique des Polymères, la Biophysique ;

— le développement de la formation pratique des étudiants par l'extension de la pratique en production ;

— le développement de la pratique pédagogique des étudiants ;

— l'introduction des disciplines nouvelles telles la programmation et calculateurs électroniques.

Un moment crucial dans l'évolution de l'enseignement de physique a eu lieu en 1974, lorsque la Faculté de Physique de Bucarest déménage dans un nouveau local, dans le cadre du Centre National de Physique, centre construit de l'initiative et sous le conseil direct du secrétaire général du Parti Communiste Roumaine, le président Nicolae Ceaușescu. Dans la cadre du Centre National de Physique se réalise une intégration efficiente enseignement-recherche scientifique-production.

A l'occasion du déménagement de la Faculté de Physique dans le cadre du Centre National de Physique, tous les laboratoires, ceux didactiques aussi bien que ceux de recherche, ont été complétement modernisés, au même niveau que les pays les plus développés, aux traditions dans l'école de physique. Dans la même période apparait, à la Faculté de Physique, la section de Physique Technologique avec deux directions de spécialisation, pour qu'en 1976 apparaissent quatre directions de spécialisation : réacteurs nucléaires, matériaux combustibles nucléaires, appareils de mesure et contrôle ainsi que matériaux électroniques et composantes électroniques.

L'enseignement de physique réalise, par l'intermède des frais émoulus de cette section, le pont tellement nécessaire entre la physique et l'industrie, dans les plans d'enseignement de cette section étant prévues, dès le début, des disciplines techniques.

La section de Physique, organisée en sept directions de spécialisation : Spectroscopie, Plasma et lassers, Biophysique, Physique des polymères, Physique du solide, Météorologie et physique de la Terre, Electronique, Physique nucléaire, aussi bien que la section de Physique Technologique ont prouvé une structure capable d'assurer une efficience maxime en ce qui concerne le pratique en production des étudiants, les diplômes et les projets de diplôme, l'intégration, le plus rapidement possible, des frais émoulus de la Faculté de Physique dans la recherche et la production.

L'activité de recherche scientifique dans le domaine de la physique constitue pour les enseignants une préoccupation constante et inséparable du procès d'enseignement. Dans le contexte de nouvelles conditions crées dans le cadre du Centre National de Physique, à l'appui des indications permenentes et du soutien conséquent accordés par le président Nicolae Ceaușescu, la recherche scientifique dans le domaine de la physique a été concentrée dans quelques programmes prioritaires, tels que :

— le programme d'énergetique nucléaire ;

— le programme de physique nucléaire ;

— le programme d'appareillage dosimètrique :

— le programme des lassers ;

— le programme des acceélérateurs ;

— le programme des matériaux nouveaux ; des composantes et dispositifs (monocristaux, cristaux liquides et solides, suprastructures) ;

— le programme de la physique de la Terre et séismologie ;

— le programme de biophysique ;

— le programme pour des sources nouvelles d'énergie (nucléaire, des sources à base les plasma, la conversion de l'énergie solaire, bioconversion etc.) ;

— le programme de la physique des polymères ;

— le programme de physique théorique (dans les domaines mentionnés plus haut).

En travaillant dans des collectifs mixtes, enseignants, chercheurs et étudiants des années supérieures d'étude, ont été abordés et résolus des thèmes figurant dans le plan de recherche de l'Institut Central de Physique, partie intégrante du Programme-directive de recherche et introduction du progrès technique.

Une attention spéciale a été accordée à la recherche scientifique à base de contrats, au moyen de laquelle ont été solutionnés des thèmes de la plus grande importance pour l'économie de notre pays. Les résultats remarquables obtenus dans le cadre de la recherche à base de contrats sont dûs, en grande partie, au soutien sans réserve accordé par le Conseil

National pour Science et Technologie, organisme dirigé par Acad. Dr. Ing. Elena Ceaușescu, dont le nom est étroitement lié au progrès de la science dans notre pays.

La période 1944—1984 représente un saut impressionnant en ce qui concerne le développement de l'enseignement et de la recherche scientifique dans notre pays. Le rythme et les changements structuraux dans le développement économique du pays jusqu'en 1990 demandent un apport de plus en plus substantiel de la science et de l'enseignement de physique au progrès de la société entière.

ANALELE UNIVERSITĂŢII BUCUREŞTI, FIZICĂ, XXXIII, 1984, pag. 7—12

# THE OSCILLATING SEMI-INFINITE RECTANGULAR WING

S. TURBATU

Faculty of Physics — University of Bucharest *

*Abstract.* By use of FOURIER transforms the aerodynamic forces on an oscillating semi-infinite rectangular wing in transonic flow are calculated. The results show that three-dimensional side-edge effects are very important.

## 1. Introduction

An important topic that is developing rapidly at the present time concerns the numerical calculation of unsteady transonic flows on aircraft wings and control surfaces, helicopter rotor blade tips, and compressor blades. In the transonic regime, the inherent nonlinearity of pressure variations, with incidence, for example, makes the aerodynamic forces and moments very sensitive to small changes in incidence of MACH number; and the folw field is an interrelated mixture of subsonic and supersonic zones.

The time averaged mean flow past an airfoil oscillating harmonically at transonic speeds differs from the steady flow obtained at rest. This difference depends on oscillation frequency and amplitude and arises because both mean and disturbance flowfilds interact nonlinearly. For small oscillation amplitudes a time linearized description usually suffices : the mean flow is conveniently solved without reference to the unsteady flow and the harmonic flow is solved without explicit reference to the unsteady disturbance amplitude. For larger amplitudes, however, the wave back-interraction induced by the primary disturbance on the mean flow cannot be discounted because the modified mean flow in turn affects the evolution of the harmonic flowfield. This effect may be significant because transonic flows are inherently nonlinear.

Linear theory [1], [2], [3], [4], [5]., wich generally assumes small unsteady disturbance amplitudes in comparison to the overall thickness, expands the unsteady solution about the known transonic flow corresponding to the stationary airfoil. Although, as shown in [1], [2], [3], the equations of motion for unsteady transonic flow can be linearized if the reduced frequency of oscillation is sufficiently large, these equations do not yield themselves to simple solutions for wings of arbitrary planforms. The simplest solution which retains many of the features of practical three-dimensional wing solutions is that for a semi-infinite rectangular wing.

---

* National Center of Physics, P. O. Box MG—11, Bucharest—Măgurele, Romania.

## 2. Basic equations and the solution

LANDAHL, M.T. [1],[2] has shown that in the linearized theory the partial differential equation of the non-dimensional perturbation velocity potential $\Phi$ (x, y, z ; t) for unsteady transonic flow reads, using non-dimensional variables,

$$\Phi_{yy} + \Phi_{zz} - 2M_{\infty}^2\Phi_{xt} - M_{\infty}^2\Phi_{tt} = 0, \tag{1}$$

where $M_{\infty}$ is the free stream MACH number.

For harmonic oscillations we set

$$\Phi(x, y, z ; t) = \mathrm{Re}\,\{\varphi\,(x, y, z)\,e^{ikt}\}, \tag{2}$$

where k is the reduced frequency, and then the equation (1) takes the form

$$\varphi_{yy} + \varphi_{zz} - 2ikM_{\infty}^2\varphi_x + M_{\infty}^2k^2\varphi = 0. \tag{3}$$

Equation (3) is valid when $k \gg |1-M|$, where $|1-M|$ is the magnitude of the largest deviation of the local MACH number from unity in the flow. $M\infty$ can be eliminated from equation (3) by means of the transformation $Y=M_{\infty}\,y$, $Z=M_{\infty}\,z$ so that only the case $M_{\infty}=1$ need to be considered. For $M_{\infty}=1$, the equation (3) becomes

$$\varphi_{yy} + \varphi_{zz} - 2ik\varphi_x + k^2\varphi = 0. \tag{4}$$

Now let us consider a quarter-infinite rectangular wing with the leading edge located along the positive y-axis and the side edge along the positive x-axis. The boundary conditions imposed on $z=+0$ are [1], [2], [6]:

$$\varphi_z\,(x,y,+0)=g(x,y) \qquad \text{on the wing} \tag{5}$$

$$\varphi\,(x,y,+0)=0 \qquad \text{outside the wing,} \tag{6}$$

where g(x,y) is a known function [1], [2, [6].

Since equation (1) is parabolic there is no upstream influence so that either LAPLACE or FOURIER transforms could be used to obtain the solution. In the present paper FOURIER transforms will be used throughout. FOURIER transformed functions are denoted by

$$\Psi(y,z;s \;=\; \mathfrak{F}\{\varphi(x,y.z)\} = \frac{1}{\sqrt{2\pi}}\int_{-\infty}^{+\infty}\varphi(x,y,z)\,e^{-isx}\,dx. \tag{7}$$

Transformation of equations (4), (5), (6) leads to

$$\Psi_{yy}(y,z;s) + \Psi_{zz}(y,z;s) + \lambda^2\Psi(y,z;s) = 0 \tag{8}$$

$$\Psi_z(y,+0;s) = G(y;s) \qquad \text{for } y>0, \tag{9}$$

$$\Psi(y,+0;s) = 0 \qquad \text{for } y<0, \tag{10}$$

where

$$\lambda = (2ks + k^2)^{1/2} \quad \text{and} \quad G(y;s) = \mathfrak{F}\{g(x,y)\}. \tag{11}$$

For convergence reasons we choose s and k to have arbitraryly small negative imaginary parts. Also that branch of $\lambda$ is chosen for $\mathrm{Im}\lambda<0$. To make λ single-valued a cut is therefore introduced along a straight line from $s=-\frac{k}{2}$ o infinity with the slope −argk. When applying the inversion formula

$$\varphi(x,y,z) \;=\; \mathcal{F}^{-1}\{\Psi(y,z;s)\} \;=\; \frac{1}{\sqrt{2\pi}}\int_{-\infty}^{+\infty}\Psi(y,z;s)\,e^{isx}\,ds \tag{12}$$

the integral should therefore be taken just below the Res — axis.

The two-dimensional boundary value problem defined by equations (8), (9), (10), can be solved in several different ways. LANDAHL, M.T. [1], [2] has shown that the LAMB's method [7] can be extended to cover also cases of arbitrary G, i.e. $G=G(y\,;\,s)$. We now derive an integral representation for the solution, which is analogous to the representation for solutions of the plane screen diffraction problem given by BURGER, A. [8].

If $\eta$ and $\zeta$ represent running coordinates in the y and z directions, respectively, then the distance R between the points (y, z) and $(\eta, \zeta)$ is given by

$$R^2=(y-\eta)^2+(z-\zeta)^2. \tag{13}$$

Now application of GREEN's theorem to the half-plane of positive $\zeta$ yields the known relation [8] :

$$\Psi\,(y,z;\,s)=\frac{1}{4i}\int_{-\infty}^{+\infty}\left\{\frac{\partial\Psi}{\partial\zeta}H_o^{(2)}(\lambda R)-\Psi\frac{\partial H_o^{(2)}}{\partial\zeta}(\lambda R)\right\}_{\zeta=+0}d\eta. \tag{14}$$

valid only when z is positive. From (13) this may be written

$$\Psi\,(y,z;\,s)=\frac{1}{4i}\int_{-\infty}^{+\infty}\left\{\frac{\partial\Psi}{\partial\zeta}H_o^{(2)}(\lambda R)+\Psi\frac{\partial H_o^{(2)}}{\partial z}(\lambda R)\right\}_{\zeta=+0}d\eta. \tag{15}$$

For negative z the integral vanishes, so that, replacing z by $-z$,

$$O=\frac{1}{4i}\int_{-\infty}^{+\infty}\left\{\frac{\partial\Psi}{\partial\zeta}H_o^{(2)}(\lambda R)-\Psi\frac{\partial H_o^{(2)}}{\partial z}(\lambda R)\right\}_{\xi=+0}d\zeta. \tag{16}$$

By adding (15) and (16) we obtain

$$\Psi\,(y,z;\,s)=\frac{1}{2i}\int_{-\infty}^{+\infty}\left\{\frac{\partial\Psi}{\partial\zeta}H_o^{(2)}(\lambda R)\right\}_{\zeta=+0}d\eta. \tag{17}$$

Introducing the notation

$$r=\sqrt{(y-\eta)^2+z^2} \tag{18}$$

and using a subscript to denote differentiation, we can write (17) as

$$\Psi\,(y,z;s)=\frac{1}{\pi}\int_{-\infty}^{+\infty}\Psi_\zeta\,(\eta,+0;s)\,d\eta\int_{r}^{+\infty}(q^2-r^2)^{-1/2}\,e^{-i\lambda q}\,dq \tag{19}$$

by using a known integral expression for the HANKEL FUNCTION [9] :

$$H_0^{(2)}(q) = -\frac{2}{\pi i}\int_1^{+\infty} (\tau^2 - 1)^{-1/2} e^{-iq\tau} d\tau \tag{20}$$

We now make the substitution

$$q - y - \eta = 2\xi \tag{21}$$

and (19) becomes

$$\Psi(y,z;s) \doteq -\frac{e^{-i\lambda y}}{\pi}\int_{-y}^{+\infty}(y+\xi)^{-1/2} d\xi \int_{\sigma}^{+\infty}(\eta-\sigma)^{-1/2} e^{-i\lambda\eta}\Psi_\zeta(\eta,+0;s)d\eta, \tag{22}$$

where $\sigma = -\xi + \frac{z^2}{4(y+\xi)}$. Now making use of (10) we may put z=0 in (22) and obtain

$$0 = \int_{-y}^{+\infty}(y+\xi)^{-1/2} e^{-2\lambda\xi} d\xi \int_{\xi}^{+\infty}(\eta+\xi)^{-1/2} e^{-i\lambda\eta}\Psi_\zeta(\eta,+0;s)\,d\eta \tag{23}$$

which is valid for all negative y only. This relation has the form of an integral equation of ABEL's type and by the uniquenees theorem for the integral equation [10] :

$$\int_{-\xi}^{+\infty}(\eta+\xi)^{-1/2} e^{-i\lambda\eta}\Psi_\zeta(\eta+0;s)\,d\eta, \tag{24}$$

which is valid for all $\xi > 0$, because in (23) th e integration over $\xi$ covers all $\xi > -y$, where y is negative.

Applying (24), we note that the inside integral in (22) vanishes when $\xi > \rho = \frac{1}{2}\left(-y + \sqrt{y^2+z^2}\right)$, so that (22) becomes

$$\Psi(y,z;s) \doteq -\frac{e^{-i\lambda y}}{\pi}\int_{-y}^{\rho}(y+\xi)^{-1/2} e^{-2i\lambda\xi} d\xi \times$$

$$\times \int_{\sigma}^{+\infty}(\eta-\sigma)^{-1/2} e^{-i\lambda\eta}\, G(\eta;s)\,d\eta \tag{25}$$

This is the solution of the boundary problem defined by the equations (8), (9), (10).

The inversion to the physical plane is easily carried out by aid of the following formula, valid for Imd<0 and x>0 :

$$\mathfrak{F}^{-1}\{e^{-ids^{1/2}}\} = \frac{1}{2}(i+1)\frac{d}{x^{3/2}}\exp\left(-i\frac{d^2}{4x}\right). \tag{26}$$

For x<0 the transform is zero. Then, from equation (25) and the Faltung theorem for FOURIER integrals, we have

$$\varphi(x,y,z) = -\frac{i+1}{2}\sqrt{\frac{k}{\pi}}\int_0^x \frac{\exp\left(-i\frac{k}{2}(x-x_1)\right)}{(x-x_1)^{3/2}}\,dx_1\int_{-y}^{\rho}(y+\xi)^{-1/2}\,d\xi\,\times$$

$$\times\int_{\sigma}^{+\infty}(y+\eta+2\xi)\,(\eta-\sigma)^{-1/2}\exp\left(-i\frac{k}{2}\,\frac{(y+\eta+2\xi)^2}{x-x_1}\right)g(x_1,\eta)\,d\eta. \quad (27)$$

This is the solution of the boundary value problem defined by tse equations (4), (5), (6).

### 3. **A special case**

In the following only the case when g does not depend on y will be considered. For this we can start from equation (25) where G=G(y ;s). The integrals in (25) can be evaluated [9] and we find that

$$\Psi(y,z;s) = -\sqrt{2}\,\frac{G}{\lambda}\exp\left(-i\frac{\lambda}{4}z^2\right)2^{1/2}\pi^{-1/2}\left(\frac{\lambda}{2}(y+\sqrt{y^2+z^2})\right)^{1/2}\times$$

$$\times\, F_1^{(1)}\left(\frac{1}{2},\frac{3}{2},i\frac{\lambda}{2}(y+\sqrt{y^2+z^2})\right) \quad (28)$$

Making use of the formula [9] :

$$C(q) \pm iS(q) = 2^{1/2}\pi^{1/2}\,F_1^{(1)}\left(\frac{1}{2},\frac{3}{2},\pm\, iq\right),$$

where C and S stands for the well-known FRESNEL integrals, we find that

$$\Psi(y,z;s) = (i-1)\frac{G}{\lambda}\exp\left(-i\frac{\lambda}{4}z^2\right)\left[C\left(\frac{\lambda}{2}(y+\sqrt{y^2+z^2})\right)-iS\left(\frac{\lambda}{2}(y+\sqrt{y^2+z^2})\right)\right] \quad (29)$$

In the particular case y→+0 this reduces to the result given in [1],, [2], [6] :

$$\Psi(y,+0;s) = (i-1)\,\frac{G}{\lambda}\left(C(\lambda y)-iS(\lambda y)\right) \quad (30)$$

The inversion may be written

$$\varphi(x,y,+0) = \int_0^x h_0(x-\xi)\exp\left(-i\frac{k}{2}(x-\xi)\right)g(\xi)\,d\xi, \quad (31)$$

where,

$$h_0(x) = \frac{1}{\sqrt{2\pi}}\,\mathscr{F}^{-1}\left\{\frac{i-1}{(2ks)^{1/4}}\int_0^y\frac{\exp(-i(2ks)^{1/2}y_1)}{\sqrt{2\pi y_1}}\,dy_1\right\}$$

For computational reasons it is convenient to performan integration by parts before evaluating the hernel. This leads to [1], [2] :

$$\varphi(x,y,+0) = h_1(x)\exp\left(-i\frac{k}{2}x\right)g(0) -$$

$$-\int_0^1 h_1(x-\xi)\frac{\partial}{\partial\xi}\left(\exp\left(-i\frac{k}{2}(x-\xi)\right)g(\xi)\right)d\xi, \qquad (32)$$

where

$$h_1(x,y) = \int_0^x h_0(\xi,y)\,d\xi = \mathcal{F}^{-1}\left\{\frac{i+1}{(2ks)^{1/4}}\int_0^1\frac{\exp\left(-i(2ks)^{1/2}y_1\right)}{2\pi s\sqrt{y_1}}dy_1\right\} =$$

$$= \frac{2^{1/4}e^{\pi i/4}}{k^{1/2}\sqrt{2\pi}}\sum_{n=0}^{\infty}\frac{e^{\frac{\pi i(5-2n)}{8}}\,x^{\frac{1-2n}{4}}\,(2k)^{\frac{n}{2}}\,e^{\frac{1+2n}{2}}}{n!\left(n+\frac{1}{2}\right)\Gamma\left(\frac{5-2n}{4}\right)}.$$

The calculation of the sectional forces and moments for translational and pitching oscillations $l_{11}$—$l_{22}$, can be reduced to the evaluation of the following integrals

$$l_{ij} = 4(\pi k)^{-1/2}\left(m_{ij}h_1(1,y)\exp\left(-i\frac{k}{2}\right) - \int_0^1 h_1(x,y)\exp\left(-i\frac{k}{2}x\right)M_{ij}dx\right),$$

where

$$m_{11}=m_{12}=ik,\quad m_{21}=m_{22}=1;$$

$$M_{11} = \frac{3}{2}k^2 + \frac{ik^3}{2}(1-x),\quad M_{12} = ik + \frac{3}{2}k^2x + \frac{ik^3}{4}(1-x^2),$$

$$M_{21} = -\frac{5}{2}ik + 2k^2(1-x) + \frac{ik^3}{4}(1-x)^2,$$

$$M_{22} = 1 - \frac{5}{2}ikx + k^2(1-x^2) + \frac{ik^3}{12}(2-3x+x^2).$$

## REFERENCES

1. M. T. LANDAHL, *Unsteady Transonic Flow*, Pergamon Press, 1961.
2. M. T. LANDAHL, The Aeronautical Research Institute of Sweden, Report 78, Stockholm, 1958.
3. M. T. LANDAHL, *Symposium Transsonicum*, Springer-Verlag, Berlin, Göttingen, Heidelberg, 1964, 414—439.
4. D. E. DAVIES, *Three Dimensional Sonic Theory, AGARD Manual on Aeroelasticity*, Part II, Aerodynamic Aspect, Ch. 4.
5. R. M. TRACI, E. D. ALBANO, J. L. FARR and H. K. CHENG, *AFFDL—TR—74—37*, June 1974.
6. S. TURBATU, *Recent Developments in Theoretical and Experimental Fluid Mechanics*, Springer-Verlag, Berlin, Heidelberg, New-York, 1979, 58—66.
7. H. LAMB, Proc. London Math. Soc., Ser. 2, Vol. 4, 1907, 190—203.
8. A. BURGER, Proc. Roy. Soc. London, Ser. A 252, 1959, 411—417.
9. M. RYSHIK and S. GRADSTEIN, *Tafeln-Summen-Produkt — und Integral*, VEB Deutscher Verlag der Wissenschaften, Berlin 1957.
10. A. ZAANEN, *Linear Analysis*, North—Holland Publishing Co., Amsterdam, 1953.

ANALELE UNIVERSITĂŢII BUCUREŞTI, FIZICĂ, XXXIII, 1984, pag. 13—16

# EFFECTIVE DEPENDENCE OF MULTI-INSTANTONS

D. ŞTEFĂNESCU

University of Bucharest, Faculty of Physics *

*Abstract.* We describe some properties of the multi-instantons for SU(2). We obtain new evaluations of the number of effective parameters describing a q—instanton for $q \geq 2$. These evaluations are obtained with the help of algebraic and geometrical techniques. We show that they are better than those obtained by other methods.

## 1. Introduction

The nonabelian gauge theories were firts considered by Yang and Mills ([5]) and, independently of them, by Shaw. The importance of nonabelian gauge theories was showed by the unified model of weak and electromagnetic interactions, based on the gauge group $SU(2)\times U(1)$, of Salam—Weinberg ([9], [10]). Very recent experimental results (the discovery at CERN of the charged W in 1983) showed that the weak interaction can be thought as mediating the exchange of particles in the weak gauge fields.

An important progress in the study of the gauge theories was the construction of the instantons given by Atiyah-Drinfeld-Hitchin-Manin ([1]). In this paper we start from their construction. We obtain some new evaluations of the number of parameters describing a q-instanton for SU(2) , where $q \geqslant 2$. The tools used for this purpose are algebraic and geometrical.

## 2. The q-instantons

Let G=SU (2). It is a nonabelian compact Lie group. Its Lie algebra L (G) can be identified with the skew-symmetric $2\times 2$ matrices which have the trace zero.

Let A be the SU (2) — potential described by

$$A(x)=\mathrm{Im}\,\frac{\bar{x}dx}{1+|x|^2}=\frac{1}{2}\cdot\frac{\bar{x}dx-d\bar{x}\cdot x}{1+|x|^2}, \tag{1}$$

where $x=x^1+x^2i+x^3j+x^4k \in H$, $\bar{x}=x^1-x^2i-x^3j-x^4k$ (in the quaternionic symbolism). We use the usual notations :

$\mathrm{Re}\,x=x^1$, $\mathrm{Im}\,x=x-\mathrm{Re}\,x=x^2i+x^3j+x^4k$, $dx=dx^1+dx^2i+dx^3j+dx^4k$, $d\bar{x}=dx^1-dx^2i-dx^3j-dx^4k$.

---

* National Center of Physics, Bucharest—Măgurele P. O. Box 5211, Romania.

The curvature F corresponding to this potential is

$$F = \mathrm{Im}\left(\frac{d\bar{x} \wedge dx}{1+|x|^2} + d\bar{x}(1+|x|^2)^{-1} \wedge dx + \frac{\bar{x}dx \wedge \bar{x}dx}{(1+|x|^2)^2}\right) = \frac{d\bar{x} \wedge dx}{(1+|x|^2)^2}. \quad (2)$$

It is self dual, i.e. $^*F = {}^-F$ (where "$*$" is the Hodge operator). If $|x| \to \infty$ then $A(x) \sim \mathrm{Im}(x^{-1}dx) = f(x)^{-1}df(x)$, where $f(x) = \frac{x}{|x|}$. This shows that A is asymptotically the gauge transform of O through the gauge transformation f (x). On the quaternionic unitary sphere we have $f(x)^{-1} = \bar{x}$ and the application $x \to \bar{x}$ from $S^3$ to $S^3$ has degree $^-1$. Therefore the relation (1) describes an anti-instanton.

Changing x with $\bar{x}$ we obtain the basic instanton described by the following potential A and field F :

$$A = \mathrm{Im}\,\frac{x d\bar{x}}{1+|x|^2},\ F = \frac{dx \wedge d\bar{x}}{(1+|x|^2)^2}. \quad (3)$$

For constructing q-instantons for $q \geqslant 2$ let's consider as in [1] the SU (2)-potential defined on $\mathbb{H}^q = \mathbb{R}^{4q}$

$$A(u) = \mathrm{Im}\,\frac{u^*du}{1+|u|^2}, \quad (4)$$

where u is the column vector of quaternionic components $u_j$

$$j = 1, 2, \ldots, q),\ u^*du = \sum_{j=1}^{q} \bar{u}_j du_j \text{ and } |u|^2 = \sum_{j=1}^{q} |u_j|^2.$$

We shall use the following result from [2].

*2. 1. Theorem. Let.* $q \geqslant 2$. $u(x) = [m(B-x)^{-1}]^*$, *where* $B \in M_{\mathrm{symm}}(q, q; \mathbb{H})$, $m = (m_1, \ldots m_q) \in \mathbb{H}^q$, $x = xI$ *(I is the unity matrix from* $M(q, q; \mathbb{H})$ ).

*Then every q—instanton for SU (2) is derived from the parameters* (m, B) *such that :*

$$B^*B + m^*m \in M(q, q; \mathbb{R}) \quad (5)$$

*For every* $x \in \mathbb{H}$ *from the relations*

$$(B-x)y = 0,\ my = 0,\ y \in \mathbb{H}^q \text{ it follows that } y = 0, \quad (6)$$

*The potential in an asymptotic gauge beeing given by the relation (4), where* $u(x) = [m(B-x)^{-1}]^*$.

*The potentials defined by (m, B) and (m′, B′) are equivalent if and only if there are* $t \in Sp(1)$, $T \in 0(q)$ *such* $m' = tmT$, $B' = T^{-1}BT$.

## 3. **Properties of the instantons**

In this section we shall establish the number of effective real parameters needed in the construction of a q-instanton for G = SU (2), where $q \geqslant 2$.

*3. 1. Proposition. If* $q \geqslant 2$ *then a q-instanton for SU (2) depends of 8q—3 real parameters.*

*Proof.* We shall evaluate by a direct computation the number of parameters on which depends a q-instanton.

By 2. 1 such a multi-instanton is described by a couple $(B,m) \in M_{symm}$ $(q, q ; |H) \times |H^q$. The couple (B, m) depends of $4\frac{q(q+1)}{2}+4q=2q^2+6q$ parameters (scince $\dim_k M_{symm}(q, q ; k)=\frac{q(q+1)}{2}\Big)$.

These parameters depend of the action of $Sp(1)=\{x \in |H ; |x|=1\}$, $0(q)=\{A \in M(q, q ; |R) ; AA^t=1_n\}$.

From the relation $B^*B+m^*m \in M(q,q ; R)$ we obtain $\frac{3q(q-1)}{2}$ equations. Therefore the number of real parameters on which depends a q-instanton for SU (2) is $2q^2+6q-\left(3+\frac{q(q-1)}{2}+\frac{3q(q-1)}{2}\right)=8q-3$.

*3. 2. Remarks.* a) The evaluation from 3. 1. agrees with that from [7]. Our proof uses only simple computations of linear algebra, while A. S. Schwarz's proof uses the Atiyah-Singer index theory.

b) The fact that a q-instanton for $G=SU(2)$ depends of 8q-3 real parameters improves some results obtained in the general case. Thus, there were constructed families of instantons depending of $5q+4$ parameters if $q \geqslant 3$ and of 13 parameters if $q=2$. Let's remark that for $q=2$ by 3. 1 we obtain $8.\,2-3=13$ parameters.

*3.3. Proposition If* $q \geqslant 3$ *then a q-instanton depends of* $\frac{1}{2}q(q+13)$ *—3 real parameters.*

*Proof.* The condition (5) of the theorem 2. 1 means that all the coefficients of i, j, k in the matrix $B^*B+m^*m \in M(q, q ; |H)$ vanish. The $\frac{3q(q-1)}{2}$ equations thus obtained define an affine algebraic variety. This variety can be realized as the intersection of a finite number of hypersurfaces from $A_{q^2+q}(R)$. This number is $q^2+q$.

Indeed, let's consider the following more general algebraic problem. Let R be a noetherian domain of dimension n, $R=S[x]$, where S is a ring and x is an indeterminate. If $a$ is an ideal of R then there are n elements $g_1, \ldots, g_n \in a$ such that $a=(g_1, \ldots, g_n)$. As in [4] this can be proved by induction over n.

If $n=1$ then R is a PID. If $n \neq 1$ let $p_1, \ldots p_m$ be the minimal prime ideals of S and $U=S \setminus \bigcup_{i=1}^{m}$. Then $\dim U^{-1}S=0$.

Therefore there is $g_1 \in U^{-1}a$ such that $U^{-1}(g_1)=U^{-1}a$. Let $R^*=R/(u)$, $a^*=(a+(u))/(u)$, where $u \in U$ is such that $ua \subset (g_1)$. By the induction there are $g^*_2, \ldots, g^*_n \in a^*$ such that $a^*=(g^*_2, \ldots, g^*_n)$. Let $g_2, \ldots, g_n \in a$ be such that $g_j \mod (g_1)=g^*_j$ for $j=2, \ldots, n$. It follows that $a=(g_1, g_2, \ldots, g_n)$.

Therefore every algebraic affine set from the affine space $A_n(k)$ where k is a commutative field, is the set-theoretical intersection of n hypersurfaces. This fact improves similar results of L. Kronecker ([3]) and F. S. Macaulay.

We deduce that the variety defined by the condition $B^* B + m^* m$ $M(q, q; R)$ is the intersection of $q^2 + q$ hypersurfaces, thus it is defined by $q^2 + q$ equations.

Since $\dim Sp(1) = 3$ and $\dim O(q) = \frac{q(q-1)}{2}$ it follows that the number of real parameters on which depends a q-instanton is $2q^2 + 6q - (3 + \frac{q(q-1)}{2} + q^2 + q) = \frac{1}{2} q(q+13) - 3$.

*3. 4. Remarks.* a) If $q > 3$ then $\frac{1}{2} q(q+13) - 3 \geqslant 8q - 3$. Therefore for $q \geqslant 3$ the proposition 3.3. gives a better evaluation than that of [7] and of the proposition 3.1.

b) It is known that for $q \geqslant 3$ they were constructed families of q-instantons depending of only $5q + 4$ parameters. Since $\frac{1}{2} q(q+13) - 3 > 5q + 4$ for $q \geqslant 3$ we obtained, for SU (2), a better evaluation.

c) If we are interested in obtaining explicitely all the effective parameters needed in the construction of the instantons we must describe the hypersurfaces used in the proof of 3. 3. Fortunately these hypersurfaces are obtained by an algorithmic method.

## REFERENCES

1. M. F. ATIYAH, V. G. DRINFELD, N. J. HITCHIN, I. I. MANIN. *Phys. Lett. 65* A, 185 (1978).
2. V. G. DRINFELD, I. I. MANIN. *Funk. Analiz. pril. 12,* 78 (1978).
3. L. KRONECKER, *J. r. ang. Math. 92,* 1 (1882).
4. D. EISENBUD, G. EVANS, *Inv. Math. 19,* (107 (1973).
5. R. L. MILLS, C. N. YANG, *Phys Rev. 96,* 191 (1954).
6. A. S. SCHWARZ, *Phys. Lett.* 67 B, 172 (1977).
7. D. ŞTEFĂNESCU, *An. Univ. Buc. — Fiz. 32,* 3 (1983).
8. D. ŞTEFĂNESCU, *Abstr. Amer. Math. Soc. 4,* 392 (1983).
9. A. SALAM, *Rev. Mod. Phys. 92,* 525 (1980).
10. S. WEINBERG, *Phys. Rev. Lett. 19,* 1264 (1967).

ANALELE UNIVERSITĂŢII BUCUREŞTI, FIZICĂ, XXXIII, 1984, pag. 17—20

# POTENTIELS EXPLOSIFS DANS LES VAPEURS DE L'ALCOOL ISOPROPILIQUE $CH_3$—CHOH—$CH_3$ ET DANS DES MELANGES DE KRYPTON ET DE VAPEURS DE L'ALCOOL IZOPROPILIQUE

G. G. BRĂTESCU, MAGDA CAZAN-CORBASCA, LIVIA DOBOS

Faculté de Physique, Université de Bucarest *

*Résumé.* On a determiné les potentiels explosifs et on a tracé les courbes de Paschen dans les vapeurs de l'alcool isopropilique à l'état pur et dans des mélanges de proportions différentes du krypton avec des vapeurs de l'alcool isopropilique. Les électrodes employées sont de Al.

## 1. Introduction

Dans cet ouvrage les auteurs ont déterminé les potentiels explosifs $V_e$ dans les vapeurs de l'alcool isopropilique et dans des mélanges de krypton et de vapeurs de l'alcool isopropilique, en employant des électrodes de Al. En même temps on a tracé les courbes de Paschen correspondantes.

On a comparé les résultats concernant les vapeurs de l'alcool isopropilique à l'état pur à ceux obtenues pour les vapeurs de l'alcool isobutilique à l'état pur mentionné dans un ouvrage antérieur /1/.

## 2. Résultats

Les déterminations ont été effectuées avec la même installation, et de la même manière que dans le cas des divers alcools étudiés /1—6/.

La courbe de paschen $V_e = f\,(pd)$ (où p est la pression du gaz et d la distance entre les électrodes), pour les vapeurs de l'alcool isopropilique est présentée dans la figure 1.

On a obtenu les valeurs :

$$V_{e_{min}} = 473 \pm 1 \text{ V} ; (pd)_{min} = 3,30 \pm 0,1 \text{ mm Torr.}$$

La figure 2 présente comparrativement les courbes de Paschen pour les vapeurs des alcools isobutilique et isopropilique, en utilisant des électrodes de Al.

On a tracé les courbes de Paschen dans les suivants mélanges : 9,10% ; 45,10% ; 64,15% 92,65% krypton en mélange avec des vapeurs de l'alcool isopropilique (masse de krypton rapporté à la masse du mélange).

Les résultats concernant le krypton à l'état pur mentionnés dans un ouvrage antérieur sont rapprochés à ceux trouvés dans la littérature de spécialité /6, 7/.

---

* Centre National de Physique, Măgurele—Bucarest, P. O. Box 5211.

PESTI MŰSZAKI E... 1848 KÖZP... TÁRA

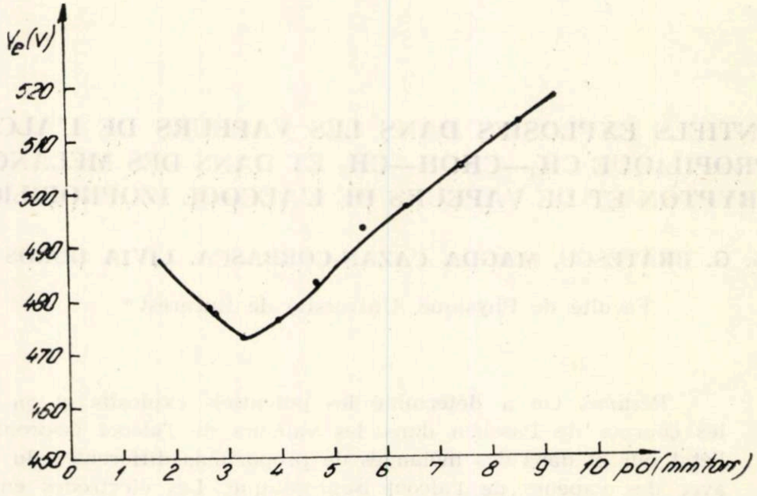

*Fig. 1* La courbe de Paschen pour les vapeurs de l'alcool isopropilique à l'état pur.

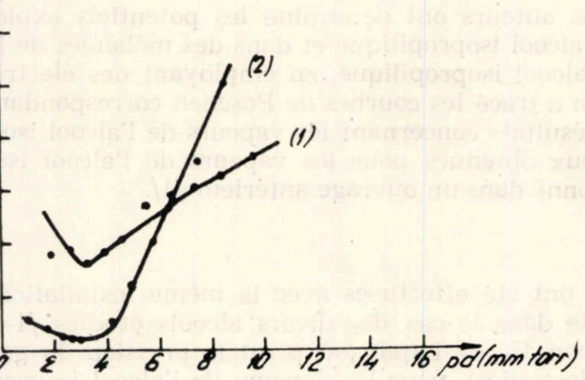

*Fig. 2* Les courbes de Paschen pour les vapeurs de l'alcool isopropilique (1) et isobutilique (2).

On présente les valeurs du potentiel explosif minime et du produit $(pd)_{min}$ correspondant, pour les constituants du mélange à l'état pur, de même que pour les mélanges étudiés, dans la tableau I.

*Tableau I.*

| Substance | Proportion % | $V_{e\,min}$ (V) | $(pd)_{min}$ (mm Torr) |
|---|---|---|---|
| Krypton | 100 | 259,00 | 11,90 |
| Mélange | 92,65 Kr | 330,05 | 4,50 |
| Mélange | 64,15 Kr | 400,80 | 6,25 |
| Mélange | 45,10 Kr | 412,75 | 6,20 |
| Mélange | 9,10 Kr | 452,50 | 3,50 |
| $CH_3—CHOH—CH_3$ | 100 | 473,00 | 3,30 |

La figure 3 présente comparativement les courbes de Paschen pour les mélanges mentionnés.

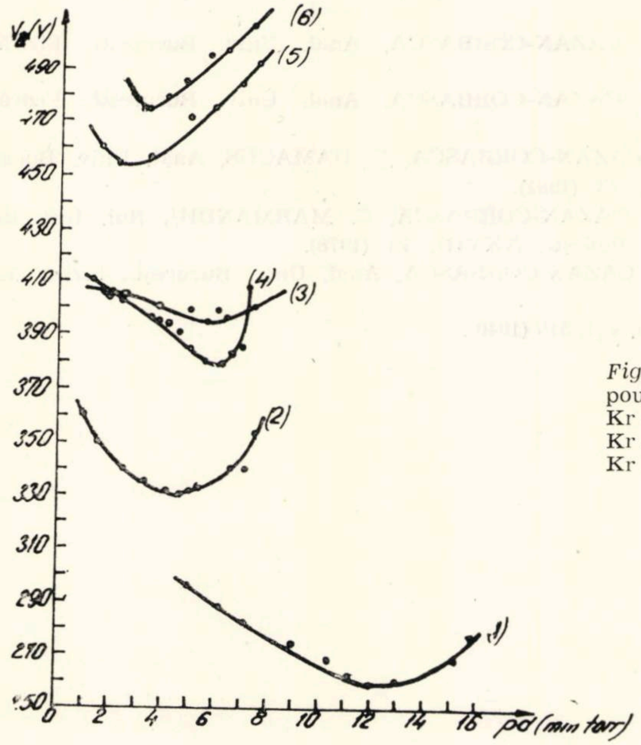

*Fig. 3* Les courbes de Paschen pour les mélanges : (1) 100% Kr ; (2) 92,65% Kr ; (3) 64,15% Kr ; (4) 45,10% Kr ; (5) 9,10% Kr ; (6) 100% $CH_3$—CHOH—$CH_3$.

## 3. Discussion des résultats

On constate pour les quatre mélanges étudiés que les valeurs des potentiels explosifs minimes se situent entre celles correspondantes aux composantes à l'état pur. Elles s'élèvent quand la proportion de Kr diminue en se raprochant de celle correspondante aux vapeurs de l'alcool, à l'état pur.

Les valeurs des produits $(pd)_{min}$ diminuent avec la concentration du Kr dans le mélange, exception faite pour le mélange présenté par la courbe nr. 2.

## 4. Conclusions

De même que dans le cas d'autres substances organiques, on constate dans le cas de l'alcool isopropilique, des valeurs plus élevés des potentiels explosifs, par comparaison aux gaz moléculaires simples, attribuées aux processus moléculaires multiples qui ont lieu dans ces substances, qui réclament une grande consummation d'énergie fournie de l'extérieur.

Les courbes de Paschen pour les vapeurs des alcools isopropilique et isobutilique ont la même allurre et des valeurs proches pour le potentiel explosif minime, de même que pour le produit (pd) minime.

## BIBLIOGRAPHIE

1. G. G. BRĂTESCU, M. CAZAN-CORBASCA, Anal. Univ. București, Fizică, 31, 17 (1982).
2. G. G. BRĂTESCU, M. CAZAN-CORBASCA, Anal. Univ. București, Fizică, 27, 11 (1978).
3. G. G. BRĂTESCU, M. CAZAN-CORBASCA, Anal. Univ. București, Fizică, 29, 9 (1980).
4. G. G. BRĂTESCU, M. CAZAN-CORBASCA, C. DAMACUS, Anal. Univ. București, Fizică, 30, 13 (1981).
5. G. G. BRĂTESCU, M. CAZAN-CORBASCA, C. MARMANDIU, Bul. Inst. de Petrol și Gaze, Ploiești, XXVIII, 73 (1978).
6. G. G. BRĂTESCU, M. CAZAN-CORBASCA, Anal. Univ. București, Fizică, 32, 7 (1983).
7. A. KRUITHOFF, Physica, VII, 519 (1940).

ANALELE UNIVERSITĂȚII BUCUREȘTI, FIZICĂ, XXXIII, 1984, pag. 21—25

# LAMB — SHIFT POLARISED ION SOURCES

NICOLAE GHERBANOVSCHI, CRISTIAN CONSTANTIN BORDEIANU *

Faculty of Physics, University of Bucharest

*Résumé.* On présente les principes théoriques qui sont utilisés dans la construction des sources d'ions polarisés et aussi les progrès obtenus, les annés derniers, dans ce domaine.

## 1. Introduction

The interactions between nucleons and nucleus can be more reallisticaly studied and better understood if they are achieved by polarised atoms and ions. Within the polarised ion and atom beams the direction of the nuclear spin are partially or totally the same. The Lamb-shift of the excited states $2S_{\frac{1}{2}}$ and $2P_{\frac{1}{2}}$ of hidrogen and deuterium atoms can be used in order to construct polarised-ion sources.

This method is preferable to that using non uniform magnetic fields, because the selective ionization possibility eliminates the contribution of the ions appeared in the residual gas from the ioniser that are diminishing the ionization degree. In consequence a low pressure into the ioniser is unneccessary and because of that the ensemble is simpler and easier to be constructed.

## 2. The properties of hydrogen atom in metastable state $2S_{\frac{1}{2}}$ the hyperfine structure; Zeeman effect

The energetic states of hydrogen atom with $n = 2$, have a fine structure. According to Dirac theory, the excited states $2S_{\frac{1}{2}}$ and $2P_{\frac{1}{2}}$ should have the same energy.

Introducing the quantification of the electromagnetic radiation H.A. Bethe shows (ref. 1) that there is a (energetic) difference between these two states (Lamb-shift). The main contribution to the $2S_{\frac{1}{2}}$ state spontaneous desintegration is due to the transitions towards the fundamental state realised by the emission of two photons. This process has a life time of $10^{-7}$ sec, much longer than the life time of $2P_{\frac{1}{2}}$ state which is $1{,}595 \cdot 10^{-9}$ sec (ref. 2).

The presence of an electric field E shortens the life times of the metastable states of the hydrogen atom because of Stark effect. H. A. Bethe and E. Salpeter show (ref. 1) that for electric fields $E < 100$ V/cm there is the following relation between the life time of $2S_{\frac{1}{2}}$ and $2P_{\frac{1}{2}}$ states :

$$\tau_S = \tau_P \, (475/E)^2 \quad \text{with E in V/cm} \tag{1}$$

---

* National Center of Phyzics, Măgurele, P. O. Box 5211, Bucharest, Romania.

In the presence of a magnetic field H, the levels are splitting each in two components, fig. 1 (Zeeman effect in fine structure). If the interaction between nuclear magnetic momentum and the electron magnetic one is taken into account (ref. 3), the fine structure splits into a hyperfine one, fig. 2.

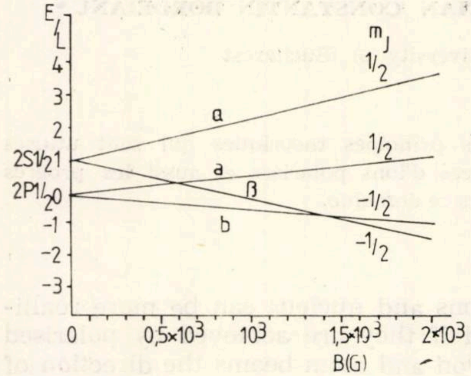

*Fig. 1* Zeeman effect on the $2S^1/_2$ a $2P^1/_2$ levels of hydrogen atom (fin structure).

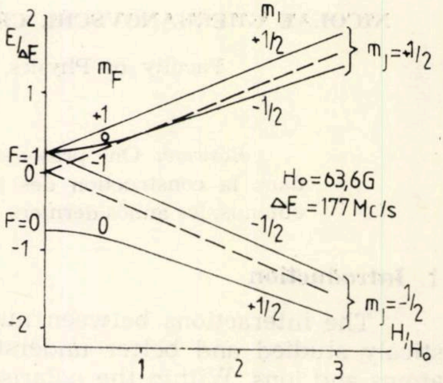

*Fig. 2* Zeeman effect on the $2S^1/_2$ levels of hydrogen atom taking into account hyperfine structure.

Due to this interaction the 2 S $^1/_2$ state splits into two subtates having an energetic difference given by :

$$\Delta E = (8/3)\, g_I \;\; (I + {}^1/_2) \cdot \frac{Z^2}{n^3} \cdot \alpha^2 \; .h.c.R \qquad (2)$$

where Z is the nucleus charge number, n is the principal quantum number, α is the fine structure constant, c is the light velocity, R is Rydberg's constant and I is the proton angular momentum.

In the presence of a magnetic field H a new splitting appears (Zeeman effect in hyperfine structure). After the calculus we have :

$$E_\pm = - g_I \mu_0 \cdot H \pm \frac{\Delta E}{2} \sqrt{1 + \frac{4 m_F}{2 \cdot I + 1} \cdot x + x^2} \qquad (3)$$

where $x = \frac{(g_J + g_I)\, \mu_0 \cdot H}{\Delta E}$, J being the electron angular momentum, $g_J$ and $g_I$ Landé factors for electron and proton respectively, $\mu_0$ Bohr-Procopiu magneton. Plus sign corresponds to F = I + 1/2 and minus one to F = I—1/2, with F = I + J.

### 3. The principle of Lamb-shift polarised ion source

In the presence of a magnetic field H normal to an electric one E only transitions α → b and β → a (fig. 1) can ocur. For H = 575 G we have :

$$\frac{\tau_s\,(\alpha)}{\tau_s\,(\beta)} = 1850 \qquad (4)$$

This means that if a hydrogen atom beam in metastable state, with a velocity of 4,4 · $10^7$ cm/sec. passes through a H = 575 G magnetic field parallel with the beam in the presence of an electric field $E = 15$ V/cm normal to H, only 3,5% of the atoms of $\alpha$ component are desintegrated whereas practically all the atoms of $\beta$ component are desintegrated. This way, at the exit from the magnetic field, a beam containing only atoms of $\alpha$ component of the $2\,S_{\frac{1}{2}}$ state is obtained. We can define the polarisattion degree : $P = N_+ - N_-$, with $N_+$ the proton fraction of $m_I = +1/2$ and $N_-$ proton fraction of $m_I = -1/2$. With this method, for P a maximum value of 50% can be obtained.

A few methods are used to grow the polarization degree : radiofrequency-transition method (ref. 2), (ref. 3), P. G. Sona's method (ref. 4) etc. We shall refer here to the spin filter method developped at Los Alamos (ref. 5). Three fields are applied in this method : an uniform magnetic field H = 575 G, an transversal electric field E and a radiofrequency field about 1600 MHz. The field ensemble constituting the spin filter can be adjusted so that through it can penetrate the atoms of one of the state H (2S) (fig. 4) components only.

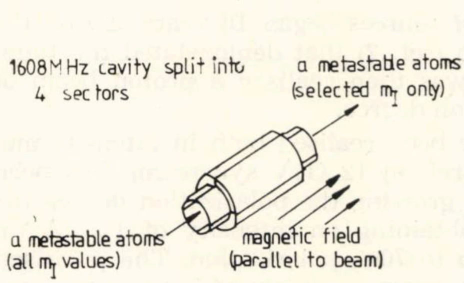
1608MHz cavity split into
4 sectors
α metastable atoms
(selected $m_I$ only)
α metastable atoms
(all $m_I$ values)
magnetic field
(parallel to beam)

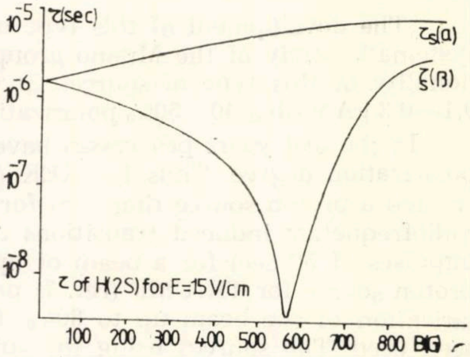

*Fig. 3* Life times of $2S_{1/2}$ State metastable atoms as a function of the magnetic field strength.

*Fig. 4* Electric and magnetic fields used in the spin filter. All but one hyperfine state are quenched when 500 eV H(2S) atom through the device.

The principle device of a Lamp-shift type polarised ion source is given in Fig. 5. In the common sources the metastable atoms are produced by charge exchange processes in Cs vapor. The following process occur (ref. 2), (ref. 9).

$$H^+ + Cs \rightarrow H\,(2S) + Cs^+$$

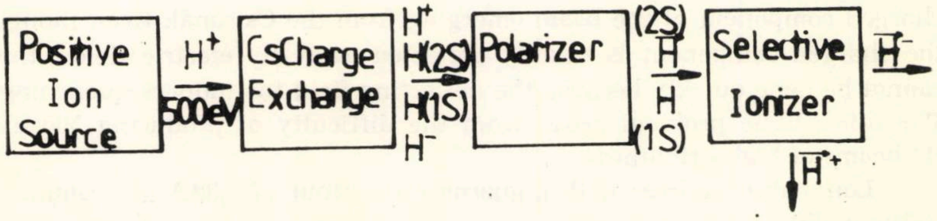
Positive Ion Source
$H^+$
500eV
CsCharge Exchange
$H^+$
H(2S)
H(1S)
$H^-$
Polarizer
(2S)
$\vec{H}$
H
(1S)
Selective Ionizer
$\vec{H}^-$
$\vec{H}^+$

*Fig. 5* Principle of the Lamb—shift polarised ion source.

The metastable atom beam passes after that through an electromagnetic field that polarizes the H (2S) atoms. The atoms polarized this way, are then selectively ionized by electron collision, electrons having an energy in 3,4 eV $<$E $<$13,4 eV, or in gaseous argon by the process :

$$H\ (2S) + Ar \rightarrow H^-\ (2S) + Ar^+ \qquad (5)$$

In the first method the selective ionization is due to the fact that the electron energy is enough only to ionize the excited atoms, the atoms in the fundamental state remaining unchanged. In the second method the selectivity is due to the fact that the negative ion fraction produced by the process :

$$H\ (1S) + Ar \rightarrow H^-\ (1S) + Ar^+ \qquad (6)$$

is negligeable with respect to the negative ion fraction produced by the process (5).

## 4. A review of the last years results

The development of this type of sources began 16 years ago by the systematic study of the Milano group (ref. 2) that demonstated the functionality of this type of sources. It was then realised a proton beam of 0,1—0,3 μA with a 40—50% polarization degree.

In the last years progresses have been realised both in intensity and polarization degree. Thus for KEK (ref. 6) 12 GeV syncrotron has been created a proton source that uses for growing the polarization degree the radiofrequency induced transitions obtaining an intensity of 1,1 μA (in impulses of 50 sec) for a beam of up to 70% polarization. The polarised proton source for TRIUMF (ref. 7) produces a current of 1 μA with a polarization of the beam up to 80%. In this case P.G. Sona's method has been used. The sources using the spin filter described give a 85% polarisation degree and even higher, but with a relatively weak intensity (0,5μA) (ref. 5).

Recent improvements of Lamb-shift type sources include the rapid change of the polarization sign (1KHz frequency) completed with the use of a spin filter allowing the passage of only one of the $2S_{\frac{1}{2}}$ state components.

While the beam intensity obtained with Lamb-shift sources does not approach the $H^+$ beam currents from atomic beam devices, Lamb-shift sources continue to be of interest because they readily provide negative ions. The intensity limitation probably arises at least in part from a fundamental problem (ref. 5) : quenching of the metastable atoms by the charged component of the beam emerging from the Cs canal. Even though the charged component is usually deflected away by electric fields, this cannot be done quickly because the deflecting field too induces quenching. The other basic problem arises from the difficulty of producing 500 eV $H^+$ beams of high brightness.

Lamb-shift sources with a guaranteed output of o,3μA are commercially avaible.

## REFERENCES

1. H. A. BETHE, E. E. SALPETER, *Quantum Mechanics of One and Two Electron Atoms.*
2. A. CESATI, F. CRISTOFORI, L. MILAZZO COLLI and P. G. SONA, Energia Nucl. (Milan) *13*, 649 (1966).
3. L. VÁLYI, *Atom and Ion Sources*, Akadémiai Kiadó, Budapest (1977).
4. P. G. SONA, *Energia Nucl.* (Milan) *14*, 295 (1967).
5. W. HAEBERLI, A.I.P. Conf. Proc., 51 (1979).
6. S. SUWA, A.I.P. Conf. Proc., 51 (1979).
7. J. L.BEVERIDGE, G. DUTTO, P. W. SCHMOR, A.I.P. Conf. Proc., 51 (1979).
8. W. ARNOLD, H. BERG, H. H. KRAUSE, J. ULBRICHT and G. CLAUSNITZER, Nucl. Instr. Meth, 143, 441 (1977).
9. L. MARINESCU, *Studii și cercetări de fizică, 8,* 819 (1976).

ANALELE UNIVERSITĂŢII BUCUREŞTI, FIZICĂ, XXXIII, 1984, pag. 27—32

# PAIR CORRELATIONS IN A MOLECULAR THEORY OF NEMATIC LIQUID CRYSTALS

**V. POPA-NIŢĂ and L. GEORGESCU**

Faculty of Physics, University of Bucharest *

*Abstract.* One obtain the single particle orientational distribution function for nematic liquid crystals varying the Helmholtz free-energy functional $F[f(\theta)]$ with respect to $f(\theta)$ under the normalization condition. We have chosen an intermolecular potential with a scalar component, a Lennard-Jones form and a long-range anisotropic component induced dipole-dipole term of the Coulomb interaction and working in a mean field approximation.

## 1. Introduction

In a microscopic development to studying the properties of a thermodynamic system obeying classical statistical mechanics, one first need to specify the potential of interaction between the particles of the system. This information with thermodynamic parameters such as density and temperature completely determine the state of the system. In the case of the liquid crystals, the intermolecular potential is not known. Even if it is known, the information would not be very helpful in microscopic calculation, since it would certainly be of an inordinately complex nature. As a compromise, when treating such a system one chooses a model potential which is tractable within the framework of the theory, but still incorporates certain realistic features. The „real" intermolecular potentials for liquid crystals must possess the following properties :

a) In liquid crystals as well as in simple fluids there are dominantly two-body additive forces. According to this assumption, the potential energy U is merely the sum of potentials due to the molecular pairs [1]. That is :

$$U(1, 2, \ldots, N) = \sum_{1 \leqslant i < j \leqslant N}^{N} v(i, j) \qquad (1)$$

where U (1, 2,...,N) is the potential energy of the system as a function of the N coordinates of the particles. We consider a macroscopic system of N classical rigid particles with position (e. g. centre of mass) specified by a vector $\vec{r}$ and orientation defined by the three Euler angles $\vec{e} = (\theta, \varphi, \chi)$

b) This potential incorporates a strong short-range repulsion and at intermediate or little range (comparable with the width of molecule) the potential must depend of the particles orientations and intermolecular distance.

---

* National Center of Physics, Măgurele, P. O. Box 5211, Bucharest, Romania.

In the study of the liquid-crystals one choose a simplified potential. Most mean-field-type treatments neglect the short-range repulsion entirely [3]. On the other hand, some previous microscopic theories have gone to the opposite extreme and centered their attention on systems of hard rods [4]. Such systems do not represent realistic models for liquid crystals.

In this work we have chosen an intermolecular two particles potential of the from

$$v(1,\ 2) = v_0(R) + w(\vec{R},\ \vec{e}_1,\ \vec{e}) \tag{2}$$

where $\vec{R} = \vec{r}_2 - \vec{r}_1$ and $R = |\vec{R}|$, with :

$$v_0(R) = 4\varepsilon\left[\left(\frac{\sigma}{R}\right)^{12} - \left(\frac{\sigma}{R}\right)^{6}\right] \tag{3}$$

which incorporates into the model a strong short-range repulsion, and at intermediate range, a moderate attraction. We have considered the familiar Lennard-Jones form, which is used for describing simple liquids ; $w(\vec{R},\ \vec{e}_1\ \vec{e}_2)$ is a long range anisotropic component induced-dipole-dipole term of the Coulomb interaction (Van der Waals forces) [5], [6] :

$$w(\vec{R},\ \vec{e}_1,\ \vec{e}_2) = -\frac{a}{R^6}(\vec{e}_1 \cdot \overleftrightarrow{T} \cdot \vec{e}_2)^2,\ a > 0 \tag{4}$$

where $\overleftrightarrow{T}$ is the symmetric tensor :

$$\overleftrightarrow{T} = \overleftrightarrow{1} - \frac{3\,\vec{R} \cdot \vec{R}}{R^2} \tag{5}$$

Given density $\rho \equiv N/V$ and temperature T, statistical mechanics of the canonical ensemble evolves from the configurational partition function [1] :

$$Q_N = \int e^{-\frac{U(1,2,\ \dots,\ N)}{kT}}\, d1 \dots dN \tag{6}$$

and the n-particle distribution functions [1] :

$$P^{(n)}(1,2,\dots,n) = \frac{N!}{Q_N(N-n)!}\int e^{-\frac{U(1,2,\ \dots,\ N)}{kT}}\, d_{n+1} \cdots dN \tag{7}$$

where k is the Boltzmann constant and we have used $d_1$ to indicate $d\vec{r}_1\, d\vec{e}_1$.

Of particular interest to a system characterized by pairwise interactions are the one — and two-particle distribution functions $P^{(1)}(1)$ and $P^{(2)}(1,2)$. When only orientational order is of concern, the physical properties are invariant under translation (for nematic liquid crystals) we can write :

$$P^{(1)}(1) \equiv P^{(1)}(\vec{r}_1,\ \vec{e}_1) = \rho f(\theta_1) \tag{7}$$

and

$$P^{(2)}(1,2) \equiv P^{(1)}(1)\,P^{(1)}(2)\,g(1,2) = \rho^2 f(\theta_1)\, f(\theta_2)\, g(1,2) \tag{8}$$

where $\theta_i$ measures the orientation of the i-th molecule relative to the director (taken along the z axis). f ($\theta$) is the *single particle orientational distribution function* and provides a measure of the long-range order, while g (1,2), a pair correlation function, describes the short-range order in the system.

In mean field approximation short-range correlations exist only in positions of centers of mass, the correlations in orientation are ignored. With this approximation, the relation (8) take the form :

$$P^{(2)}(1,2) = \rho^2 f(\theta_1)\, f(\theta_2)\, g(R) \tag{9}$$

The form of the orientational distribution function is empirical determinated from the property of molecular axis to align parallel with the director [2].

We shall determine explicit the form of function f ($\theta$) varying the Helmholtz free-energy functional F[f($\theta$)] with respect to f($\Theta$), working with the potential (2) in approximation (9)

## 2. The calculus of the orientational distribution function

From the expression of Helmholtz free-energy functional $F[f(\theta)] = E - TS$ we calculate the system energy and entropy.

The energy :

$$E = \langle U(1,2,\dots,N) \rangle = \frac{\int U(1,2,\dots,N)\, e^{-\frac{U(1,2,\dots,N)}{kT}}\, d1 \dots dN}{Q_N} =$$

$$= \frac{1}{2} N(N-1) \frac{\int v(1,2)\, e^{-\frac{U(1,2,\dots,N)}{kT}}\, d1 \dots dN}{Q_N}$$

From eqs. (2) and (7) we obtain :

$$E = \frac{V}{2} \int v_0(R) P^{(2)}(1,2)\, d\vec{R}\, d\vec{e}_1\, d\vec{e}_2 + \frac{V}{2} \int w(\vec{R},\vec{e}_1,\vec{e}_2)\, P^{(2)}(1,2)\, d\vec{R}\, d\vec{e}_1\, d\vec{e}_2.$$

From eq. (9) and the normalization :

$$\int f(\theta)\, d\vec{e} = 1$$

and express $\vec{R}$ in a spherical coordinate system we obtain :

$$E = 4\pi \frac{V\rho^2}{2} \int_0^\infty v_0(R)\, g(R) R^2\, dR + \frac{V\rho^2}{3} \int w(\vec{R},\vec{e}_1,\vec{e}_2)\, g(R)\, f(\theta_1)\, f(\theta_2)\, d\vec{R}\, d\vec{e}_1 d\vec{e}_2$$

On obtain the entropy S from expanding the expression :

$$S = -\frac{k}{N!} \int P^{(N)}(1,2,\dots,N) \ln \left[ \frac{P^{(N)}(1,2,\dots,N)}{N!} \right] d1 \dots dN$$

in a cluester series and then truncated at $N = 2$ :

$$S = S_{\mathrm{ideal}} - Nk \ln\rho + k \ln N! - Nk \int f(\theta) \ln f(\theta)\, d\vec{e} - \frac{1}{2} N\rho k \int g(R) \ln g(R)\, d\vec{R} + \ldots$$

Finally, on obtain the following expresion for the free energy :

$$F = F_0 + 4\pi \frac{V\rho^2}{2} \int_0^\infty v_0(R)\, g(R)\, R^2\, dR +$$

$$+ \frac{V\rho^2}{2} \int w(\vec{R}, \vec{e}_1, \vec{e}_2)\, g(R)\, f(\theta_1)\, f(\theta_2)\, d\vec{R}\, d\vec{e}_1 d\vec{e}_2 + NkT \int f(\theta) \ln f(\theta)\, d\vec{e} +$$

$$+ \frac{1}{2} NkT \int g(R) \ln g(R)\, d\vec{R} + \ldots \qquad (11)$$

To calculate the second integral from the right term of (11) we use the eqs. (4) and (5). We introduce a spherical coordinate system with polar axis $\vec{n}$ and express $\vec{e}_1$ and $\vec{e}_2$ in this coordinate system. Since the nematic liquid crystal molecules are uniaxial, all azimuthal angles $\varphi_1$ and $\varphi_2$ are equally probable. The average over these angles then works out to be

$$\langle(\vec{e}_1 \cdot \overleftrightarrow{T} \cdot \vec{e}_2)^2\rangle_{\varphi_1, \varphi_2} = \int_0^{2\pi} d\varphi_1 \int_0^{2\pi} d\varphi_2 (\vec{e}_1 \cdot \overleftrightarrow{T} \cdot \vec{e}_2)^2 =$$

$$= \frac{1}{4}\Big[\sin^2\theta_1 \sin^2\theta_2 (T_{xx}^2 + T_{yy}^2 + 2T_{xy}^2) + 4\cos^2\theta_1 \cos^2\theta_2\, T_{zz}^2 +$$

$$+ 2(\sin^2\theta_1 \cos^2\theta_2 + \sin^2\theta_2 \cos^2\theta_1)(T_{xz}^2 + T_{yz}^2)\Big] \qquad (12)$$

where the $T_{ij}$ are the cartesian components of $\overleftrightarrow{T}$.

Next, we average (12) over polar angles $\theta_1$, $\theta_2$. From the symmetry of the nematic state, the distribution function $f(\theta)$ is related to the order parameter $\eta$ by

$$\int_0^\pi \frac{1}{2}(3\cos^2\theta - 1)\, f(\theta) \sin\theta\, d\theta = \langle P_2(\cos\theta)\rangle = \eta \qquad (13)$$

where $P_2(\cos\theta) = \frac{1}{2}(3\cos^2\theta - 1)$ is the Legendre's polynomial of the second order.

The interaction averaged over all orientations of the two molecules becomes :

$$\langle w(R)\rangle_{\vec{e}_1, \vec{e}_2} = -\frac{a}{9R^6}\Big[T_{xx}^2 + T_{yy}^2 + T_{zz}^2 + 2(T_{xy}^2 + T_{xz}^2 + T_{yz}^2) +$$

$$+ \eta(4T_{zz}^2 + 2T_{xz}^2 + 2T_{yz}^2 - 2T_{xx}^2 - 2T_{yy}^2 - 4T_{xy}^2) +$$

$$+ \eta^2(T_{xx}^2 + T_{yy}^2 + 2T_{xy}^2 + 4T_{zz}^2 - 4T_{xz}^2 - 4T_{yz}^2)\Big] \qquad (14$$

Finally, we must average (14) over all orientations of the vector $\vec{R} = (R.\ \theta,\ \varphi)$. We express R in the same spherical coordinate system as before (with $\vec{n}$ the polar vector). Let $\Phi$ and $\theta$ be the azimuthal and polar angles of $\vec{R}$. Since the nematic state is cylindrically symmetric, all values of $\Phi$ are equally probable and obtain from relation (14) :

$$\langle w\rangle_{\vec{e}_1,\vec{e}_2,\Phi} = -\frac{a}{9R^6}\left[6+6\eta\,(3\cos^2\theta-1)+9\eta^2(1-8\cos^2\theta+9\cos^4\theta)\right] \quad (15)$$

In mean field approximation, on assume that all angles $\Theta$ are equally probable, i.e. the centers of mass of the molecules are completely random even at short range. With this assumption $< \cos^2\theta > = \frac{1}{3}$ and :

$$\langle w\rangle_{\vec{e}_1,\vec{e}_2,\varphi,\theta} = -\frac{2a}{3R^6}\left[1+\frac{n^2}{5}\right] \quad (16)$$

In relation (11) has the final form :

$$F = F_0 + 4\pi\frac{V\rho^2}{2}\int_0^\infty v_0(R)g(R)\,R^2\,dR - \frac{V\rho^2}{2}\,\frac{2a}{3}\left[1+\frac{n^2}{5}\right]\int_0^\infty\frac{g(R)}{R^4}\,dR$$

$$+ NkT\!\int f(\theta)\ln f(\theta)\,d\vec{e} + \frac{1}{2}NkT\!\int g(R)\ln g(R)\,d\vec{R} + \ldots$$

Varying the free-energy with respect to $f(\theta)$, finally we obtain :

$$f(\theta) = \frac{1}{Z}\exp\left[\frac{2\rho aI}{15kT}\,\eta P_2(\cos\theta)\right] \quad (17)$$

where the normalization Z is :

$$Z = \int_0^{2\pi} d\varphi\int_0^{\pi}\exp\left[\frac{2\rho aI}{15kT}\,\eta p_2(\cos\theta)\right]\sin\theta\,d\theta \quad (18)$$

where I is the integral

$$I = \int_0^\infty \frac{1}{R^4}\,g(R)\,dR \quad (19)$$

The form of the orientational distribution function chosen from the symmetry of nematic state and used in the theory is the following :

$$f(\theta) = \frac{1}{Z}e^{\alpha n P_2(\cos\theta)} \quad (20)$$

where $\alpha$ is a parameter depending on the nature of liquid crystal. Maier-Saupe mean field theory predicts for $\alpha$ a value of $\approx 6.8$. Theoretically

Wulf's calculations [7] suggests that $\alpha$ may be smaller that the mean field value. From eq. (17) this parameter can be evaluated for different nematic liquid crystals, used the pair correlation function g (R).

## 3. Conclusions

The orientational distribution function describes how the nematic liquid crystals molecules are distributed among the possible directions about the director ; it gives the probability of finding a molecule at some prescribed angle $\theta$ from the director $\vec{n}$. With this function we can calculate the average value of cantities important for the nematic state.

The form (17), theoretically calculated from the minimum condition of the free-energy, has the correct angular dependence $P_2$ (cos $\theta$) and one observe the dependence on the nature of the liquid crystals by the intermediary of p, a, I. The calculus of I is possible only if the form of the radial function g(R) is known. It is possible to determine g(R) from the equation BBGKY.

### REFERENCES

1. I. Z. FISHER, *Statistical Theory of Liquids*, The University of Chicago Press, 1966.
T. L. HILL, *Statistical Mechanics*, McGraw-Hill, 1956.
2. G. R. LUCKHURST and G. W. GRAY, *The Molecular Physics of Liquid Crystals*, Academic Press, 1979.
3. S. CHAKRAVARTY and C. W. WOO, Phys. Rev. A11, 713 (1975) ; L. SHEN, H. K. SIM, Y. M. SHIH and C. W. WOO, Mol. Cryst. Liq. Cryst. 39, 229 (1977) ; M. A. LEE and C. W. WOO, Phys. Rev. A16, 750 (1977).
4. R. L. COLDWELL, T. P. HENRY and C. W. WOO, Phys. Rev. A10, 897 (1974).
5. J. D. PARSONS, J. de Phys., 37, 1187 (1976).
6. C. A. CROXTON, *Statistical Mechanics of The Liquid Surface*, John Wiley of Sons, 1979.
7. A. WULF, J. Chem. Phys., 64, 104 (1976).

ANALELE UNIVERSITĂȚII BUCUREȘTI, FIZICĂ, XXXIII, 1984, pag. 33—36

# PULSED NMR SPECTROMETER

ST. LEVAI
Department of Physics, University of Bucharest *

S. LEVAI
Building Institute of Bucharest

M. CATRINESCU
Polytechnic Institute of Bucharest

*Abstract.* In order to study of the liquid state a pulsed NMR Spectrometer was designed and built on the purpose of measuring the relaxation times spinlattice $T_1$ and spin-spin $T_2$.

One of the main problems of modern statistical physics is the liquid state study. Its solution has to do with the thermal motion of molecules and liquid structure. These problemes are important for both, theoretical and applied research since liquid media are the ones where the majority of chemical reactions take place, the liquid is the most important thermal agent in energetic sistems, the biological processes take place in liquid media too. Up to now a considerable amount of experimental and theoretical popers have appeared, nevertheless new experimental data are needed if one takes into account the complexity of the problems encountered.

The nuclear magnetic rezonance is an important tool in this field, beside optical, spectroscopic, nuclear and other research.

In order to study the liquids experimentaly a pulsed NMR spectrometer was designed and built on the purpose of measuring the relaxation times spin-lattice $T_1$ and spin-spin $T_2$. The measurements range from 100$\mu$s and tens of seconds. The errors of measurements in optimum conditions is $2^0/_0$.

Figure 1 shows the block diagram of the spectrometer. The main block is a 4 MHz oscilator stabilized by the a quarz crystal. This fre-

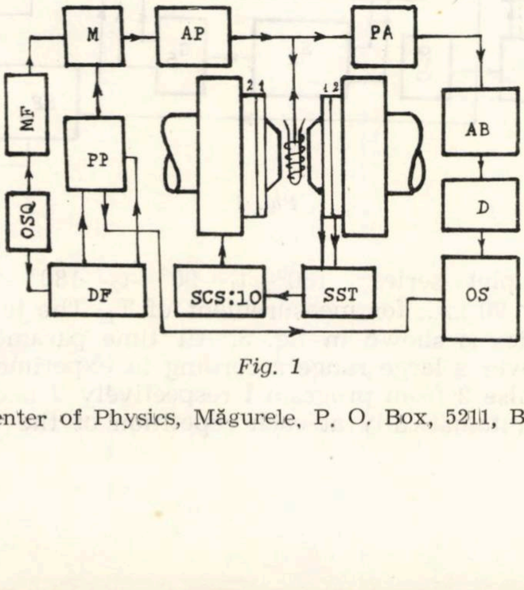

*Fig. 1*

---

* National Center of Physics, Măgurele, P. O. Box, 5211, Bucharest, Romania.

quency is multiplied 9 times MF block which yields the working current of 36 MHz. The imput of modulator block M consists of the 36 MHz signal and video pulses yieded by the pulse programme generator PP. The programming block receives two video signals of different frequencies f and F from the frequency divider DF, through two mechanical selectors $SM_1$ and $SM_2$.

The radiofrequency pulses obtained from the modulator are amplified by the power amplifier AP and applied to the coil inside wich the study-sample is placed.

The NMR signals are amplified. detected and visualised on the CRO screen OS.

Figure 2 shows the work diagram of the pulse programmer. It performes the following programes ;

I. Pair of pulses ; 90°—t—180° and their repetition ofter $T = 1/F$ seconds, for measurement of the relaxation times $T_2$, or 180°—t—90° for the measurement of $T_1$.

II.The simple triplet ; 90°—$t_1$—90°—$t_2$—180° and their repetition ofter T seconds, for the measurement of $T_1$.

III. The series Carr-Purcell ; 90°—$t_1$—180°—2$t_1$—180°—2$t_1$—180°..... for measurement of $T_2$.

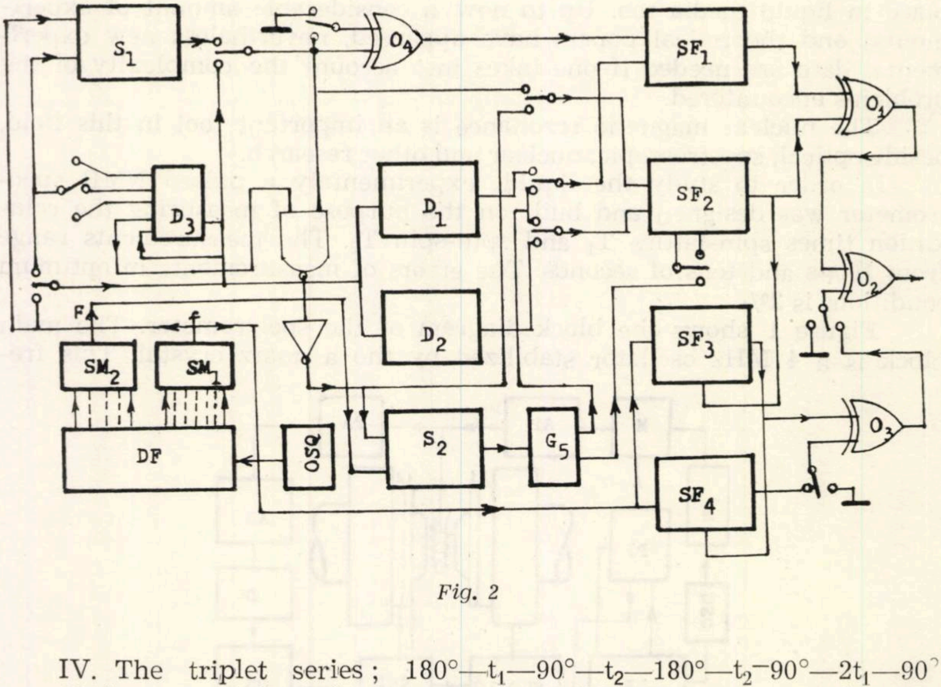

*Fig. 2*

IV. The triplet series ; 180°—$t_1$—90°—$t_2$—180°—$t_2$—90°—2$t_1$—90° $t_2$ — 180° — $t_2$ — 90°......, for measurement of $T_1$. The temporal diagram of these sequencies is shown in fig. 3. All time parameters t, $t_1$, $t_2$, T could be varied over a large range according to experimental needs. The shifting of the pulse 2 from program I respectively 2 and 3 in program II is performed automatically at each repetition of the experiment (ofter T s) by means of the two frequency dividers $D_1$ and $D_2$ wich divide the frequency f (chosen accordingly with $SM_1$), 99 respectively 100. The step between pulse 2 with respect to 1 is determined by selection of frequency f. The duration of series is determined by the choice of the

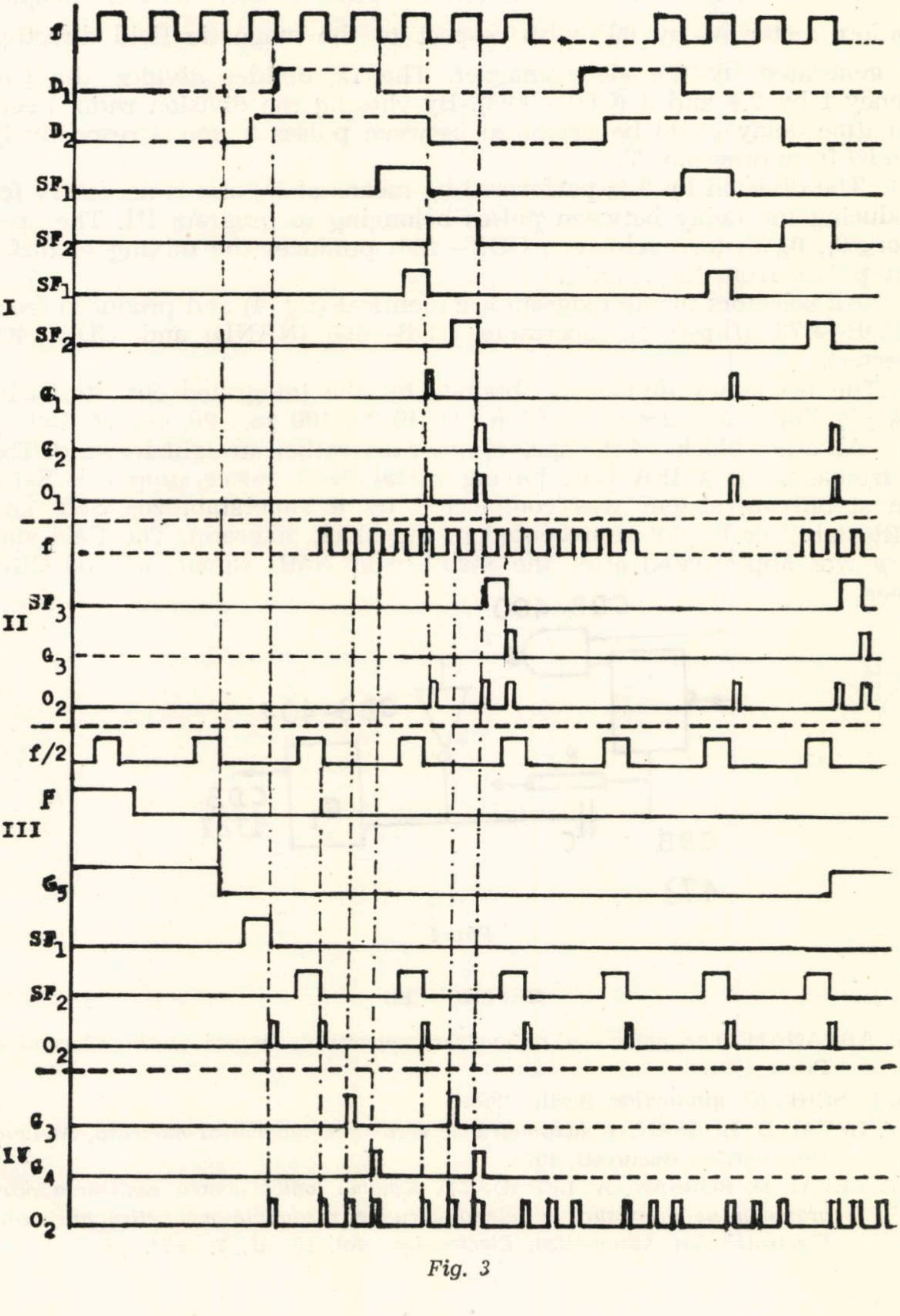
f
D1
D2
SF1
SF2
SF1
I
SF2
G1
G2
O1
f
SF3
II
G3
O2
f/2
F
III
G5
SF1
SF2
O2
G3
IV
G4
O2

*Fig. 3*

pulse duration yielded by the generator $G_5$ (monostable CDB-4121) wich is trigered by the reference pulse F by means of the selector $S_2$.

The pulses of duration $\tau$ are selected and formed in the selection and formation blocks $SF_1 ... SF_4$. Their shape of a given duration is produced by the square pulse generators (monostable CDB—4121). The duration of 90° and 180° are obtained manually by adjusting the time constant RC of the generator circuit. The 90° pulse rotates the total magnetization vector $\vec{M}$ by 90° with respect to the magnetic field direction $\vec{H}$ generated by the electromagnet. The $D_3$ divider divides the frequency f by 2,4 and 8 (CDB—493). By chosing the division ratio a certain time delay could be produced between pulses 2 and 3 respectively 3 and 4 from program IV.

The division by 2 is performed by means of $D_3$ and is necessary for producing the delay between pulses belonging to program III. The operators $0_1$, $0_2$, $0_3$ (or exclusive ; CDB—486) produces the mixing of different pulses from $SF_1 \ldots SF_4$.

All selectors in the diagram are identical (fig. 4) and produced from a CDB—473 (flip-flop), operators CDB—400 (NAND) and CDB—406 inverter).

The frequency divider is obtained by the integrated circuits CDB-493, yielding 7 decades of division (20, 40 80, 100 μs... 20, 40, 80, 100 s).

All other blocks of the spectrometer are rather straight forward. The electromagnet is a IFA type having a stabilized power supply SCS-10. The stabilizing sistem was complected by a superstabilizer SST and NMR stabilizer (is not reprezented in the block diagram). The field stability was appreceated after the stability of NMR signals on the CRO screen.

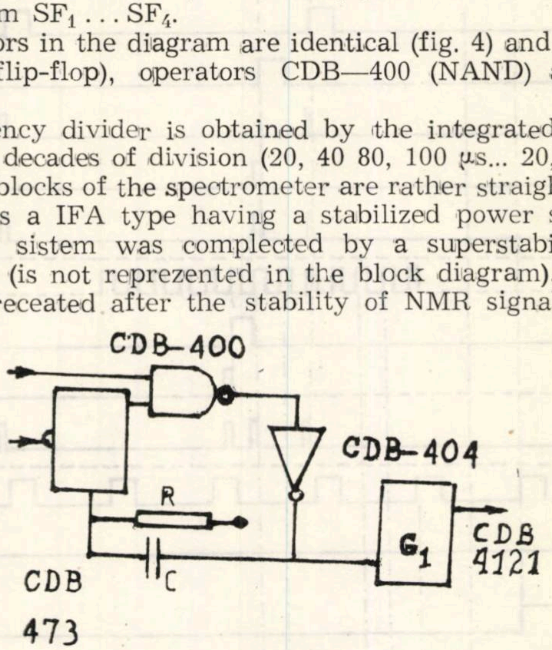

*Fig. 4*

## REFERENCES

1. A. ABRAGAM, *The principles of nuclear magnetism*, Oxford at the Clarendon Press, 1961.
2. A. LÖSCHE, *Kerninduction*, Berlin, 1959.
3. ST. LEVAI, D. BORSAN, *Relaxometru de rezonanță magnetică nucleară*, Analele Universității București, 1970.
4. ST. LEVAI, D. BORȘAN, A. LEPĂDATU, *Schema logică pentru realizarea programelor de impulsuri la relaxometru de rezonanță magnetică nucleară. Electrotehnica Automatica, Electronica.* vol. 19, nr. 2, 1975.

ANALELE UNIVERSITĂŢII BUCUREŞTI, FIZICĂ, XXXIII, 1984, pag. 37—41

# LA PROPAGATION DES ULTRA-SONS DANS LES LIQUIDES $CCl_4$ ET $CHCl_3$, ET DANS LE MELANGE $CCl_4+CHCl_3$

V. DIMA
Faculté de Physique, Université de Bucarest *
N. FLOREA
Institut de Constructions, Bucarest **

*Résumé.* A partir des considérations statistiques sur l'état liquide on calcule la fonction radiale de distribution et sur cette base on calcule la vitesse des ultra-sons dans les liquides purs $CCl_4$ et $CHCl_3$, et dans le mélange $CCl_4+CHCl_3$. Dans le cas du mélange les interactions entre les molécules de la même espèce et d'espèces différentes sont décrites par un potentiel moyen qui dépend de la concentration. Les valeurs calculées sont présentées par rapport à celles mesurées par la méthode des impulsions transmises. Entre les valeurs théoriques et les valeurs expérimentales il y a un accord satisfaisant.

## A. Liquides purs

### 1. *Fonction radiale de distribution*

Nous allons considérer le modèle statistique du liquide où tous les paramètres thermodynamiques peuvent s'exprimer sur la base de la fonction radiale de distribution g (r). La fonction g (r) peut être déterminée par la solution des équations integro-différentielles /1/ qu'elle satisfait. Pour la description des intéractions moléculaires nous allons adopter un potentiel Lennard-Jones ayant la forme :

$$\left.\begin{aligned} \Phi(r) &= 4\varepsilon\left[\left(\frac{a}{r}\right)^{12} - \left(\frac{a}{r}\right)^{6}\right], & r &\geqslant a \\ \Phi(r) &= \infty, & r &< a \end{aligned}\right\} \qquad (1)$$

où ε est un paramètre énergétique qui correspond à la valeur minimale du potentiel Φ (r) et a — le diamètre de collision ou la longuer caractéristique de la molécule.

Le choix de ce type de potentiel, valable pour des interactions entre des molécules à symmétrie sphérique, se justifie par le fait que les liquides que nous sommes proposé d'investiguer, le tétrachlorure de carbone et le chloroforme se rapprochent de cette symmétrie sphérique. Dans un ouvrage antérieur /2/ nous avons décrit la méthode de calcul de la fonction g (r) pour un certain liquide pour lequel on connaissait les paramètres Lennard-Jones a et ε ainsi que la densité et la masse molaire. Nous allons présenter ici seulement les résultats obtenus pour la fonction g (r) dans le cas des deux liquides mentionnés ci-dessus.

---

* Centre National de Physique, P.O. Box 5211, Măgurele, Bucarest.
** Bd. Republicii, 176, sector II, Bucarest.

Les calculs on été faits pour un intervalle large de température. celle-ci étant variée de 10 en 10 dégrés. Pour $CHCl_3$ le domaine de température été compris entre 233 K et 333 K et pour $CCl_4$ entre 253 K et 343 K. Pour la valeur $x = \frac{r}{a}$ nous avons considéré 30 valeurs comprises entre 1 et 3. Le domaine $x \varepsilon (1,3)$ constitue une précision suffisante pour les liquides où l'on suppose que l'ordre des particules se manifeste sur des distances d'un ordre de deux ou trois diamètres moléculaires. Les valeurs de la fonction g(x) pour deux températures extrêmes correspondant aux deux substances étudiées sont présentées dans le tableau 1 et représentées graphiquement dans les figures 1 et 2.

*Tableau 1*

| | $CCl_4$ : a = 5,881 $10^{-10}$m<br>ε = 4,512 $10^{-21}$J | | $CHCl_3$ : a = 5,430 $10^{-10}$m<br>ε = 4,512 $10^{-21}$J | |
|---|---|---|---|---|
| x | g(x)<br>T = 253 K | g(x)<br>T = 343 k | g(x)<br>T = 233 K | g(x)<br>T = 333 K |
| 1,00 | 0,6756 | 0,9155 | 0,6134 | 0,8855 |
| 1,04 | 1,5705 | 1,6725 | 1,5422 | 1,6513 |
| 1,08 | 2,2023 | 2,1055 | 2,2408 | 2,0990 |
| 1,12 | 2,4093 | 2,1887 | 2,4901 | 2,1907 |
| 1,16 | 2,2609 | 2,0711 | 2,3804 | 2,0753 |
| 1,20 | 2,0276 | 1,8781 | 2,0827 | 1,8823 |
| 1,24 | 1,7808 | 1,6787 | 1,8199 | 1,6824 |
| 1,32 | 1,3779 | 1,3465 | 1,3944 | 1,3499 |
| 1,40 | 1,1184 | 1,1222 | 1,1245 | 1,1263 |
| 1,48 | 0,9597 | 0,9778 | 0,9621 | 0,9832 |
| 1,56 | 0,8686 | 0,8900 | 0,8703 | 0,8965 |
| 1,64 | 0,8219 | 0,8418 | 0,8242 | 0,8491 |
| 1,72 | 0,8090 | 0,8244 | 0,8123 | 0,8318 |
| 1,80 | 0,8245 | 0,8331 | 0,8287 | 0,8400 |
| 1,88 | 0,8663 | 0,8669 | 0,8711 | 0,8723 |
| 1,96 | 0,9309 | 0,9234 | 0,9355 | 0,9262 |
| 2,00 | 0,9729 | 0,9617 | 0,9768 | 0,9626 |
| 2,04 | 1,0172 | 1,0025 | 1,0203 | 1,0014 |
| 2,12 | 1,1027 | 1,0774 | 1,1050 | 1,0730 |
| 2,20 | 1,1436 | 1,1136 | 1,1457 | 1,1078 |
| 2,28 | 1,1319 | 1,1085 | 1,1328 | 1,1031 |
| 2,36 | 1,0897 | 1,0788 | 1,0895 | 1,0751 |
| 2,44 | 1,0412 | 1,0419 | 1,0402 | 1,0403 |
| 2,52 | 1,0008 | 1,0087 | 0,9989 | 1,0089 |
| 2,60 | 0,9705 | 0,9824 | 0,9697 | 0,9839 |
| 2,68 | 0,9582 | 0,9684 | 0,9601 | 0,9718 |
| 2,76 | 0,9543 | 0,9621 | 0,9573 | 0,9660 |
| 2,84 | 0,9587 | 0,9635 | 0,9618 | 0,9670 |
| 2,92 | 0,9692 | 0,9710 | 0,9712 | 0,9734 |
| 3,00 | 1,0458 | 1,0159 | 1,0455 | 1,0130 |

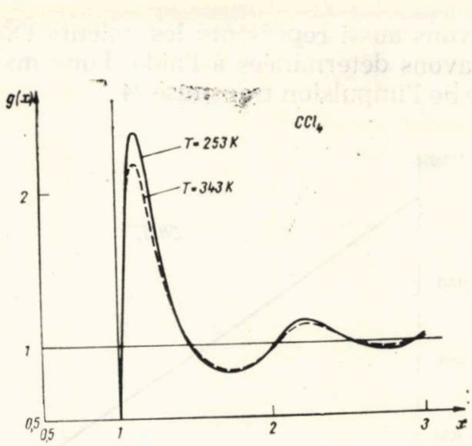

*Fig. 1.* La fonction radiale de distribution pour CCl$_4$

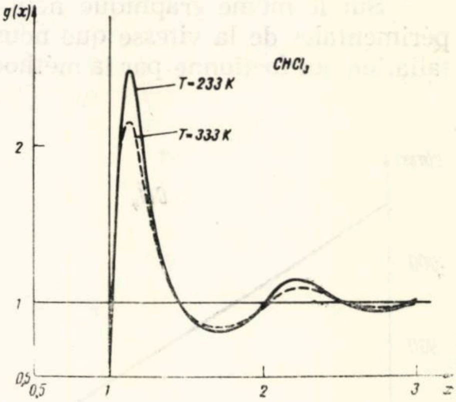

*Fig. 2.* La fonction radiale de distribution pour CHCl$_3$

Les courbes obtenues pour CCL$_4$ et CHCl$_3$ ont le même aspect que celles obtenues pour d'autres liquides /3/. La presence des premiers maxima indique cette fois l'ordre proche qui existe dans le liquide et la continuité des courbes nous permet d'afirmer que dans le liquide des mouvements de translation des particules de même que des mouvements d'oscillation autour d'une position fixe sont possibles, les premiers étant prédominants à des températures proches de celle d'ébullition. A mesure que la temperature s'acroît, les maxima et les minima semblent moins prononcés, ce qui montre que l'ordre local se restreint d'avantage.

## 2. *Vitesse de propagation des ultra-sons*

La fonction g (x) étant connue, nous pourrons calculer la vitesse de propagation des ultra-sons dans un certain liquide à l'aide de l'expresion suivante /3/ :

$$c=\left[\frac{R}{\mu}\left(T+\frac{\gamma-1}{\alpha_p}\right)+\frac{16\pi N^2\rho\varepsilon a^3}{\mu}\int_1^3\left(\frac{10}{x^{10}}-\frac{3}{x^4}\right)g(x)\,dx\right]^{\frac{1}{2}} \quad (2)$$

où $\gamma$ est le coefficient adiabatique,
$\alpha_p$ — coefficient de dilatation isobar
$\mu$ — masse molaire,
N — numéro d'Avogadro.

La fonction g (x) étant obtenus sous forme numérique nous avons résolu l'intégrale numérique de la relation (2) à l'aide du calculateur en utilisant la méthode des trapèzes. Nous avons effectué à cet effet un programme FORTRAN que nous avons roulé sur un calculateur FELIX 256. Les calculs on été effectués pour les mêmes valeurs de la température pour lesquelles nous avons calculé la fonction g (x). Dans les figures 3 et 4 sont présentées les valeurs calculées de la vitesse de propagation des ultra-sons en CCL$_4$, respectivement CHCL$_3$.

Sur le même graphique nous avons aussi représenté les valeurs expérimentales de la vitesse que nous avons déterminées à l'aide d'une installation qui foctionne par la méthode de l'impulsion transmise /4/.

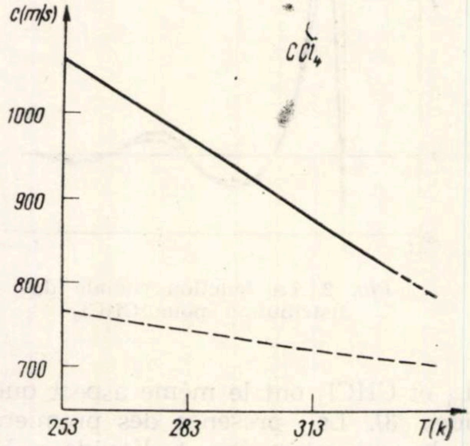

*Fig. 3.* La fonction c(T) pour $CCl_4$.
——— valeurs expérimentales
- - - - - valeurs théoriques

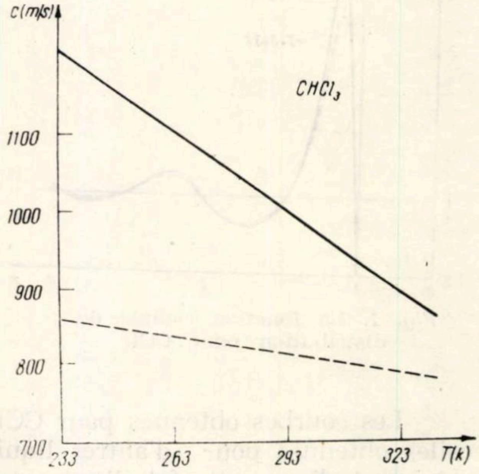

*Fig. 4.* La fonction c(T) pour $CHCl_3$.
——— valeurs expérimentales
- - - - - valeurs théoriques

Comme on remarque du graphique, tant théoriquement que par voie expérimentale, on obtient une variation linéairement décroissante de la vitesse avec le température.

Pour les deux liquides, les vitesses calculées sont d'habitude moindres que celles expérimentales, et la pante de la droite expérimentale est plus grande que la pante correspondant à la droite théorique. Ceci fait que, à mesure que la température augmente, il y ait un meilleur accord entre les valeurs théoriques et expérimentales.

### B. **Melange binaire $CHCl_3+CCl_4$**

Les deux liquides qui composant le mélange considéré ont des paramètres a et ε rapprochés ent tant que valeur de sorte que, pour la description des interactions moléculaires, on peut considérer un potentiel moyen qui dépend de la fraction molaire du mélange. Suivant la méthode de calcul décrite par nous dans l'ouvrage /5/, nous avons d'abord calculé la fonction g (x) pour chaque concentration et ensuite la valeur de la vitesse de propagation des ultra-sons. Nous avons travaillé à une seule température $t = 20°C$ et nous avons calculé la valeur c pour 11 concentrations. Pour les mêmes concentrations nous avons mesuré la vitesse des ultrasons avec la même installation utilisée au cas des liquides purs. Les déterminations expérimentales ont été faites avec une erreur de 1 %.

Les résultats théoriques et expérimentaux sont présentés dans la figure 5.

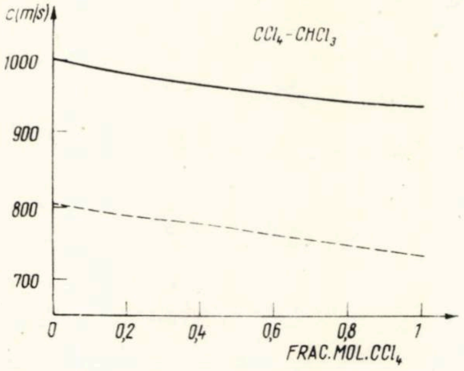

*Fig. 5.* Dépendance de la vitesse des ultra-sons de la concentration du mélange $CCl_4+CHCl_3$

—— valeurs expérimentales
- - - - - valeurs théoriques

Comme on remarque sur le graphique, la courbe de concentration obtenue théoriquement présente le même trait que celle obtenue expérimentalement. La courbe théorique est située au-dessous de celle expérimentale, une situation naturelle si nous nous souvenons que les vitesses théoriques des composantes pures sont moindres que les vitesses expérimentales correspondantes. Le fait que dans le cas du mélange étudié la courbe théorique donne une dépendance de la vitesse à partir de la concentration, semblable à celle produite par la courbe expérimentale, indique le cadre correct d'application dela théorie du potentiel moyen.

## REFERENCES

1. J. KIRKWOOD, V. LEWINSON, B. ALDER, J. Chem. Phys., 20, 929, 1952.
2. N. FLOREA, V. DIMA, *Analele Universității București,* Fizică, XXX, 51, 1981.
3. V. DIMA, *Teza de doctorat,* Universitatea București, 1974.
4. N. FLOREA, *Teza de doctorat,* Universitatea București, 1981.
5. N. FLOREA, V. DIMA, *Analele Universității București,* Fizică, XXXI, 23, 1982.

ANALELE UNIVERSITĂȚII BUCUREȘTI, FIZICA, XXXIII, 1984, pag. 43—49

# ON THE THICKNESS AND STOICHIOMETRY OF CUPROUS SULPHIDE FOR THIN FILM $Cu_2$ S/CdS ELECTRON-VOLTAIC CELLS

**A. DAFINEI and I. LICEA**

Faculty of Physics, University of Bucharest *

*Abstract.* In this work an electrochemical study of the thickness and stoichiometry of the thin films of cuprous sulphide entering in the composition of the thin film electron-voltaic $Cu_2S/CdS$ cells is made. A method based on the constant current coulometry which allows a rapid determination of the thickness and composition of $Cu_{2-x}S$ thin film is used. The experimental data may be explained directly by means of some nomograms.

## 1. Introduction

The studies performed in the last ten years pointed out the fact that conversion efficiency and other properties of the thin film $Cu_2S/CdS$ cells are affected strongly on the thickness of the cuprous sulphide layer and also on his composition. The best results are obtained using a $Cu_{2-x}S$ layer with $x < 0{,}005$ which assures a most favorable stoichiometry in order to obtain a great conversion efficiency. As it is well-know, the electron-voltaic effect appears when the electrons from a β-source are incident on the $Cu_{2-x}S$ layer of the cells. Penetrating this layer they form electron-hole pairs predominantly in the CdS layer and these charge carriers are separated by the electric field existing in the junction. The main feature of the electron-voltaic energy conversion is that the shunt resistance, $R_{sh} = \left|\frac{dV}{dI}\right|_{V=0}$ has a more significant effect on the I—V caracteristic than the series resistance, which can be assumed to be negligible [1]. This fact is assured by the fabrication technology of the cells, using the „dry“ barrier rather than the „wet“ barrier method as in the case of the cells fabricated for photo-voltaic energy conversion [1, 2].

The low values of the shunt resistance may arise due to some factors which include structural properties of the CdS and $Cu_{2-x}S$ layers and also the possible presence of $Cu_{2-x}S$ tracks in the CdS. Besides the forming process of the $Cu_{2-x}S$ layer, other factors, as the oxydation in time or the electrochemical decomposition caused by electric field, can modify the composition and structure of the cuprous sulphide layer.

---

* National Center of Physics, P. O. Box 5211, Măgurele — Bucharest, Romania.

Consequently, it is important to know the thickness and the composition of the $Cu_{2-x}S$ layer in order to assure a most favorable generation and separation of the charge carriers.

The purpose of this work is to present a study involving an analysis of the thickness and composition of some $Cu_{2-x}S$ thin films by means of the constant current coulometry method. Although this method is destructive, it is suitable because his rapidity, when a sample out of a great number of cells obtained in similar conditions must be analysed. The obtained results allow to understand better the work mechanism of the $Cu_2S$/CdS electron-voltaic cells and the possibility to optimise the conversion efficiency.

## 2. Electrochemical analysis

The cells are obtained [2] by the „dry“ barrier fabrication technique, involving the vacuum evaporation of a cooper compound on the surface of the CdS layer followed by a bake in order to convert the surface region to $Cu_{2-x}$ S. A typical cell consists by a cadmium sulphide layer of 15—20μm deposited on a glass substrate which has been previously covered with conducting SnO. The top layer of CdS has been converted in p-type $Cu_{2-x}S$ and the metalic grid (the positive terminal) has been fixed to the $Cu_{2-x}$ S by indium film.

In order to obtain some information on the possible values of x, a method based on the study of the electromotive force of the electrochemical cell Cu/ $Cu^{2+}_{aq}$ /$Cu_{2-x}$ S may be used. This method has been proposed first for the study of the $Cu_{2-x}S$ layer in the thin film $Cu_2S$/CdS solar cells [3,4].

The electromotive force $E_x$ of the electrochemical cell Cu/$Cu^{2+}_{aq}$/ $Cu_{2-x}$ S is related to the chemical potentials of pure copper and copper in cuprous sulphide, $\mu^{c}cu$ and $\mu^{x}cu$ by the relation.

$$-2N_A qE_x = \mu^{x}cu - \mu^{\circ}cu \tag{1}$$

where $N_A$ is Avogadro's number.
Taking into account that

$$\mu^{x}cu = \mu^{\circ}cu + k_B N_A T \ln a\,(Cu) \tag{2}$$

the copper activity is given by :

$$a\,(Cu) = e^{-\frac{2qE_x}{k_B T}} \tag{3}$$

if the cuprous sulphide in equilibrium with copper is chosen as a reference state so that the copper activity for $E_x = 0$ is a (Cu) = 1. From the relation (3) one may see that $E_x$ can be related to the real stoichiometry of the $Cu_{2-x}S$ sample. The passing of an electric current through the considered cell leads to the appearance of the reaction $Cu_{2-y}S$ — aqueous solution

$$Cu_{2-x}S + 2(x' - x)e^{-} \rightarrow Cu_{2-x}S + (x - x')Cu^{2+} \tag{4}$$

It is easily to establish that the differance (x—x') appearing in the quoted reaction can be related with the mass sample, the current value and the time which it flows. In this way one can modify by a known amount the stoichiometric, ratio of the sample. The influence of this change on the electromotive force of the electrochemical cell and, consequently, on the copper activity may be determined.

## 3. Stoichiometry and thickness of the cuprous sulphide layer

In order to determine the departure from the stoichiometry of the $Cu_{2-x}S$ layer, a classical device with three electrodes :

| | | | |
|---|---|---|---|
| *Platinum electrode*<br>Calomel electrode | *Sodium acetate*<br>aqueons solution | $Cu_{2-x}$ S | Pt |

has been used. The experimental set-up used in the measurements is given in Fig. 1. The sample electrode and the platinum electrode are immersed in a supersaturated sodium acetate solution at the room temperature. The referance electrode (calomel electrode) is immersed in a supersaturated KCl solution. The sample electrode consists in a teflon plate in which the sample is inserted. In order to assure a uniform field both sample and platinum electrodes are plane ; also, a little window (0,28 sq. cm) from the sample has been separated with an insulating epoxy film.

In the sample the reduction takes place in three steps, as follows :

$$Cu_2O + H^2O + 2e^- \rightarrow 2Cu^\circ + 2OH^- \tag{5}$$

$$Cu_{2-x}S + xe^- \rightarrow \frac{2-x}{2} Cu_2S + \frac{x}{2} S^{2-} \tag{6}$$

$$\frac{2-x}{2} Cu_2S + (2-x)e^- \rightarrow (2-x)Cu^\circ + \frac{2-x}{2} S^{2-} \tag{7}$$

The completion, of each step is signaled by a change in the electrical voltage between the sample electrode and the reference calomel electrode. These variation in time are plotted by a X—Y recorder. In the reactions (6) and (7) the requered quantities of electricity $q_1$ and $q_2$ are, respectively,

$$q_1 = xe^- \; ; \qquad q_2 = (2-x)e^- \tag{8}$$

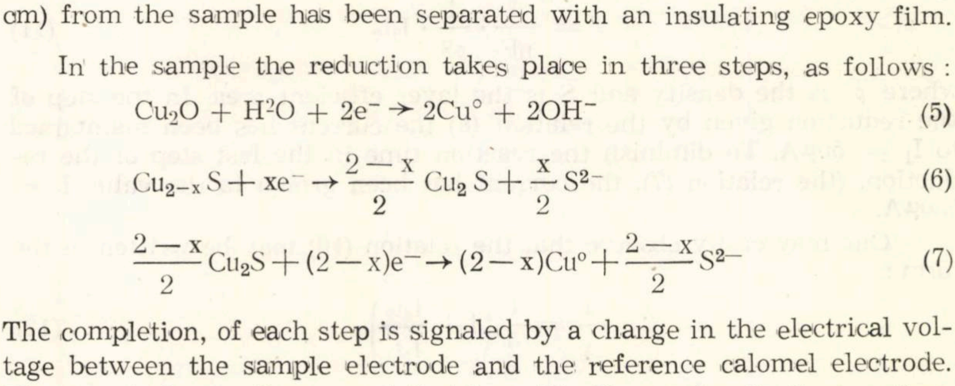

*Fig. 1.* Experimental set-up.

The departure from the stoichiometry x is determined by the quantities of electricity, so that :

$$x = \frac{2q_1}{q_1 + q_2} \tag{9}$$

or

$$x = \frac{2I_1t_1}{I_1t_1 + I_2t_2} \tag{10}$$

where $I_1$ and $I_2$ are the values of the current flowing through the cell in time of the two steps of reduction, $t_1$ and $t_2$ being respectively the duration of the (6) and (7) reactions. The relation (7) may be used in order to calculate the thickness of the $Cu_{2-x}S$ film. From the Faraday's law of electrolysis we have, $m = \frac{A}{n} \cdot \frac{1}{F} \cdot It$,here F is Faraday's constant, n is the number of transfered electrons, A is the molar mass. The layer thickness may be expressed by

$$d = \frac{A}{nF} \cdot \frac{1}{\rho S} \cdot I_2t_2 \tag{11}$$

where $\rho$ is the density and S is the layer efficient area. In the step of the reduction given by the relation (6) the current has been maintained to $I_1 = 50\mu A$. To diminish the reaction time in the last step of the reduction, (the relation (7), the current has been grown to the value $I_2 = 550\mu A$.

One may easily observe that the relation (10) may be written in the form :

$$\frac{1}{x} = \frac{1}{2}\left(1 + \frac{I_2t_2}{I_1t_1}\right) \tag{12}$$

The ralation (11) and (12) may be used to give some nomograms which represent straight lines, allowing to determine directly the thickness and the departure of stoichiometry of the $Cu_{2-x}S$ layers.

In Fig. 2, we plotted the nomograms giving the thickness d = f (t) for various current conditions. In the calculus the following values of the parameters have been used : $A = 0{,}159$ kg/mol, $\rho = 5{,}6 \cdot 10^3$ Kg/ m$^3$, $F = 96500$C/mol, $S = 2{,}8 \cdot 10^{-5}$ m$^2$.

In Fig. 3 we plotted the nomogrames giving the departure of the stoichiometry $x = f(t_2/t_1)$ for various, values of the ratio $I_2/I_1$.

The measured samples belong to three different sets out of which two have been thermally treated. The curves giving the dependence of the voltage versus the time for the wholle set of sample are plotted in Fig. 4.

The voltage between the sample electrode and the calomel electrode presents jumps when passes from a kind of reaction to an other kind of reaction. The to part of the curve refers to the reaction (5), the $t_1^i$ part refers to the reaction (6) and the $t_2^i(1 \leqslant i \leqslant 3)$ refers to the reaction (7). In the above notation the index indicates the number of the sample.

The last bearing of the curve is given by the electrochemical deposition of coopper from the solution. In the treated samples 2 and 3 one observe a growth of the $CuO_2$ amount marked by an extension of the bearing which coresponds to the first reaction.

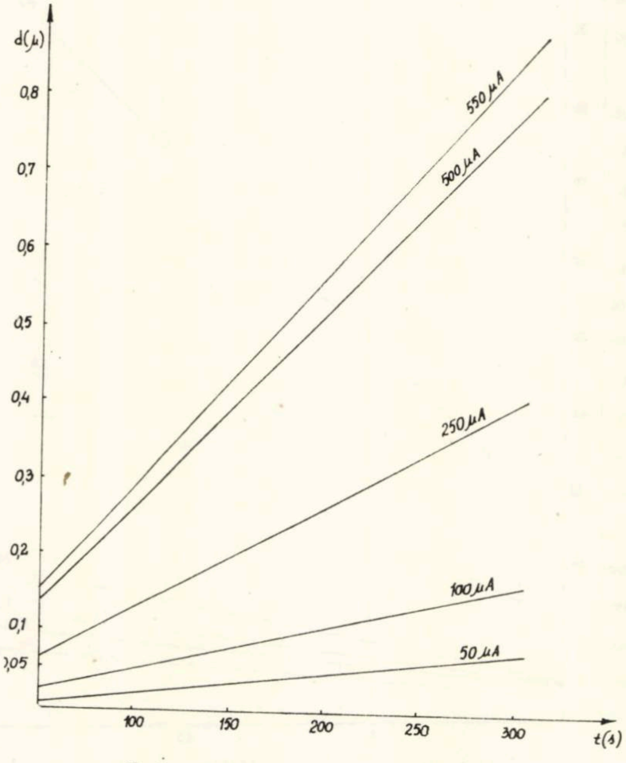

Fig. 2 The nomograms $d = f(t)$ for various current conditions.

By means of the obtained nomograms it is possible to explain the reaction times in terms of thickness and composition of the samples. The values obtained for the thickness and the departure from the stoichiometry are given in Table 1.

*Tabela 1*

| Nr. | Thickness (μm) | Composition | Voc(mV) | $\eta$(%) |
|---|---|---|---|---|
| 1. | 0,45 | $Cu_{1\,87}S$ | 12,5 | 2,16 |
| 2. | 0,36 | $Cu_{1\,89}S$ | 19,75 | 0,78 |
| 3. | 0,28 | $Cu_{1.79}S$ | 2,87 | 0,25 |

These measurements are important also because they give some information on the relation between the composition and thickness of $Cu_{2-x}S$ layers and the conversion parameters of thin film $Cu_2S/CdS$ electron-voltaic cells. The measurements of the conversion efficiency and of the open circuite voltage for the three beta cells from the studied set at an irradiation with 75 kV electrons are given also in Table 1 [2].

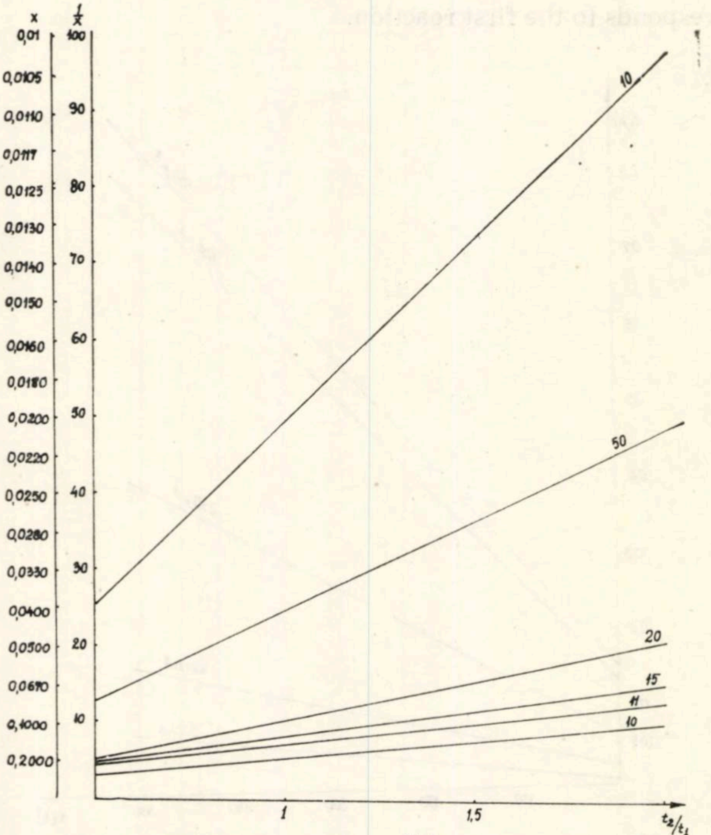

Fig. 3 The nomograms $x = f\left(\frac{t_2}{t_1}\right)$ for various ratios $\frac{I_2}{I_1}$

For the studied cells, the stoichiometry of the $Cu_{2-x}S$ layer influences the open circuit voltage while the growth of the layer thickness determines the generation of the secondary electrons in an appropriate region for the collecting process. These problems will be treated in an apart study.

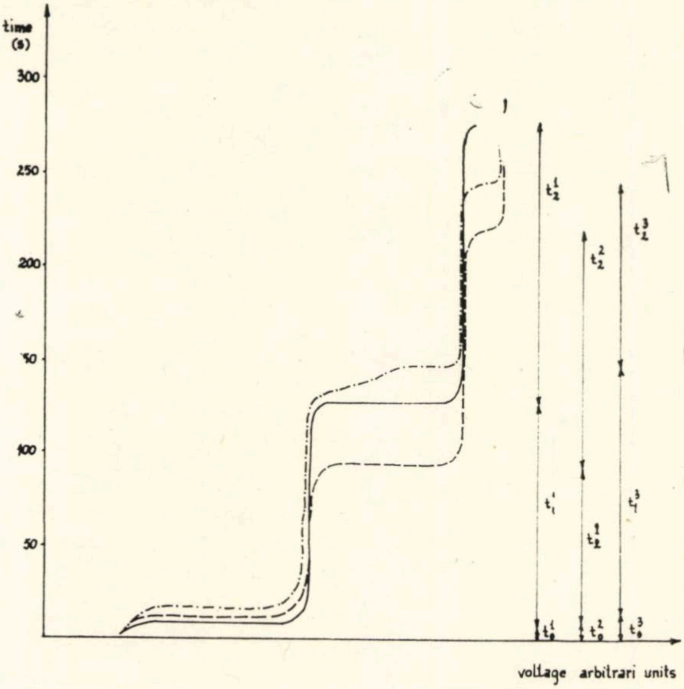

Fig. 4 Dependence of the voltage versus the time.

## REFERENCES

1. R. W. GLEW, F. J. BRYANT, *Solid-State Electronics, 18*, 839 (1975).
2. A.DAFINEI, Rev. Roum. Phys., (to be published).
3. E. CASTEL and J. VEDEL Analysis, *3*, 487 (1975).
4. B. BARON, A. W. CATALANO, E. A. FAGEN, *Proceedings of the 13 th IEE Photovoltaic specialists Conference*, Washington 1978.

ANALELE UNIVERSITĂŢII BUCUREŞTI, FIZICĂ, XXXIII, 1984, pag. 51—56

# PHOTOCONDUCTIVITY OF EVAPORATED CdSe THIN FILMS

**I. SPĂNULESCU, I. SECĂREANU**
Faculty of Physics, University of Bucharest *
**TALAL KHALASS**
Faculty of Science, University of October **
**N. BĂLŢĂŢEANU**
Central Institute of Physics, Măgurele—Bucharest***
**IBRAHIM ZAKĂR ABDI**
College of Science, University of Mosul ****

*Abstract.* In this paper the photoconductivity of the CdSe thin films obtained by thermal evaporation in vacuum in various conditions is studied. The effect of 7—10 MeV electron radiation on photoconduction properties of evaporated CdSe layers is also investigated.

## 1. Introduction

Semiconductor compounds of $A^2B^6$ type are often used in electronics and microelectronics, in optics, dosimetry of the ionised radiations etc. Among these, the CdSe thin films have been less studied, although they finds also many applications, especially in optoelectronics and energetics (solar cells) [1—5].

Optical and photoelectrical properties of the CdSe thin films have been, also, less studied [6, 7]. In the vorks of Bogdanovici and col. [7], and also in papers [8—10] is showed that the photocurrent value and the aspect of spectra characteristics of the photoconduction strongly depend on the preparation conditions, especially on the temperature at which the CdSe evaporation take place, and therefore on the stoichiometry of the CdSe thin films. No more data concerning photoconduction of the CdSe thin films in the mentioned papers are given.

In this paper we have proposed the study of the photoconductivity of the CdSe thin films obtained by thermal evaporation and condensation in vacuum in various experimental conditions.

## 2. Experimental

The CdSe thin films were obtained by thermal evaporation and condensation in vacuum at approximate pressure of $10^{-5}$ torr. For deposition of the films, it has been used supports of silica glass heated at temperature varying between 25° and 380° [11]. Layers with thickness between 0.06 and 3.5 μm were obtained. The evaporation temperatures were 700° and 760°C.

---

*, *** National Center of Physics, P. O. Box MG—11, Măgurele, Bucharest, Romania.

** University of October, Lattakia, Siria.

**** University of Mosul, Mosul, Iraq.

For elucidation of the photoconduction mechanism, CdSe thin films were subjectet to irradiation with 7 MeV and respective 10 MeV accelerated electrons.

Photoconduction spectra for CdSe policrystaline thin films have been raised by the aid of monochromator with Si prism of the type SPM-2. As a source of light a wolfram lamp was used. Film illumination was made frontal, in continuous regime. The distance between the indium electrodes ranged between 1—3 mm.The meassurements have been effected principally at room temperature ($T \simeq 293$ K).

## 3. **Results and discussion**

Our experiments showed that, according to optical absorption spectra, the photoconduction spectra of CdSe thin films strongly depend on the samples preparation conditions, especially on the support temperature (Fig. 1). As it is seen in figure 1 the photocurrent increases with support temperatura, reaching a maximum for $T_s \simeq 250°C$, after which it begins to decrease for $T_s \gtrsim 300°C$ (Fig. 1, curve 4). Practically, in all cases of the studied spectra one can put in evidence, at least, two big maxima, less or more marked, situated at $\lambda_1 \simeq 0.530—0.560$ μm and $\lambda_2 \simeq 0.675$ μm respectivelly (Fig. 1), corresponding to wavelengths smaller than $\lambda_g \simeq 0.73$ λm which is characteristic to the fundamental absorption edge.

Our experiments showed that the photoconduction spectra depend, also, on the temperature at which CdSe evaporation take place, hence on the samples stoichiometry. Since in the case of this compound, selenium is much more volatile than cadmium, for high evaporation temperatures (when CdSe dissociation appear), and for lower support temperatures, the CdSe thin films with a large quantity of nonstoichiometrical Cd atoms (that is in surplus) will grow. In these situation Se vacancies will introduce donor levels which partially compensate acceptor levels created of Cd vacancies or of crystal defects.

As Hauffe and Flint [12] showed, by heating CdSe in Cd vapours, the samples photoconduction increases, while, after heating CdSe in Se vapours (which can complete Se vacancies in the lattice) the photoconduction of the respective samples decreases. The larger concentration of the excess Cd atoms which result for $T_s \lesssim 250°C$ leads to a small value of the dark resistance of the CdSe thin films, as it was clarly observed in our experiments too. A partial reevaporation from the support of the nonstoichiometrical Cd atoms and the increasing of the film resistance take also place with the increase in the support temperature. The best (maximum) ratio between the resistance at ilumination and that at dark is obtained for $T_s$ varying between 200°C and 250°C (Fig. 1, curves 2 and 3) when the photocurrent has the maximum value too.

To verify the influence of the evaporation temperature, CdSe layers have been obtained at a constant support temperature, namely $T_s \simeq 150°C$, modifying only the source temperature. The obtained results are represented in figure 2. As it is seen from figure 2, for $T_{source} = 780°C$, when an intense CdSe dissociation take place, the photocurrent has a value practically two times greater than in the case of $T_{source} = 760°C$. This results must be also correlated with the 150°C support temperature when a large part of Se atoms (unreacted) will be reflected from support, while the nonstoichimetrical Cd atoms will be maintained, acheving a convenient (best) ratio between aceptor levels created from surplus Cd vacancies and defects, and the donor level given by Se vacancies.

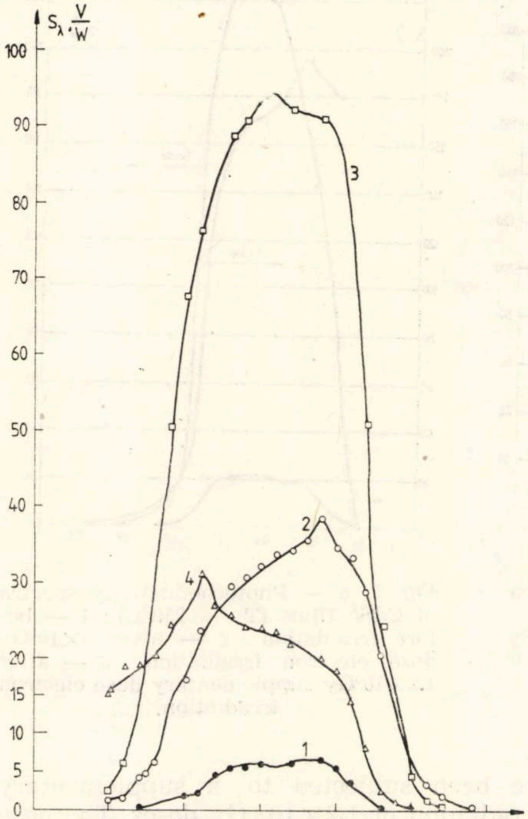

*Fig. 1.* Protoconductivity spectra of CdSe thin films : 1 — $T_s$ = 100°C ; 2 — $T_s$ = 200°C ; 3 — $T_s$ = 250°C ; 4 — $T_s$ = 300°C.

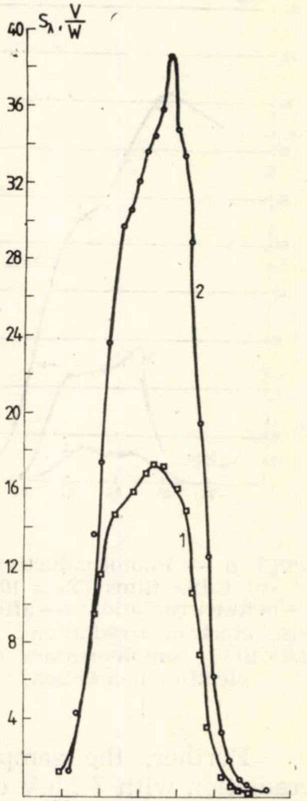

*Fig. 2.* Photoconductivity spectra of CdSe thin films $T_s$ = 150°C) : 1 — $T_{source}$ = = 760 C ; 2 — $T_{source}$ = 780°C.

The essential role of the nonstoichiometrical Cd atoms or the Se vacancies together with other recombination or trapping centers, in the kinetics, nature and spectral characteristics of the photocurrent for CdSe thin films can be confirmed by irradiation experiments on the respective layers with 7-10 MeV electron radiation. Thus, as it is seen from figure 3 a, b, curves 2, after irradiation with 10 MeV electron radiation of $5 \times 10^5$ Gy doses, a strong activation of the CdSe thin films take place, especially for the samples obtained at small support temperature ($T_s \simeq 100°C$), where photocurrent value is increased more than 25 times (Fig. 3 a, curve 2). During the irradiation with electron radiation, both a migration of the defects and impurity atoms (exces of Cd) and a partial completion of the Se vacancies take place in these samples therefore an improvement of the crystalline structure is observed.

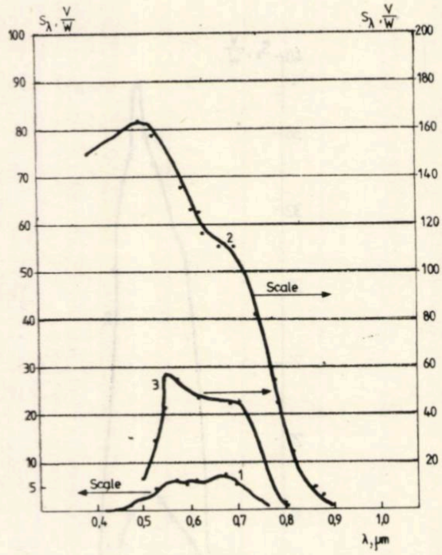

*Fig. 3, a* — Photoconductivity spectra of CdSe films ($T_s = 100$ C) : 1 — before irradiation; 2— after $5\times10^5$Gy dose electron irradiation ; 3 — after $1.2\times10^5$Gy supplementary dose electron irradiation.

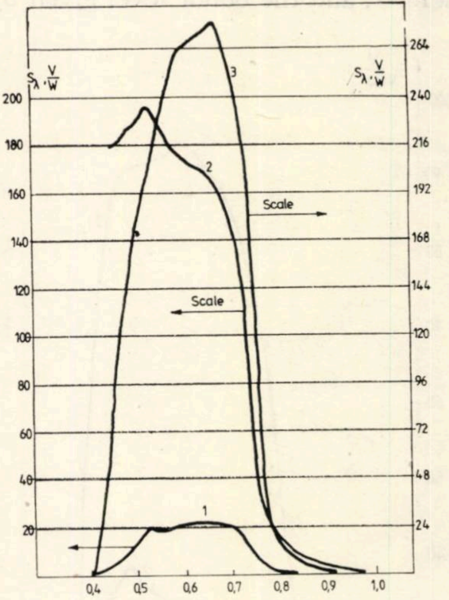

*Fig. 3, b* — Photoconductivity spectra of CdSe films ($T_s = 250$°C) : 1 — before irradiation ; 2 — after $5\times10^5$Gy dose electron irradiation ; 3 — after $1.2\times10^5$Gy supplementary dose electron irradiation.

Further, the samples have been subjected to a supplementary irradiation with 7 MeV electron radiation of $1.2\times10^5$ Gy doses. The dose and the energy value of the irradiation have been taken small to avoid the possibility to exceed the „optimal" threshold of the irradiation conditions, when the maximum photocurrent value is obtained. As is observed in figure 3, for certain samples a stronger increase in the photocurrent value took place, namely for layers obtained at high support temperatures (Fig. 3, b curve 3) while for the smaller support temperatures, a considerable decrease of the photocurrent is observed (Fig. 3, a, curve 3). These results present a much practical and theoretical importance, especially for the „nonthermal" photocurrent sensitivation, and the improvement of the solar cells parameters obtained with thin films of such semiconductor compounds.

In the CdSe photoconduction spectra a main maximum is observed at $\lambda \approx 0.7$ μm. which is associated with the exciton transitions corresponding to the fundamental absorbtion. The wide maximum from the region $\lambda = (0.5 \div 0.55)$ μm which been very intense and clear at high support temperatures after irradiation with electron radiation, can be put in correspondence with the transitions of excitonical type from the second subband of the valence band in the minimum of the conduction band of CdSe. For CdSe there are characteristic especially crystallites with hexagonal structure of the wurtzit type, for which the split of the valence band, due to the spin-orbit interaction, leads to the appearance of three subbands in the $\Gamma(\vec{k} = o)$ point (Fig. 4). In this case in the photocurrent spectra of the CdSe with hexagonal structure, three maxima must be observed, fact which is experimentaly obtained indeed (Fig. 5). The width and the intensities of these maxima will be influenced by the type and concentrations of impurities and defects which are present in the crystallites of the respective layers, depending on the preparation conditions and (or) treatment conditions (of activation of the respective layers) [6, 13, 14].

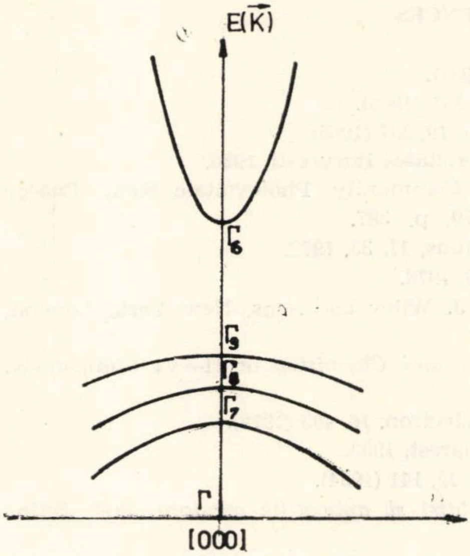

*Fig. 4.* The aspect of energetic bands in $\Gamma$ ($\vec{k}$ = 0) point of CdSe hexagonal crystals.

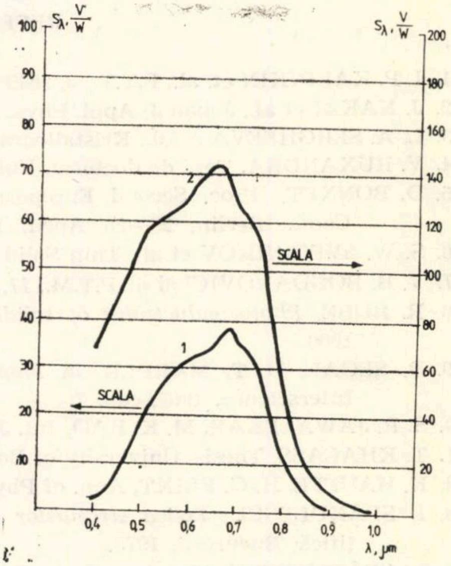

*Fig. 5* — Photoconductivity spectra of CdSe thin films ($T_s$ = 150°C) : 1 — before irradiation ; 2 —after $5 \times 10^5$Gy dose electron irradiation.

## 4. Conclusions

The photoconduction spectra of the CdSe thin films strongly depend on the samples preparation conditions, especially on the support temperature and on the temperature at which evaporation take place. The photocurrent for these layers increases with the support temperature, after which it begin to slowly decrease for $T \simeq$ 300 C. Also for the same condensation temperature it is observed the increase of the photocurrent with the increase of the evaporation temperature from $T_{ev} = 740°C$ to $T_{ev} \simeq 780°C$ when is obtained the maximum effect.

The nonstoichiometrical Cd atoms as the Se vacancies together with other capture centers in CdSe crystallites plays an essential role in the kinetics, the nature and in the spectral curve of the photocurrent for CdSe thin films. The irradiation with 10 MeV electron radiation of about $5\times10^5$ Gy doses leads to a strong sensitivation of the CdSe thin films especially for those obtained at small $T_s$ for which a spectacular increase of the photocurrent is observed.

The „nonthermal" sensitivization method of CdSe thin films by the irradiation with the optimal electron radiation doses is based on the migration effect of the defects and impurities atoms (excess of Cd), and also on the partial completion of the Se vacancies (donor levels). The effect is much strong for the layers obtained at high support temperatures and more reduced for the samples obtained at small support temperatures.

## REFERENCES

1. I. P. KALINKIN et. al., F.T.T., *3,* 2640 (1961).
2. J. NAKAI et al., Japan J. Appl. Phys., *4,* 545 (1965).
3. L. A. SERGHEEVA et al., Kristallografia *10,* 237 (1965).
4. V. RUXANDRA, Teză de doctorat, Universitatea București, 1980.
5. D. BONNET. Proc. Second European Community Photovoltaic Solar Energy Conf., Berlin, 23—26 April, 1979, p. 387.
6. S. W. SVECINIKOV et al., Thin Solid Films, *11.* 33, 1972.
7. V. B. BOGDANOVICI și al.,P.T.M., *11,* 76, 1973.
8. R. BUBE, *Photoconductivity of solids.* J. Wiley and sons, New York, London, 1960.
9. B. SEGAL, D. T. MARPLE, in *Physics and Chemistry* of II—VI Compounds, Interscience, 1967, cap. 7.
10. S. R. JAWALEKAR, M. K. RAO, Int. J. Electron, *16,* 483 (1979).
11. T. KHALASS, Thesis, University of Bucharest, 1983.
12. K. HAUFFE, H. G. FLINT, Ann. of Phys. *15,* 141 (1954).
13. I. SPÂNULESCU, *Fizica straturilor subțiri și aplicațiile acestora,* Edit. Științifică, București, 1975.
14. I. SPÂNULESCU, *Celule solare,* Edit. Științifică și Enciclopedică. București, 1983.

ANALELE UNIVERSITĂŢII BUCUREŞTI, FIZICĂ, XXXIII, 1984, pag. 57—64

# ON THE ELECTRICAL PROPERTIES OF SOME ORGANIC SEMICONDUCTORS

**I. CĂPLĂNUŞ**
Faculty of Physics, University of Bucharest *
**G. I. RUSU, C. H. BUDEANU**
Faculty of Physics, University "A. I. Cuza" of Jassy**

*Abstract.* In the paper the temperature dependence of the electrical conductivity for organic compounds conteining $Ni^{+2}$ and $Cd^{+2}$ in their molecules are studied. The general formulae of the investigated compoundsare presented in the Fig. 1. The substituents M, $R_1$ and $R_2$ are listed in the Table I.

For the investigations, the thin film samples deposited from solution have been used.

To obtain a stability of the film structure as well as a reproductibility of the electrical properties all samples have previously been submitted to a heat treatment.

The values of the thermal activation energy, calculated from the dependence $\ln \sigma = f\left(\frac{1}{T}\right)$ are correlated with chemical structure of the respective compounds.

The Seebeck coeficient is positive for all investigated samples.

## 1. Introduction

In recent years, the organic semiconducting compounds are intensively studied due to their interesting properties which are of theoretical, experimental and practical importance [1—7]. Particulary, the electrical properties of the organic semiconductors are very important for the applications of these materials in electronics, electrotechnics and other fields [1,5—7, 12—15].

The electrical conductivity and other properties such as thermoconduction, photoconductivity, luminiscence, etc. of the organic semiconductors are in chose connection with their molecular structure [1, 2, 12—14].

The experimental data on the electrical and thermoelectrical properties of the organic semiconductors are widespread in the literatura, but the reproductibility of these are not of a high order [1, 4, 15—17].

It is well known, that the electrical properties of semiconducting materials strongly depend on the preparation conductions of the investigated sample [1, 9, 11—14]. We remark, that in these papers experimental data were discussed with respect to a relative small number of samples obtained under different conductions. Thuse it is difficult to compare the results presented by different authors.

---

* National Center of Physics, Măgurele—Bucharest, P. O. Box 5211.
** Calea 23 August no. 11, Jassy — 6600.

Therefore, it is important to a establish a correlation between preparation technology, physical properties and molecular structure for a great number of organic semiconducting samples obtained under similar conductions.

In this paper are studied the electrical and thermoelectrical properties of some new organic compounds conteining $Ni^{+2}$ and $Cd^{+2}$ in their molecules.

## 2. Experimental procedure

The general formulae of the investigated compounds are presented in the Fig. 1. The substituents M,$R_1$ and $R_2$ are listed in the Table I

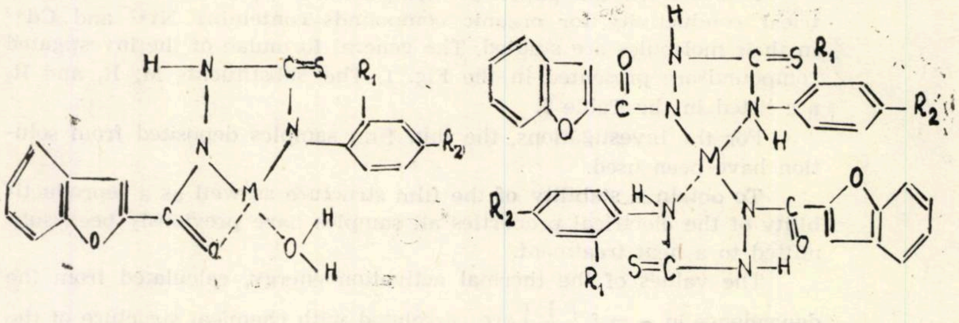

Formulae A Formulae B

*Fig. 1.* Chemical formulaes of the compounds

*TABLE I*

| Compound | General Chemical Formula | $R_1$ | $R_2$ |
|---|---|---|---|
| A.1 | A | — H | H |
| A.2 | A | — $CH_3$ | — H |
| A.3 | A | — H | — $OC_2H_5$ |
| B.1 | B | — H | — H |
| B.2 | B | — $CH_3$ | — H |
| B.3 | B | H | — $OC_2H_5$ |

In [5] the preparation method of the compounds and some their physical and chemical properties are described.

The investigated compounds are derivatives of the thiosemicharbazide complexed with Ni and Cd cations.

The molecular structure and purity of the substances were proved by both chemical analyses and spectral measurements.

All studied compounds are in the polycristalline form.

For the investigation of the electrical and thermoelectrical properties the thin films deposited from pyridine solutions of the compounds have been used.

The films were deposited onto glass substrates.

The experimental conditions for obtaining of samples with uniform thickness on the large substrate region have been established.

For the study of the temperature dependence of the electrical conductivity the surface cells were used. The silver electrodes were deposited onto substrate before the film preparation.

For low electric fields ($E < 10V^2/cm$) the experiments showed that the silver electrodes constitute the ohmic contacts.

The thickness of the films has been measured by an interferometric method and for investigated samples the obtained values were ranged between 0.15 and 2.85 μm. With a metallographic microscope the surface structure of the films has been investigated.

The experimental arrangement used for the electrical resistivity measurement and its temperature dependence is similar with that described in [6, 9].

For a large number of sample, the Seebeck coeficient has been measured using an experimental technique presented in [1, 10]. The temperature difference between the electrodes was of 10—15 k. The Seebeck voltage was determined by the standard d.c. potențiometric method.

## 3. Experimental results and discussion

The investigations revealed that the film structure depends on the its thickness. For smaller, values of the thickness ($d < 0.80$ μm) the films had generally a granular structure. The size of the film granules depends both on the preparation conditions and film thickness. A structure with greater granules was observed for high values of the thickness. For higher thicknesses the films are characterized by a continuous structure.

The increase of the thickness causes an increase in the electrical conductivity. For the thicknesses $d > 2$μm, the electrical conductivity of the films, $\sigma$ tends to a constant values which depends on the molecular structure of the compounds and preparation conditions of the films. A similar behaviour was also found for after organic semiconductors in thin films [6, 7, 12].

Experimentally, was established that studied compounds have analogous electrical properties.

In a series of previous paper [5—7, 12—14], we have showed that a stable structure and a reproductibility of electrical properties of organic semiconducting films may be obtained if the samples are submitted to a heat treatment. This treatment consist of several subsequent heatings and coolings in determined temperature domain $\Delta T$, characteristic for each compound. For the investigated compounds the values of $\Delta T$ are indicated in the Table II. The thermal stability of the studied substances in this temperature range was verified. The upper limits of $\Delta T$ are to 50—55 K smaller than the melting points of the respective compounds.

The temperature dependence of the electrical conductivity during the heat treatment has been studied.

It is known [6, 7, 9, 11—14], that these investigations give information about the structure modifications in the thin films during the heat treatment.

For this category of compounds, we suppose that the temperature dependence of the electrical conductivity obeys the well-known exponential low [1, 4, 6] :

$$\sigma = \sigma_0 \exp\left(-\frac{\Delta E}{2kT}\right).$$

where $\Delta E$ is thermal activation energy of electrical conduction and parameters $\sigma_0$ and $\Delta E$ do not dependent on the temperature.

Accordingly, for a numerous samples the aspect of the curves $\ln\sigma = f\left(\frac{10^3}{T}\right)$ was analysed.

Was established that aspect of these curves depend on molecular structure of the compounds, preparation conditions of the films and film thickness.

For two samples of compounds A. 1 and B. 3 the dependences $\ln\sigma = f\left(\frac{10^3}{T}\right)$ are represented in Fig. 2 and 3. Some characteristic parameters of respective samples are presented in the Table II.

In the mentioned figures each sample was subjected to two subsequent heatings and coolings.

It can be observed, that the investigated films have a similar behaviour in respect to the dependence $\ln\sigma = f\left(\frac{10^3}{T}\right)$ during heat treatment.

At the first heating, a decrease in electrical conductivity $\sigma$ with increasing temperature has been observed in the lower temperature range.

This fact is probably due to the elimination of the adsorbed and absorbed gases, as well as of certain impurities introduced in the films during their preparation. Also, some changes in the film structure occur.

It is known that these factors strongly influenced the electrical properties of the anorganic and organic semiconductors in thin films [1, 9, 11].

Starting with a temperature $T_c$, characteristic for each compound is noticed to increase with temperature, the dependences $\ln\sigma = f\left(\frac{10^3}{T}\right)$ being typical curves for semiconducting materials.

At first cooling, the electrical conductivity decreases but without returning to its initial value. In this case the curve show two distinct portions : one with a smaller slope, within the low temperature range, where the compounds are characterized by an extrinsec conduction, and other within the higher temperature range, where we consider that the compounds possess an intrinsec conduction.

Continuing the series of heatings and coolings, curves similar to those of first cooling are obtained coming nearer to each other so that

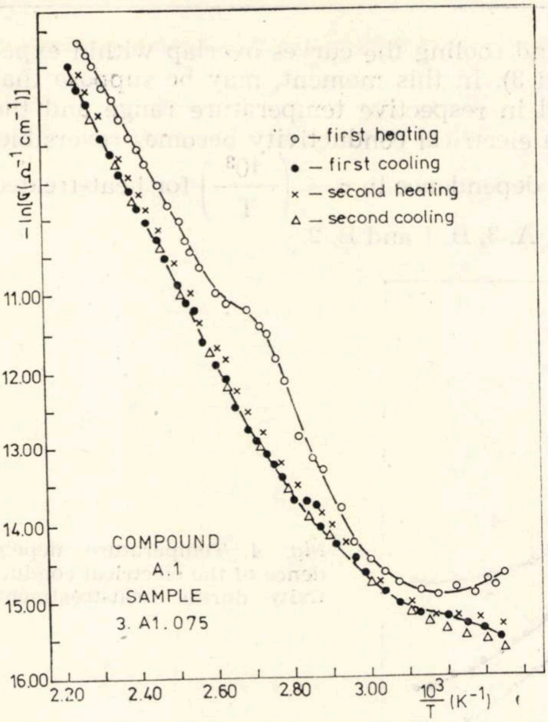

*Fig. 2.* Temperature dependence the electrical conductivity during heat-treatment for the compound $A_1$

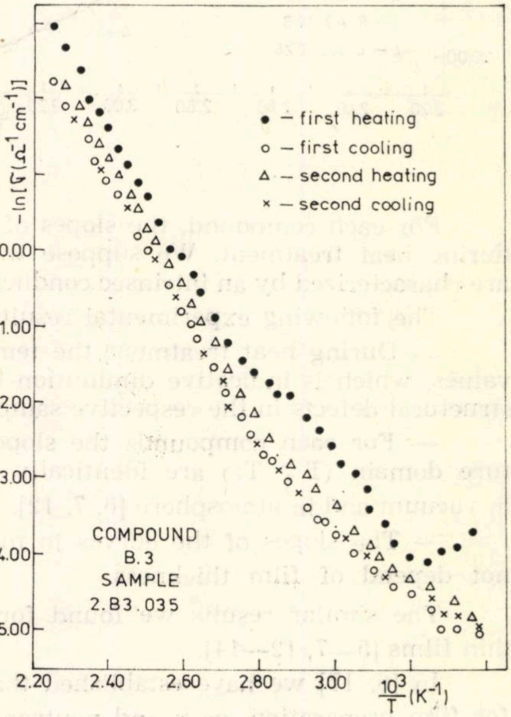

*Fig. 3.* Temperature dependence of the electrical conductivity during heat-treatment for the compound B.3.

after 2—4 succesive heatings and cooling the curves overlap within experimental errors (sec. Fig. 2 and 3). In this moment, may be suppose that the film structure is stabilized in respective temperature range and the temperature dependence of the electrical conductivity becomes reversible.

In Fig. 4 are presented the dependence $\ln \sigma = \left(\frac{10^3}{T}\right)$ for heat-treated samples of the compounds A. 2, A. 3, B. 1 and B. 2.

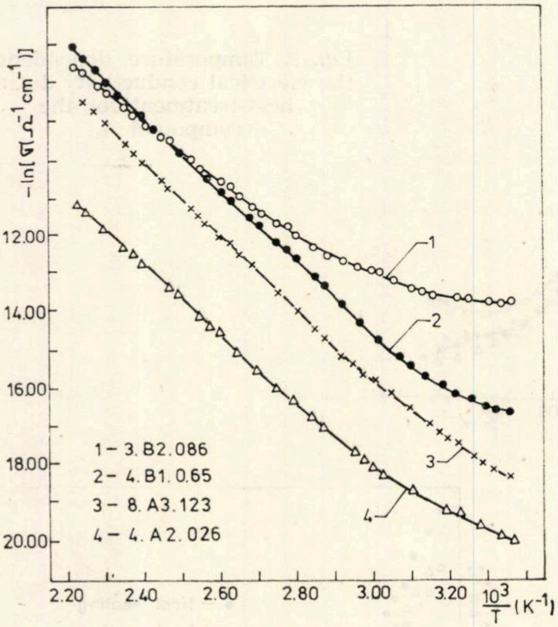

*Fig. 4* Temperature dependence of the electrical conductivity during heat-treatment.

For each compound, the slopes of the curves for $T > T_c$ are parallel during heat treatment. We suppose that within this temperature range are characterized by an intrinsec conduction.

The following experimental results justifie this hypothesis :

— During heat treatment the temperatures $T_c$ shift towards lower values, which is indicative diminution of the impurity concentration and structural defects in the respective sample.

— For each compounds the slopes of the curves in this temperature domain ($T > T_c$) are identically if the measurements are carried in vacuum and in atmosphere [6, 7, 12].

— The slopes of the curves in mentioned temperature ranges does not depend of film thickness.

The similar results we found for other organic semiconductors in thin films [5—7, 12—14].

In [6, 17] we have established that the change of the solvent used for film preparation, or γ and neutron irradiation of the samples determine a modification of the dependence $\ln \sigma = f\left(\frac{10^3}{T}\right)$ in the extrinsec conduction domain.

For many organic semiconductors, there is a good agreement between the values of activation energy $\Delta E$ calculated from the curves $\ln \sigma = f\left(\frac{10^3}{T}\right)$ in the intrinsec conduction domain and those determined from the scattering reflexion spectra of the compound [12, 13, 17].

For investigated compounds the values of $\Delta E$ calculated from temperature dependences of the electrical conductivity in the intrinsic conduction range are given in the Table III (The calculations were performed taking into account the mentioned formula for temperature dependence of the $\sigma$).

*Table II*

| SAMPLE | $\Delta T$ (K) | $T_c$ (K) | $\sigma_s$ ($\Omega^{-1}.cm^{-1}$) | $\Delta E_i$ (eV) | $\Delta E$ (eV) |
|---|---|---|---|---|---|
| 3.A1.075 | 297—450 | 356 | $5.08\times10^{-4}$ | 0.45 | 1.80 |
| 4.A2.026 | 297—447 | 352 | $1.30\times10^{-5}$ | 0.60 | 1.60 |
| 8.A3.123 | 300—450 | 360 | $2.06\times10^{-3}$ | 0.65 | 1.70 |
| 4.B1.065 | 297—445 | 312 | $8.80\times10^{-3}$ | 0.65 | 1.60 |
| 3.B2.086 | 297—465 | 360 | $5.52\times10^{-3}$ | 0.40 | 1.30 |
| 2.B3.035 | 394—450 | 358 | $9.25\times10^{-3}$ | 0.35 | 1.45 |

*Table III*

| Compound | SAMPLE | d (μm) | $\sigma_c$ ($\Omega^{-1}.cm^{-1}$) | $\sigma_t$ ($\Omega^{-1}.cm^{-1}$) |
|---|---|---|---|---|
| A.1. | 3.A1.075 | 0.75 | $4.54\times10^{-7}$ | $1.50\times10^{-7}$ |
| A.2 | 4.A2.026 | 0.26 | $1.80\times10^{-8}$ | $1.93\times10^{-9}$ |
| A.3 | 8.A3.123 | 1.23 | $8.25\times10^{-8}$ | $8.90\times10^{-9}$ |
| B.1 | 4.B1.065 | 0.65 | $7.72\times10^{-7}$ | $5.80\times10^{-8}$ |
| B.2 | 3.B2.086 | 0.86 | $2.70\times10^{-6}$ | $1.28\times10^{-6}$ |
| B.3 | 2.B3.035 | 0.35 | $1.22\times10^{-6}$ | $1.67\times10^{-7}$ |

Also, in the Tables II and III there indicated the following characteristic parameters of the studied samples : d-the film thickness, $\sigma_c$ — electrical conductivity at room temperature before heat treatment, $\sigma_t$ — electrical conductivity at room temperature after heat treatment, $\Delta T$ — temperature range within which the heat treatment has been performed, $T_c$ characteristic temperature for heat-treated samples, $\sigma_s$ — the value of electrical conductivity for upper limit of $\Delta T$, $\Delta E_i$ — the activation energy for lower temperatures.

From the analysisi of our results, it can assumed that the differences in electrical properties of studied substances are determined mainly by their chemical structure.

Particularly, the values of $\Delta E$ depend on this structure. As a first remark we must mention that $\Delta E$ have smaller values for the compounds with extended conjugation.

It is observed, that the compounds conteining $Cd^{+2}$ in their molecules are characterized by smaller values of $\Delta E$. This fact is caused by increase of the conjugation system in respective compounds.

The insertion in the molecule of the $-CH_3$ substituente determines a decrease in the activation energy. Also, the substition of the $-CH_3$ group by $-OC_2H_5$ group causes an increase of the activation energy.

These results are in agreement with the experimental data obtained for many organic semiconductors [1, 5—7, 12—14, 16, 17].

The sign of the Seebeck coefficient is positive for all investigated samples, i.e. these have a p-type electrical conduction. The experiments show that in the temperature range 300—400 K, the seebeck coefficient slowly depends on the temperature.

## REFERENCES

1. F. GUTMANN, L. LYONS, *Organiceshie poluprovodniki*, Mir, Moskva, 1970.
2. * * * *Recent Advances in the Quantum Theory of Polymers*, Springer Verlag, Berlin—Heidelberg—New York, 1980.
3. A. SUSSMAN, J. Appl. Phys. *38*, 2538 (1967).
4. M. LAMPERT, P. MARK, *Curent Injection in Solids*, Academic Press, New-York, London, 1970.
5. G. I. RUSU, V. SUNEL, C. H. BUDEANU, An. ştiinţ. Univ. Iaşi, secţ. Ib, XX/2, 119 (1979).
6. G. I. RUSU, V. SUNEL, M. GHEORGHIU, An. ştiinţ. Univ. Iaşi, secţ. Ib, T XXVII, 57 (1977).
7. G. I. RUSU, M. OLENIK. I. ZUGRĂVESCU. Makrom Cheme, 175, 1651 (1974).
8. C. H. BUDEANU şi colab., An. ştiinţ. Univ. Iaşi, secţ. Ic, XIX/1, 59 (1973).
9. G. I. RUSU,Phys. Stat. Sol. (a), 4, 775 (1971), An. ştiinţ. Univ. Iaşi, Ib, XV/2, 149, (1969), Candidatkia Dissertatsia (Univ. Leningrad, 1969).
10. V. M. GLAZOV, A. S. OHOTIN, R. P. BOROVIKOVA, *Metodj issledovaniya termoelektricheshih svoisv poluprovodnikov*, Atomizdat, Moskva, 1969.
11. * * * *Handbook of Thin Films Technology*, Edited by L. I. Maissel and Glang, McGraw Hill Book Comp., 1970.
12. G. I. RUSU, Scientific sesion „Progress in Physics", Craiova, 29 sept. — 1 oct. 1983.
13. M. SPIRATOR, G. I. RUSU, A. AIRINEI, Angew. Makromolek. Chem. 107, 33, (1982).
14. M. SPIRATOS, G. I. RUSU, A. AIRINEI, A. CIOBANU, Polymer, Bulletin, 6, 243 (1982).
15. M. VODENICHAROVA, Phys, Stat. Sol. (a), *28*, 263 (1975).
16. I. GOLOVCENCO, G. I. RUSU, M. RUSU, V. ŞTEFAN, An. ştiinţ. Univ. Iaşi, secţ. Ib, T. XVII/1, 61 (1971), An. ştiinţ. Univ. Iaşi, secţ. Ib, T. XVIII/1, 9, (1972).
17. G. I. RUSU, A. AIRINEI, M. SPIRATOS, G. SINGUREL, An. ştiinţ. Univ. Iaşi, secţ. Ib, T. XXIV, 103, (1980).

ANALELE UNIVERSITĂŢII BUCUREŞTI, FIZICĂ, XXXIII, 1984, pag. 65—70

# THE g VALUES OF $Er^{3+}$ ION IN YAG

**C. CIUCU**
Faculty of Physics, University of Bucharest *
**S. GEORGESCU**
Institute for Physics and Technology for Radiation Devices**

*Abstract.* The wave functions for the fundamental Stark level of $Er^{3+}$ in yttrium aluminum garnet have been determined. With this wavefunctions the g factors were calculated, paying attention to the relative orientation of the quantifications axes of the crystal field and those of the gyromagnetic tensor.

## 1. Introduction

The $Er^{3+}$ ion (configuration $4f^{11}$) has a spectral line scheme with many luminescente lines which was enough studied in the literature. So it was obtained stimulated emision from the levels $^4S_{3/2}$ $^4I_{11/2}$ and $^4I_{31/2}$ /1, 2, 3/. In the last years it was payed attention on the $Y_3Al_5O_{12}$ (YAG) dopped with $Er^{3+}$ due to two factors : i) it was obtained stimulated emision at the wavelenght $\lambda \simeq 3\mu m$ (transition $^4I_{11/2} \rightarrow {^4I_{13/2}}$ ), and ii) it was possible to use great concentrations of the active ion till the complecte substitution of $Y^{3+}$ ion with $Er^{3+}$. The lower emision threshold was obtained for a concentration of the active ion from about 33% (atomic procents about yttrium).

The lower leve of the $Er^{3+}$ ion is $^4I_{15/2}$. This level is well izolated from the next one ($^4I_{13/2}$) at about 6000 $cm^{-1}$. This fact makes possible that the „J-mixing" effects to be neglected. Also the term $^4I$ has the largest contribution at the level $^4I_{15/2}$ so that in a first aproximation Russell-Saunders coupling can be used.

These asumptions make possible an easy approach of the lower level in the crystal field and to obtained the wavefunctions of this level.

In this paper we tried to make a conection bettwen the crystal field parameters ($B^k_q$) and the gyromagnetic factors. To do this using the crystal field parameters $B^k_q$ from the literature and making the diagonalization of the crystal field interaction matrix we obtained the wavefunctions for the Stark levels. With these wavefunctions we calculated the gyromagnetic factors $g_x$, $g_y$, $g_z$. It was payed attention to the relative orientation of the quantifications axes of the crystal field and those of the gyromagnetic tensor. To do this we have to obtain the rotation matrix for $J = 15/2$.

---

* National Center of Physics, P. O. Box 5211, Măgurele, Bucharest.
** National Center of Physics, P. O. Box 5206, Măgurele, Bucharest.

## 2. Crystal field splitting

The $Er^{3+}$ ion substitutes the $Y^{3+}$ ion in the crystal lattice. The point group symmetry at this site is $D_2$. For this symmetry the double-valued representations of $R_3$ are descomposed according to :

$$D_J \rightarrow (J + 1/2)\,\Gamma_5 \tag{1}$$

so in our case the level ${}^4I_{15/2}$ is splitting in eight Kramers doublets.

In the case of rare earth ions the crystal field interaction is weak as compared with the „free ion" interactions and can be considered as a perturbation on the free ion levels.

A free ion level with total angular momentum J is (2J + 1) — fold degenerate. This degeneracy is removed by the crystal field interaction. The eigenvectors for the Kramers doublets can be written as linear combinations of $|JM_j>$ eingefunctions

$$| \Psi_j > = \sum_i a^j_r \,|\, JM_i > \qquad \text{and} \qquad | \widetilde{\Psi} > = T \,|\, \Psi_j > \; j = \overline{1,8} \tag{2}$$

where T is time inversal operator. In our case considering the Russell-Saunders coupling as a good aproximation and neglecting the „J-mixing" we can write for the lowest doublet

$$| \Psi > = \sum_i a_i \,|\, {}^4I_{15/2}M_i > \tag{3}$$

Due to the temporal inversion, in the absence of the magnetic field, we take eight values for the $M_i$; 13/2, 9/2, 5/2, 1/2, —3/2, —7/2, —11/2, —15/2. To obtain the $a_i$ we have to diagonalize the 8 × 8 energetic matrix of the crystal field in the basis $| M >$.

The crystal field potential for $D_2$ symmetry written with the ireducible tensorial operators for ${}^4f$ elecrons has nine terms

$$V = B^2_0C^2_0 + B^2_2(C^2_2 + C^2_{-2}) + B^4_0C^4_0 + B^4_2(C^4_2 + C^4_{-2}) + B^4_4(C^4_4 + C^4_{-4}) + \\ + B^6_0C^6_0 + B^6_2(C^6_2 + C^6_{-2}) + B^6_4(C^6_4 + C^6_{-4}) + B^6_6(C^6_6 + C^6_{-6}) \tag{4}$$

where the quantities $B^k_q$ are considered as simple coefficents of expansion to be determined empirically from the experimenta data ; $C^k_q$ are ireducible tensor operators of rank k being conected to the spherical harmonics by :

$$C^k_q = \sqrt{\frac{4\pi}{2k+1}}\, Y^q_k \tag{5}$$

In the case of $l^N$ configuration the matrix elements of the cristal field are given by :

$$< l^N WUSLJM_J \,|\, B^k_qC^k_q \,|\, l^N W'U'S'L'J'M'_J > = B^k_q \delta(S,S')(-1)^l(-1)^{J-M} \\ (-1)^{S+L'+J+k}(2l+1)\begin{pmatrix} J & k & J' \\ -M_J & q & M'_J \end{pmatrix}\begin{pmatrix} l & k & l \\ 0 & 0 & 0 \end{pmatrix}\begin{Bmatrix} J & J' & k \\ L' & L & S \end{Bmatrix}[J, J']^{1/2} < l^N WUSL \,\|\, U^{(k)} \,\| \\ \| \, l^N W'U'S'L' > \tag{6}$$

where it was used the notation $[J] = (2J+1)$. The integral W and U label the irreducible representations of $R_7$ and $G_2$, respectively, necessary to specify the state of the configuration $f^N$ ; $U^{(k)}$ are unitary operators expressed by Racah /4/

$$U_q^{(k)} = \sum_{l=1}^{N} (u_q^{(k)})_i \tag{7}$$

where the sumation is made after the interest electrons of rare earth, and

$$< nl \parallel u^{(k)} \parallel n'l' > = \delta(n.n')\delta(l,l') \tag{8}$$

In our case $l = 3$, $S = 3/2$, $L = L' = 6$, $J = J' = 15/2$, $W = W' = (111)$, $U = U' = (20)$ and $k = 2, 4, 6$.

The evaluation of the matrix elements (4) was made using the 3—j and 6—j symbols of the tables /5/ and the double reduced matrix elements from those of Nielson and Koster /6/.

The matrix elements (6) can be handled more easy with the folowing notation

$$< f^N\,(111)\,(20)\,{}^4I_{15/2}\,M_j \mid B_q^k C_q^k \mid f^N\,(111)\,(20)\,{}^4I_{15/2}\,M_J' > =$$

$$= - B_q^k \begin{pmatrix} \frac{15}{2} & k & \frac{15}{2} \\ -M_J & q & M_J \end{pmatrix} h\,(k) \tag{9}$$

where h (k) represented the remaining factors in the expression (6) and

$$\begin{aligned} h\,(2) &= 0.643803 \\ h\,(4) &= 0.\ 685094 \\ h\,(6) &= 1.800032 \end{aligned} \tag{10}$$

Using the$B_q^k$ parameters obtained by Morrison, Wortman and Karayianis /7/ we obtained for the fundamental Stark level the following wavefunctions ;

$$|\psi > = 0.59051|13/2 > + 0.01172|9/2 > - 0.53507|5/2 > - 0.11730|1/2 > - 0.42641|-3/2 > - 0.17346|-7/2 > + 0.22190|-11/2 > + 0.29991\ | -15/2 >$$

$$|\,\widetilde{\Psi} > = T\,|\,\Psi > \tag{11}$$

In acordance with the usal convection /8/ for the case of twofold symmetry $|\psi>$ is used as the wavefunction which contain $M = 1/2$.

It must be notied that the functions are written in the quantification system of the crystal field which does not coincide with those of the gjromagnetic tensor.

## 3. Magnetic field interaction

In the case of an ion with an odd number of electrons located in a crystal with a symmetry lower than a cubic one, the crystal field rise the degenerancy till Kramers doublets. This remaining degenerancy is removed by the magnetic field, which is odd at temporal inversion.

A first aproximation (and a good one) for the interaction between an ion with many electrons and the magnetic field is ;

$$H_m = \sum_i \beta\vec{H}(\vec{l}_i + 2\vec{s}_i = \beta\vec{H}\,\vec{L} + 2\vec{S}) \qquad (12)$$

where $\beta$ in Bohr's magneton.

In our case $H_m \langle\langle V$ and it can be considered as a perturbation of crystal field levels. Since we expressed by (11) the functions for the lower Stark level through $| SLJM>$ states and because $\vec{L} + 2\vec{S}$ is vector as $\vec{J}$ we can write (in the absence of „J-mixing")

$$<SLJM \mid L_j + 2S_j \mid SLJM'> = g_L <SLJM \mid J_j \mid SLJM'> \qquad (13)$$

where $j = x, y, z$ and $g_L$ is the Landé factor which has the formula

$$g_L = 1 + \frac{J(J+1) - L(L+1) + S(S+1)}{2J(J+1)} \qquad (14)$$

As we said before, the axis for local symmetry (x′, y′, z′) don't coincide with those of the gyromagnetic tensor,
If a rotation $R^{15/2}(0. - \pi/2, \pi)$ is performed, the x′, y′, z′ axis of the crystal field will coincide with x, y, z axis of gyromagnetic tensor. The elements of this matrix are calculated using Wigner's formula /9/

$$R_J(\alpha, \beta, \gamma)_{MM''} = e^{-iM\alpha} e^{-iM''\gamma} x$$

$$x \sum_t (-1)^t \frac{\sqrt{(J+M)!(J-M)!(J+M')!(J-M')!}}{(J+M-t)!(J-M'-t)!(t-M+M')!t!} \left(\cos\frac{\beta}{2}\right)^{2J-2t-M'+M}$$

$$\left(\sin\frac{\beta}{2}\right)^{2t+M'-M} \qquad (15)$$

Due to temporal inversion this matrix is reduced to 8×8. Once the rotation is made the wavefunctions obtained for the ground state are ;
$|\varphi> = 0.30668 \mid 13/2> + 0.07864 \mid 9/2> ,- 0.21313 \mid 1/2> + 0.12790 \mid$
$\mid -3/2 > + 0.75460 \mid -7/2> + 0.18082 \mid -11/2> - 0.54841 \mid$
$\mid -15/2>$ (16
and

$$\mid \tilde{\varphi} > = T \mid \varphi >$$

With the wavefunctions (16) we could calculate the g factors. For H paralel with z axis, we have

$$g_z = 2 < \varphi \mid L_z + 2S_z \mid \varphi > = 2g_{\perp} \sum_i \mid a_i' \mid^2 |M_i> \qquad (17)$$

$a'_i$ being the coefficents obtained after the rotation was made and are given in (16). We obtain

$$g_z = -10.29$$

In the case of axial symmetry, g has the expression /10/

$$g_\perp = g_L (J + 1/2)$$

and only the state $M = \pm 1/2$ has a contribution to $g_\perp$

For a lower symmetry than the axial one $g_x$ and $g_y$ are defined. In this case, all M states that differ by 2 contribute to $g_x$ and$_y$g (the z axismbeing of order two), Rubins /11/ gives compact expressions for $g_x$ and $g_y$. The symmetry of these expressions as reffered to interchange of x and y axis it is recongnisable from the expressions given below

$$g^x_y = -g_L \Big(\pm a'_1 a'_8 \sqrt{4J(J+1) - 13\cdot15} + a'_1 a'_7 \sqrt{4J(J+1) - 11\cdot13} \pm$$

$$\pm a'_2 a'_7 \sqrt{4J(J+1) - 9\cdot11} + a'_2 a'_6 \sqrt{4J(J+1) - 7\cdot9} \pm$$

$$\pm a'_3 a'_6 \sqrt{4J(J+1) - 5\cdot7} + a'_3 a'_5 \sqrt{4J(J+1) - 3\cdot5} \pm$$

$$\pm a'_4 a'_5 \sqrt{4J(J+1) - 3} + \frac{1}{2} a'^2_4 \sqrt{4J(J+1) + 1}$$

Thus, for forming the rotation matrix $R^{(15/2)}_{MM'}$ $(\alpha,\beta,\gamma)$the interchange of x and y axis leads to the factor $e^{i\pi/2\Delta M}$ with $\Delta M$ even, which lies in multiplying the lines of the lines of this matrix alternatively with 1 and —1. Thus $a'_i \rightarrow -a'_i$ for in odd which according to (18) leads to interchange of $g_x$ and $g_y$.

In our case we obtained

$$| g_x | = 1\cdot60$$

$$| g_y | = 3\cdot26$$

## 4. **Conclusions**

The separation of the full Hamiltonian into two parts ; „free ion" and „crystal field" gives the possibility to solve the problem of rare earth ion embeded in a crystal.

Using the set of crystal field parameters publised by Morrison Wortmann and Karayianis /7/ and making two simplifications (LS coupling and negect of J-mixing) the wavefunctions for the ground level were obtained. These wavefunctions were used to calculate the g factors. The g factors calculated with the parameters /7/ are in reasonable agreement with the measured ones.

In practice, these resultates may have to be modified slightly because of such effects as the coupling of different J manifolds by the crystal field /12/, the covalent reduction of the orbital moment /13, 14/ and the dynamical lowering of the symmetry through lattice vibrations /15/.

## REFERENCES

1. Z. J. KISS, R. C. DUNCAN, Proc. IRE, 50, 1532 (1962).
2. E. SNITZER, R. WOODCOCK, Appl. Phis. Lett. 6, 45 (1965).
3. L. F. JOHNSON, I. E. GENSIC, L. G. Van UITERT Appl. Phys. Lett. 7, 127, (1965).
4. G. RACH, Phis. Rev., 76, 1352, (1949).
5. M. ROTENBERG, R. BIVINS, M. METROPOLIS and J. WOOTEN Jr., The 3—j and 6—j Symbols, Technology Press, M.I.T. (1959).
6. C. W. NIELSON, G. F. KOSTER, *Spectroscopic Coefficents for* $p^n$, $d^n$ *and* $f^n$ *Configurations* (The MIT Press, Cambridge Mass. 1963).
7. C. A. MORRISON, D. E. WORTMANN, N. KARAYIANIS, J. Phis. C. Solid State Phys. 9, L1, 91, (1976).
8. K. H. HELLWEGE Ann. Phis. 4, 95, (1949).
9. A. R. EDMONDS, *Angular Momentum in Quantum Mechanics,* Princeton Univ. Press, Princeton, New Jersey, 1960.
10. B. G. WYBOURNE, *Spectroscopic Properties of Rare Earths,* Wiley, New York, 1965.
11. R. S. RUBINS, Phys. Rev. B1, 139 (1970).
12. R. J. ELLIOTT, K. Â. H. STEVENS, Proc. Roy. Soc. (London), A218 553, (1953).
13. B. BLEANEY, Proc. Roy. Soc. (London) A277, 289 (1964).
14. J. D. AXE, G. BURNS, Phys. Rev. 152, 331 (1966).
15. M. INOUE, Phys. Rev. Lett. 11, 196 (1963).

ANALELE UNIVERSITĂŢII BUCUREŞTI, FIZICĂ, XXXIII, 1984, pag. 71—75

# LA TRANSMISSION DE LA LUMIÈRE À TRAVERS DES FILMS DE POLYÉTHYLÈNE

**E. BARNA, LIVIA MARIA IONESCU, M. COJOCARU**
Faculté de Physique, Univérsité de Bucarest *

*Résumé.* La transmission de la lumière polarisée à travers des films de polyéthylène cristallisé depand de la grandeur, de la forme, de l'orientation et de l'arrangement des cristallites. Les mesures de la transmission $T_{+}$, $T_{//}$ et $T_{\times}$ en function de la direction de polarisation de la lumière incidente donnent des informations permettant d'établir des hypothèses sur les procès qui mènent à la modification de la transmission.

## 1. Introduction

La transmission de la lumière polarisée à travers des films permet d'obtenir rapidement des information suffisamment précises sur la structure confirmées et par d'autres techniques experimentales. Lorsqu'on envisage une corrélation entre la valeur de l'intensité de la lumière transmise, determinée expérimentalement, et la valeur théoretique, il faut tenir compte que la première inclue et l'intensité de la lumière diffusée dans l'ouverture de la cellule du photomètre [1] :

$$I_{exp} = \left[ I_{THÉORIQUE} + \int_{\Omega=0}^{2\pi} \int_{\theta=0}^{\theta m} I_{DIF}(\theta,\omega) \sin\theta \, d\theta \, d\Omega / I_{INCIDENT} \right] \qquad 1.$$

où $\theta_m$ est l'angle maximum de l'ouverture du photomètre.

En pratique, la contribution du facteur de diffusion de l'intensité effectivement transmise peut être, très importante.

En function de la géomètrie de la ligne de mesure, caractérisée par les angles formeés entre l'analyseur, le polariseur et l'axe optique de l'échantillon avec une direction de référance, on peut déterminer les valeurs particulières suivantes de l'intensité transmise (fig. 1) :

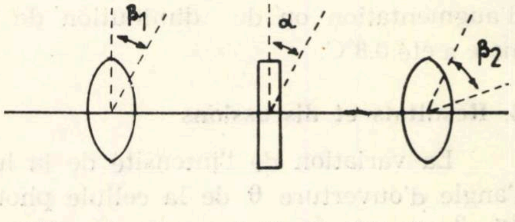

*Fig. 1.* Les angles formés par l'analyseur, le polariseur et l'axe optique de l'échantillon avec une direction de référence.

---

* Centre National de Physique, Măgurele, Bucarest B. P. 5211 Roumanie.

$$T_{\parallel} \text{ lorsque } \beta_1 = \beta_2 = 0$$

$$T_{+} \text{ lorsque } \beta_1 = 0,\ \beta_2 = 90^\circ$$

$$T_{\times} \text{ lorsque } \beta_1 = 45^\circ,\ \beta_2 = -45^\circ$$

Dans le cas de la transmission de la lumière polariseé $T_+$ à travers des systèmes polymères cristallisés (croïssance bidimensionnelle) on obtient l'expression suivante pour l'intensité effectivement transmise [3] :

$$T_+ = \pi N_s\, k^2 \Delta_s^2 A_s^2 \cdot \cos^2 \rho_2\, d^2 \int_{a=0}^{\theta=\theta max} [2-2J_0(\omega) - \omega J_1(\omega)]^2 (\sin\theta/_{\omega^4}) d\theta \qquad 2.$$

Dans cette relation $A_s = 4\pi R^2$ (R-le rayon des sphérulites) et $\Delta_s$ la birefringence des suférulites. La quantité $\rho_2$ a l'expression suivante :

$$\cos\varphi_2 = \cos\theta/_{[\cos^2\theta + \sin^2\theta \sin^2\omega]^{1/2}} \qquad 3.$$

d est l'épaisseur des sphérulites, $J_0$ et $J_1$ sont des fonctions Bessel d'ordre zero et de premier ordre repectivement, et d'argument $\omega = kR \cdot \sin\theta$.

Cette intégrale peut être effectuée par voie numérique, en obtenant généralement un accord satisfaisant avec les resultats experimentaux.

Quant-à la valeur $T_{\parallel}$, un calcul rigureux [2] mène à l'expression suivante :

$$T_{\parallel} = 1 + q^2 \left[ S_1(0)^2 + 2qS_1(0) + \frac{1}{I_0} \cdot \int_0^{\theta m} J_\nu(\theta) \sin\theta \, d\theta \right] \qquad 4.$$

ou $q = \dfrac{Nd^2\lambda^2}{2\pi}$ et N est le nombre de centres de diffusion dans 1 $cm^3$, et $S_1(0)$ le coefficient de diffusion à l'angle $\theta = 0$.

## 2. Technique experimentale

Les expériences ont été effectuées sur une ligne optique ayant pour source un laser HeNe. L'intensité de la lumière effectivement transmise est enregistrée automatiquement, l'ouverture maximale etant 4°. Les films de polyéthylène ont été obtenus par l'évaporation lente des solutions, et soumis ultérieurement aux traitements thermique et mecaniques adéquants.

L'épaisseur des films étudiés a été comprise entre 0,4—1,0 mm.

Les mesures de la transmission de la lumière en function de la température ont été effectueés sur des échantillons placés dans la cellule du spectrophotomètre Perkin Elmer. En régime isotherme la température a été contrôlée avec une precision de 0,2°C, alors qu'en régime d'augmentation ou de diminution de la température, l'erreur maximale a été 0,8°C.

## 3. Résultats et discussions

La variation de l'intensité de la lumière transmise en function de l'angle d'ouverture θ de la cellule photomètrique est présentée dans la fig. 2.

On observe un accord satisfaisant entre les résultats expérimentaux et la courbe théoretique. Les petites différences qui apparaissent pourtant entre les deux courbes peuvent être expliqueés, soit par l'apparition de certains défauts dans les sphérulites, acompagniée d'une distribution des dimensions des sphérulites (courbe expérimentale), soit par l'apparition de la croissance tridimensionnelle et l'emission de la diffussion multiple de la lumière aux petits angles [4] (courbe theoretique).

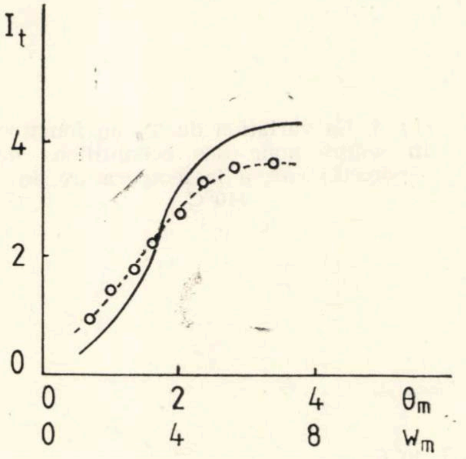

*Fig. 2.* La variation de l'intensité de la lumière effectivement transmise en fonction de l'ouverture de la cellule du photomètre. O : points expérimentaux ; ——— : courbe théorique.

Le procès de cristallisation des échantillons de polyéthylène orientés ou nonorientés a été observé pendant la cristallisation isothèrme. On peut voir ainsi (fig 3, 4 et 5) la modification des intensités $T_{//}$, $T_{+}$ et $T_{\times}$ pour les echantillons initialement chauffés à 150°C et mentenus ensuite à la température de cristallisation $t_c = 110°$ C. La deminution de la température a été assez rapide pour qu'on puisse afirmer que les modifications de l'intensité effectivement transmise sont dûes aux modifications de structure, provoquées par la cristallisation isothèrme à la température mentionnée.

Les coefficients d'extension des échantillons orientés sont :

$$\alpha_1 = 1,\ \alpha_2 = 1{,}5,\ \alpha_3 = 2{,}2.$$

On observe que pour les échantillons nonorientés ou avec une faible orientation, $T_{//}$ passe par une valeur minime pendant le processus de cristallisation. L'expression de l'intensité transmise indique une diminution pour celle-ci alors que le nombre de sphérulites à l'orientation aléatoire augmmente (le cas des échantillons nonorientés), ce qui est confirmé expérimentalement.

Pour les échantillons à haut degré d'orientation, la croissance des cristallites se produit notamment suivant la direction d'orientation, ce qui mène à une augmentation du paramètre d'ordre dans le système. D'après la relation (4), dans les échantillons à haut degré d'extension ($\alpha = 2{,}2$) a lieu une faible diminution de la quantité $T_{//}$ . Les trois courbes expérimentales montrent qu'à la fin du processus de croissance des sphérulites, a lieu une augmentation de l'intensité effectivement transmise. Ce phénomène peut être expliqué par la prépondérence du dernier terme de la relation (1) qui devient comparable au $\Delta I$ théorique.

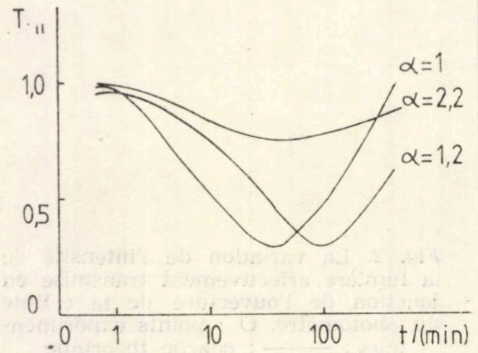

*Fig. 3.* La variation de $T_{\parallel}$ en fonction du temps pour des échantillons de polyéthylène, à la température de 110°C.

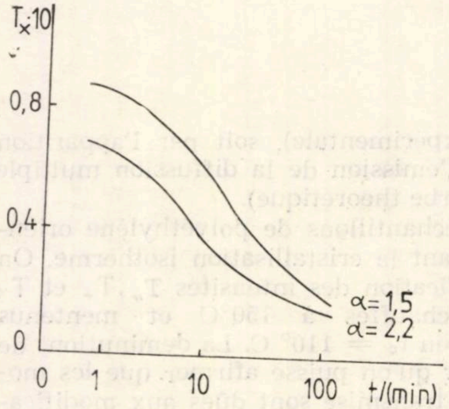

*Fig. 4.* La variation de $T_x$ en fonction du temps pour des échantillons de polyéthylène, à la température de 110°C.

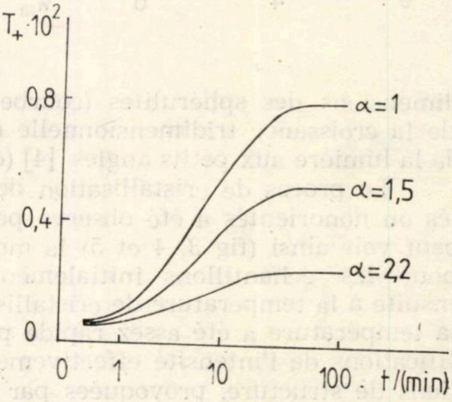

*Fig. 5.* La variation du $T_+$ en fonction du temps pour des échantillons de polyéthylène, à la température de 110°C.

La variation de l'intensité $T_+$ pendant le procès de cristallisation est bien différente de celle constanteé pour l'intensité $T_{\parallel}$.

Pour des échantillons nonorientés ($\alpha = 1$), l'analyse théorique montre une transmission nulle ; l'augmentation constateé expérimentalement pour l'intensité effectivement transmise doit être atribuée seulement à l'augmentation de l'intensité de la lumière diffusée aux petits angles par les formations sphérulitiques en croissance, intensité qui est captée dans l'ouverture de la cellule du photomètre. L'augmentation moins importante de l'intensité effectivement transmise dans les échantillons orientés est probablement une conséquence de la faible tendence de croissance sphérulitique des echantillons orientés [5].

Les variations de l'intensité $T_\times$ présentent aussi certaines particularités. Pour les échantillons nonorientés ($\alpha = 1$), la courbe $T_\times$ s'identifie avec la courbe $T_+$. Pour les échantillons à grandes extensions, $T_\times$ résulte de la biréfringence des regions amorphes orientées. La transmission initiale devient maxime lorsque l'élongation augmente, et diminue pendant le procès de cristallisation. La diminution de l'intensité transmise avec l'augmentation du degré de cristallisation peut être considérée comme une conséquence de la disparition de la lumière diffusée du champ du photomètre alors que les sphérulites augmentent. Cet effet est considérablement diminué pour des élongations plus importantes.

Dans la fig. 6, nous avons représenté la variation de la lumière transmise avec la température de l'échantillon, pour une vitesse de variation de la température 4°/min.

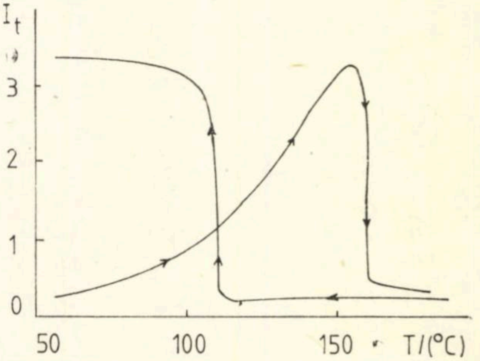

*Fig. 6.* La variation de l'intensité de la lumière effectivement transmise en fonction de la température pour un échantillon de polyéthylène chauffé à une vitesse de 4°/min.

Entre 65° et 152° C l'intensité de la lumière augmente ; dans cet intérvale de température a lieu la modification de la structure interne des sphérulites, se produit la recristallisation et le changement de leurs dimensions. A 152°C le polymère passe à l'état fondu, les derniers noyaux restant visible jusqu'à la temperature de 160°C, quand se produit l'extinction. Lorsqu'on refroidit l'échantillon, la transmission apparaît à 110°C, la pente de variation étant pourtant très rapide.

En examinant la variation de l'intensité de la lumière effectivement transmise, nous avons mis en évidence les différentes étapes du procès de cristallisation dan les polymères, sans arriver toutefois à donner une information précise sur le degré de cristallisation.

## REFERENCES

1. S. CLOUGH, J. J. VAN AARTSEN, R. STEIN, J. Appl. Phys. *36*, 3072, (1965).
2. R. STEIN, P. R. WILSON, J. Appl. Phys, *33*, 1914, (1962).
3. H. C. VAN DE HULST, *Light scattering by Small Particles*, Wiley, New York, section 4.4, 4.5.
4. R. STEIN, T. HOTTA, J. Appl. Phys. *35*, 2237, (1964).
5. J. T. COBERSTEIN, R. STEIN, J. Polym. Sci. $A_2$, *18*, 199 (1980).

ANALELE UNIVERSITĂŢII BUCUREŞTI, FIZICĂ, XXXIII, 1984, pag. 77—84

# ETUDE DE LA POLYDISPERSITE DES COPOLYMERES POLYSTYRENE-POLYMETHACRYLATE DE METHYLE (PS—PMMA)

LIVIA MARIA IONESCU, M. COJOCARU

Faculté de Physique, Université de Bucarest *

*Résumé.* Les copolymères PS—PMMA ont été caractérisés du point de vue des masses moléculaires et des rayons de giration, par diffusion de la lumière et ultracentrifugation de sédimentation.

La présence du copolymère dans les échantillons a été établie qualitativement.

L'analyse a montré qu'il s'agit prépondérément de copolymères statistiques, présentant une assez grande hétérogénéité en composition et un haut degré d'inhomogénéité d'après les masses moléculaires.

## 1. Introduction

Bien que les copolymères de méthacrylate de méthyle avec le styrène et d'autres dérivés vinyliques trouvent des applications très importantes, notamment dans l'industrie des peintures et vernis, une étude exhaustive de cette classe de composés macromoléculaires est loin d'être réalisée /1—5/.

Un premier problème qui se pose après la copolymérisation c'est de connaître avec précision le type de copolymère qui en résulte (statistique, séquencé ou greffé).

Il est nécessaire aussi de caractériser la dispersité en composition et en masse.

L'analyse complexe des résultats de la diffusion de la lumière et de l'ultracentrifugation appliquées aux solutions de copolymères, peut apporter des réponses à ces questions.

## 2. La polydispersité en composition des copolymères

La théorie développée par Bushuk et Benoît sur la diffusion de la lumière par les solutions de copolymères /6,7/ peut être appliquée à l'étude quantitative de la dispersion en composition des copolymères.

Des mesures de la masse moléculaire apparente $M_{ap}$ en trois solvants différents permettront ainsi de déterminer la masse moléculaire réelle $\overline{M}_w$

---

* Centre National de Physique, Măgurele—Bucarest, B. P. 5211, Romania.

du copolymère et les masses moléculaires $\overline{M}_w^A$ et $\overline{M}_w^B$ des deux composants A et B, d'après la relation :

$$M_{ap} = \frac{\nu_A \nu_B}{\nu_0^2}\overline{M}_w + \frac{\nu_A(\nu_A - \nu_B)}{\nu_0^2} w \overline{M}_w^A + \frac{\nu_B(\nu_B - \nu_A)}{\nu_0^2}(1\ w)\overline{M}_w^B \tag{1}$$

ou bien :

$$M_{ap} = \overline{M}_w + 2\frac{\nu_A \nu_B}{\nu_0} P + \left(\frac{\nu_A - \nu_B}{\nu_0}\right)^2 Q \tag{2}$$

Dans ces relations $\nu_0, \nu_A, \nu_B$ sont les incréments d'indice de réfraction du copolymère et respectivement ceux de ses deux composants A et B. La composition globale en poids du copolymère en motifs de type A est définie par :

$$w = \frac{c_A}{c} = \frac{c_A}{c_A + c_B}$$

oú c est la concentration du copolymère et $c_A, c_B$ les concentrations respectives des unités A et B.

Les paramètres d'homogénéité en composition P et Q ont les expressions suivantes :

$$P = \frac{1}{2}\left[(1 - w)(\overline{M}_w - \overline{M}_w^B) - w(\overline{M}_w - \overline{M}_w^A)\right] \tag{3}$$

$$Q = w(1 - w)(\overline{M}_w^A + \overline{M}_w^B - \overline{M}_w) \tag{4}$$

La relation (1) montre que pour homogénéité en composition $(\nu_A = \nu_B = \nu_0)$ on obtient $M_{ap} = \overline{M}_w$. Alors l'écart du rapport $M_{ap}/\overline{M}_w$ par rapport à l'unité est lié au degré d'hétérogénéité en composition. En représentant la variation du rapport $M_{ap}/\overline{M}_w$ en fonction de $(\nu_A - \nu_B)/\nu_0$, on obtient une parabole à axe vertical, qui permet de déterminer $\overline{M}_w$, P et Q (ou $\overline{M}_w, \overline{M}_w^A, \overline{M}_w^B$).

Plus adéquat que Q, le paramètre $Q/M_w$ caractérise la polydispersité en composition du copolymère.

Bushuk et Benoît introduisent aussi la quantité $Q/Q_{max}$ comme mesure quantitative de la dispersité en composition des copolymères, l'indice maximum de la dispersité en composition de la chaîne étant : $Q_{max}/\overline{M}_w = w(1 - w)$.

Benoît et Wippler /8/, en étudiant la dépendence angulaire de l'intensité diffusée par les solutions de copolymères, ont établi des relations qui permettent de déterminer expérimentalement, par diffusion de la lumière, les dimensions des pelotes statistiques.

Dans le cadre de cette analyse de la structure d'un copolymère, le rayon de giration apparent de la molécule de copolymère $R_{ap}$ peut être exprimé par la relation :

$$M_{ap}\overline{R}^2_{ap} = \frac{\overline{M}_w^A \overline{R}_A^2}{w} y^2 + \frac{\overline{M}_w^B \overline{R}_B^2}{1 - w}(1 - y)^2 + 2\frac{\overline{M}_w^{AB} \overline{R}_{AB}^2}{w(1 - w)} y(1 - y) \tag{5}$$

où

$$\overline{M}_w^{AB} = \frac{1}{2}\left[\overline{M}_w - w\overline{M}_w^{A} - (1-w)\,\overline{M}_w^{B}\right]$$

et y w $\nu_A/\nu_0$.

Dans la relation (5), $R_A$ et $R_B$ sont respectivement les rayons de giration des motifs A et des motifs B autour de leurs centres de masses respectifs. La quantité $R_{AB}$ est définie par la relation gènérale : $\overline{R}^2_{AB} = \frac{1}{2}\,(\overline{R}^2_A + \overline{R}^2_B + 1)$ $\overline{1^2}$ étant l'écart quadratique moyen entre les deux centres de messes.

On peut donc déterminer $\overline{R^2_A}, \overline{R^2_B}$ et $\overline{1^2}$ par des mesures de diffusion de la lumière en trois solvants différents. Si l'on admet que ces grandeurs géométriques ne dépendent pas de la nature du solvant utilisé, la courbe représentative $M_{ap}\,\overline{R^2_{ap}}$ en fonction de y est, également ici, une parabole à axe vertical, et dont la concavité est donnée par le coefficient de $y^2$. L'analyse de la fonction (5) indique que la parabole obtenue expérimentalement a une concavité positive lorsque le copolymère polydispersé est statistique et négative lorsqu'il est, au contraire, séquencé.

On conaît aussi l'influence de la polydispersité en masse sur le rayon de giration apparent. Les variations de ce paramètre en fonction du facteur y et des indices de polydispersité ont été explicités /9, 10/.

### 3. La polydispersité d'après la mase moléculaire

Une autre possibilité d'analyse et d'identification du type de copolymère est offerte par l'étude de la distribution d'après la masse moléculaire :

$$q_w(M) = \frac{dw}{dM} \qquad (6)$$

oú dw représente la fraction en poids des macromolécules ayant la masse moléculaire comprise entre M et M + dM, ou bien d'après la constante de sédimentation :

$$q_w(S) = \frac{dw}{dS} \qquad (7)$$

dw étant dans ce dernier cas la fraction en poids des macromolécules dont la constante de sédimentation se situe dans l'intervale S, S + dS.

Dans le cas d'un copolymère séquencé, la courbe de distribution d'après la masse moléculaire est unimodale, tandis que pour un mélange de deux homopolymères elle est bimodale.

Une des méthodes les plus efficientes d'analyse de la polymolécularité c'est de dissoudre le polymère et de le placer dans le champ de pesanteur artificielle de forte amplitude de l'ultracentrifugeuse /11/. Lorsque les deux composants d'un copolymère formé à partir de deux types de monomères, ont des densités différentes, la fonction de distribution présentera soit deux maximums, soit un seul maximum, selon les deux cas suivants : la réaction de copolymérisation n'a pas eu lieu, respectivement la copolymérisation s'est développée en conditions de conversion totale.

## 4. Technique expérimentale

Deux copolymères polystyrène-polyméthacrylate de méthyle : PS-PMMA F 14 et PS-PMMA F 15, même ainsi que leurs prélèvements ont été étudiés par diffusion de la lumière et ultracentrifugation.

Les mesures de diffusion de la lumière sur les solutions de ces copolymères en cinq solvants différents ont été effectuées à l'aide d'un photogoniodiffusomètre construit à IFTAR-Bucarest. Les techniques habituelles ont été utilisées pour la préparation et la purification des solutions et des solvants.

L'incrément d'indice de réfraction a été déterminé à l'aide d'un réfractomètre Pulfrich PR 2.

Les mesures de degré de polymolécularité ont été effectuées sur une ultracentrifugeuse MOM—3170/b. Les photogrammes ainsi obtenues ont été analysées d'après la méthodologie habituelle.

## 5. Résultats et discussions

La mase moléculaire moyenne apparente $M_{ap}$ et le rayon de giration apparent $R_{ap}$ du copolymère PS-PMMA F 14 (la fraction en poids du PS dans le copolymère $w = 0{,}42$ ; conversion 53%) ont été déterminés pour methyléthylcétone, dioxane, tétrachlorure de carbone, toluène et benzène. Ces résultats sont rassemblés dans le tableau 1.

*Tableau 1*

| Solvant | $M_{ap} \cdot 10^{-5}$ | $\left(\overline{R^2_{ap}}\right)^{\frac{1}{2}}$ (Å) |
|---|---|---|
| Methyléthylcétone | 3,1 | 780 |
| Dioxane | 3,2 | 800 |
| Tétrachlorure de carbone | 3,5 | 870 |
| Toluène | 3,7 | 910 |
| Benzène | 3,8 | 940 |

Les masses moléculaires $\overline{M}_w$, $\overline{M}^A_W$, $\overline{M}^B_W$ de l'équation (1) ont été obtenues en résolvant un système de trois équations pour les valeurs de $M_{ap}$ obtenues en trois solvants diffrénts (dioxane, toluène, tétrachlorure de carbone). Ces valeurs sont présentées dans le tableau 2.

*Tableau 2*

| PS—PMMA | $\overline{M}_w \cdot 10^{-5}$ | $\overline{M}^A_w \cdot 10^{-5}$ | $\overline{M}^B_w \cdot 10^{-5}$ | $\frac{P}{\overline{M}_w}$ | $\frac{Q}{\overline{M}_w}$ | $\frac{Q}{Q_{max}}$ |
|---|---|---|---|---|---|---|
| F 14 | 3,1 | 1,8 | 4,0 | —0,24 | 0,23 | 0,30 |

Les paramètres P et Q, calculés à partir des relations (3) et (4), ont été utilisés pour déterminer les rapports $P/\overline{M}_w$, $Q/\overline{M}_w$ et $Q/Q_{max}$ dont les valeurs sont inclues dans le tableau 2.

Les résultats de l'analyse de la dispersité en composition du copolymère PS-PMMA F 14 sont illustrés dans la figure 1, représentant la variation de la quantité $M_{ap}/\overline{M}_w$ en fonction du rapport $(\nu^A - \nu^B)/\nu_0$. Sur la même figure ont été tracées les variations théoriques pour $P = O$ et $Q/\overline{M}_w$ donné.

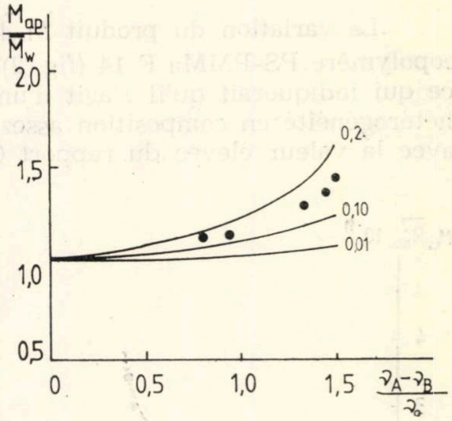

*Fig. 1.* La variation du rapport $M_{ap}/\overline{M}_w$ en fonction du rapport $(\nu_A - \nu_B)/\nu_0$, pour le copolymère PS—PMMA F 14. ● : points expérimentaux ; ——— : courbes théoriques obtenues pour $P=0$ et $Q/\overline{M}_w$ donné. Les valeurs $Q/\overline{M}_w$ sont indiquées sur les courbes respectives.

La valeur élevée du rapport $P/\overline{M}_w$ (considéré comme une mesure de la polydispersité en masse) indique un produit hétérogène par rapport aux masses moléculaires.

Le rapport $Q/Q_{max}$, caractérisant la polydispersité en composition, a une valeur élevée (0,30), ce qui indiquerait une hétérogénéité en composition du copolymère.

On observe que pour ce copolymère, avec une dispersité en composition assez élevée, l'inégalité qui fait la distinction entre un copolymère et un mélange d'homopolymères :

$$\overline{M}_w > w\overline{M}_w^A + (1-w)\overline{M}_w^B$$

est vérifiée, ce qui prouve qui l'échantillon contient du copolymère. L'inégalité a un caractère pur qualitatif, ne donnant aucune information quant-à la quantité de copolymère ou de mélange d'homopolymères dans l'échantillon. Nous pensons que dans le cas du copolymère PS-PMMA F 14 il s'agit pluôt d'un mélange de copolymère et des deux homopolymères A et B, avec la prépondérence nette du copolymère.

Les mesures de diffusion de la lumière ont été utilisées également pour déterminer les paramètres structuraux nécessaires pour l'identification du type de copolymère et pour sa caractérisation quant-à l'hétéogénéité en composition.

Les valeurs $R_{ap}$ mesuré en trois solvants différants ont été utilisées pour calculer les paramètres structuraux $R_A$, $R_B$, et $R_{AB}$ de l'équation (5) en résolvent un système de trois équations. Ont été déterminées ainsi les valeurs suivantes :

$$\left(\overline{R_A^2}\right)^{\frac{1}{2}} = 970\ A^0 \qquad \left(\overline{R_B^2}\right)^{\frac{1}{2}} = 700\ A^0 \qquad \left(\overline{R_{AB}^2}\right)^{\frac{1}{2}} = 840\ A^0$$

La variation du produit $M_{ap}\overline{R_{ap}^2}$ en fonction du paramètre y pour le copolymère PS-PMMa F 14 (fig. 2) est une parabole à concavité positive, ce qui indiquerait qu'il s'agit d'un copolymère statistique, affecté d'une hétérogénéité en composition assez élevée. Cette conclusion est en acord avec la valeur élevée du rapport $Q/Q_{max}$.

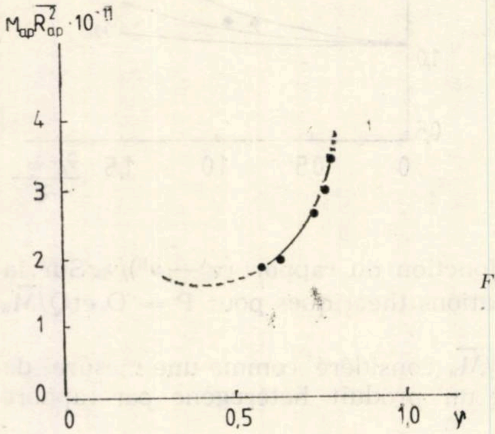

*Fig.* 2. La variation du produit $M_{ap}\ R_{ap}^2$ en fonction du paramètre y, pour le copolymère PS—PMMA F 14.

La polydispersité en masse des copolymères PS-PMMA F 14 et PS-PMMA F 15 a été caractérisée à l'aide des courbes respectives de distribution en masse (fig. 3 et 4). On peut observer ainsi que les deux fonctions de distribution d'après la constante de sédimentation sont unimodales et assez larges, ce qui prouve que de la réaction de copolymérisation ont résulté composés macromoléculaires polydispersés par rapport à la masse moléculaire. Les valeurs de la masse moléculaire des copolymères étudiés, présentées dans le tableau 3, sont de l'ordre de centaines des milliers, spécifiques donc pour les hauts polymères.

*Tableau 3*

| Copolymère | $\overline{M}_w \cdot 10^{-5}$ | $\overline{M}_{S[\eta]} \cdot 10^{-5}$ | $U = \frac{\overline{M}_w}{\overline{M}_{S[\eta]}} - 1$ |
|---|---|---|---|
| PS—PMMA F 14 | 3,1 | 2,0 | 0,55 |
| PS—PMMA F 15 | 4,8 | 3,4 | 0,41 |

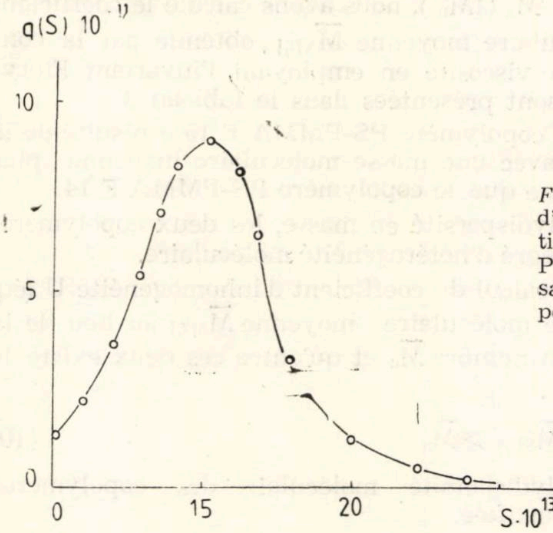

*Fig. 3.* La fonction de distribution d'après la constante de sédimentation, pour le copolymère PS—PMMA F 14, 20 min. après la réalisation de la vitesse de régime et pour une concentration c = 0,7 g/dl.

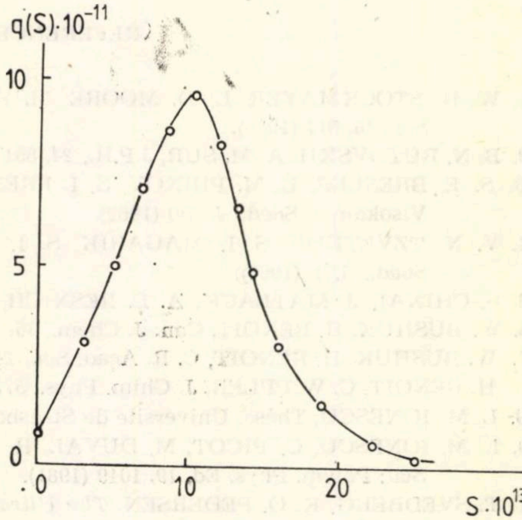

*Fig. 4.* La fonction de distribution d'après la constante de sédimentation, pour le copolymère PS—PMMA F 15, 20 min. après la réalisation de la vitesse de régime et pour une concentration c = 0,7 g/dl.

Le degré d'inhomogénéité moléculaire peut être évalué, tant qualitativement, à l'aide des fonctions de distribution d'après la constante de sédimentation, que quantitativement, en utilisant le coefficient d'inhomogénéité Schulz /12/ :

$$U = \frac{\overline{M}_w}{\overline{M}_n} - 1 \tag{9}$$

Puisque le degré d'inhomogénéité moléculaire peut être exprimé par le rapport de n'importe quelles deux masses moléculaires consécutives

/13/ (et donc pas spécialement $\overline{M}_w$ et $\overline{M}_n$ ), nous avons calculé le coefficient U à l'aide de la masse moléculaire moyenne $\overline{M}_{S[\eta]}$ , obtenue par la constante de sédimentation et la viscosité en employant l'invariant Flory-Mandelkern /14/.Ces valeurs sont présentées dans le tableau 3.

La conclusion est que le copolymère PS-PMMA F 15 a résulté de la réaction de copolymèrisation avec une masse moléculaire moyenne plus élevée et un peu plus homogène que le copolymère PS-PMMA F 14.

En ce qui concerne la polydispersité en masse, les deux copolymères sont caractérisés par un haut degré d'hétérogénéité moléculaire.

Etant donné que dans le calcul du coefficient d'inhomogénéité U (éq. 9) nous avons utilisé la masse moléculaire moyenne $\overline{M}_{S[\eta]}$ au lieu de la masse moléculaire moyenne en nombre $\overline{M}_n$ et qu'entre ces deux existe la relation :

$$\overline{M}_{S[\eta]} > \overline{M}_n \qquad (10)$$

la conclusion quant-à la polydispersité moléculaire des copolymères étudiés apparait tout-à fait justifiée.

## REFERENCES

1. W. H. STOCKMAYER, L. D. MOORE, M. FIXMAN, B. N. EPSTEIN. J. Polym. Sci., *16,* 517 (1955).
2. B. N. RUTOVSKII, A. M. SUR, J.P.H., *24,* 851 (1951).
3. S. E. BRESLER, L. M. PIRKOV, S. I. FRENKEL, S. I. KLENIN, L. A. LAIUS, Visokomol. Soed., *4,* 250 (1962).
4. V. N. TZVETKOV, S. I. MAGARIK, S. I. KLENIN, V. E. ESKIN, Visokomol. Soed., *5,* 1 (1963).
5. S. CHINAI, J. MATLACK, A. E. RESNICH, J. Polym. Sci.. *17,* 391 (1955).
6. W. BUSHUK, H. BENOIT, Can. J. Chem., *36,* 1616 (1958).
7. W. BUSHUK, H. BENOIT, C. R. Acad. Sci., *246,* 3167 (1958).
8. H. BENOIT, C. WIPPLER, J. Chim. Phys., 57, 524 (1960).
9. L. M. IONESCU, Thèse, Université de Strasbourg (1976).
10. L. M. IONESCU, C. PICOT, M. DUVAL, R. DUPLESSIX, H. BENOIT, J. Polym Sci : Polym. Phys. Ed. *19,* 1019 (1981).
11. T. SVEDBERG, K. O. PEDERSEN, *The Ultracentrifuge,* Clarendon Press, Oxford, Londres (1940).
12. G. V. SCHULZ, Z. Phys. Chem., *43,* 25 (1939).
13. S. I. FRENKEL, *Vedenie v statisticeskuiu teoriu polimerizatii,* Nauka, Moskva (1965).
14. P. J. FLORY, *Principles of Polymer Chemistry,* Cornell Univ. Press, Ithaca, New York (1953).

ANALELE UNIVERSITĂȚII BUCUREȘTI, FIZICĂ, XXXIII, 1984, pag. 85—92

# THE LATERAL INHOMOGENEITY OF THE MANTLE BENEATH THE VRANCEA ZONE

ȘT. LASCU, ELENA DECU, M. CIOBANU

Faculty of Phys:cs, University of Bucharest *

*Abstract.* Using the residuals of the registered travel-time at the seismological stations in Romania we came to the conclusion of a regional variation in the crust and upper mantle structure beneath these stations. Out of the magnitudes and travel-time residuals of the earthquakes occurring in Vrancea there resulted some of their azymuthal anomalies that lead to the conclusion of existence of some lateral nonhomogeneites of the upper mantle beneath the Vrancea zone.

## 1. Introduction

The lateral nonhomogeneity of the uppermantle was pointed out by more authors for many seismic zone too. Generally, such nonhomogeneities were showed from the travel-time anomalies. Utsu [12], taking into account the travel time anomalies in Japonese region considers that these are to be caused mostly by the existence of a high velocity zone of the Pacific lithospheric plate descending beneath the Asian continent. Kebeasy [5] were showed anomalies of the P travel-time in the Northern and Eastern parts of the Circum Pacific region and suggested two models of velocity structure for this zone. Recently, Maki [8, 9] showed the existence of some systematic variations of the travel-time residuals at the Japonese seismological stations, both for teleseismic and for local shallow earthquakes.

For the Vrancea seismic zone lateral anomalies of the travel-time of intermediate earthquales occurring in this zone showed [6, 7]. The cause of these are considered to be lithospheric subplate descending, the one that is responsable for producing of the earthquakes too, and that provokes lateral nonhomogeneities in the velocity structure. In the present study new proofs concerning the lateral nonhomogeneities of the upper mantle in and around the Vrancea zone are brought using the P travel-time anomalies registered at the Romanian seismological stations as well as the magnitudes residuals which have been obtained at the seismological stations that registered the earthquakes occurring in this zone.

## 2. Materials and method

The travel-time data were compiled from EDR, for earthquakes occurred during four years from 1979 to 1982, these ones having the quality that within the catalogues the epicentral distance is calculated to a hundredth of degree, and P arrivals were read to a tenth of a second. From these catalogues we compiled the special coordinates and origin times of the eartquakes, the epicentral distances, the azymuths, the P and PKP arrivals, together with their residuals as well as magnitudes.

---

* National Center of Physics, Măgurele, Bucharest, P. O. Box 5211.

Only the registers of the earthquakes within at least 15 seismological stations and having their coordinates determined with an unimportant error were kept. Out of more than six thousand travel-time data have been used those ones representing more than 100 P travel times registered by each seismological stations, having residuals $|r| \leqslant 5$ seconds. The mean residuals have been calculated for each station and for each P and PKP wave type, the results are given in the table 1, were we noticed by n the number of observing data that were used, and by R the reliability, defined by the same method as Jeffreys [4] and Herrin [2] but for residuals $|r| \leqslant 5$ seconds.

*Table 1*

| Seismological stations | P | | | PKP | |
|---|---|---|---|---|---|
| | n | δt, s | R | n | δt, s |
| MLR | 1256 | 1.45±1.46 | 0.64 | 230 | 1.22±1.10 |
| VRI | 549 | 0.72±1.62 | 0.66 | 71 | 1.53±1.36 |
| CMP | 409 | 0.83±1.73 | 0.68 | 57 | 1.06±2.13 |
| SSR | 287 | 0.22±1.30 | 0.80 | 62 | 1.39±1.46 |
| DEV | 243 | 0.88±1.43 | 0.74 | 72 | 1.04±2.36 |
| CJR | 146 | 0.79±1.47 | 0.73 | 56 | 0.28±1.63 |
| TIM | 134 | 0.86±1.38 | 0.63 | | |
| BUC | 124 | 1.38±1.45 | 0.58 | | |
| CFR | 117 | —0.80±1.86 | 0.75 | | |
| DRA | 105 | 0.46±1.75 | 0.73 | | |

For the ten stations having enough observing data the P residuals hystograms were represented, their examples being presented in Figs 1 and 2 for MLR and VRI stations because the most existing data for these ones.

The registered data for four intermediate earthquakes occurred in the Vrancea zone in the period between 1979—1981 (see table 2) and having magnitudes more than 4.7 and which were registered by a larger number of seismological stations were taken from EDR too.

*Table 2*

| Date | Origin time | φ deg. | λ deg. | Depth. km. | Mag. |
|---|---|---|---|---|---|
| 1979 V 31 | 07 20 06.30 | +45.552 | +26.327 | 120 | 5.1 |
| 1979 IX 11 | 15 36 54.20 | +45.560 | +26.298 | 154 | 5.1 |
| 1980 I 14 | 15 07 54.00 | +45.791 | +26.620 | 143 | 4.7 |
| 1981 VII 18 | 00 02 59.46 | +45.618 | +26.340 | 152 | 5.0 |

### 3. The regional variation of the travel-time residuals

As it is seen in table 1 mean P residuals present pronounced variation at the seismological stations for which these have been calculated, leading to the conclusion of a difference between the crust structure and that of upper mantle beneath the respective seismological stations. A difference of about a second was marked between the two means of the residuals at MLR and VRI stations, stations that were installed near to the Vrancea seismic zone and for which near values of the two measures were expected. Taking into account the fact that the observing data for two stations is large enough, and the residuals hystograms — as shown in Figs 1 and 2 — show distributions close to a gaussian curve, the respective values can be taken as reliable measures. The R values are close

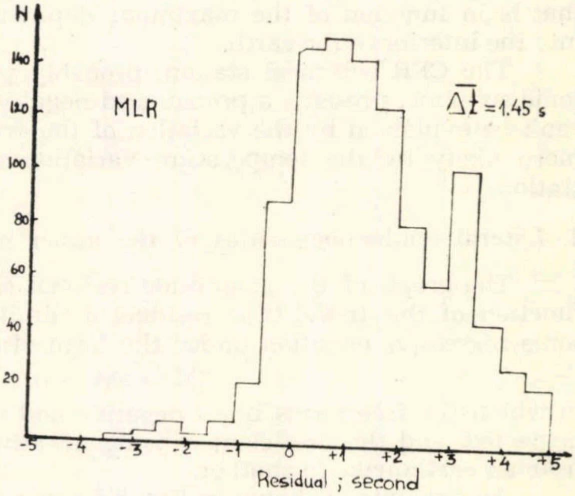

*Fig. 1*

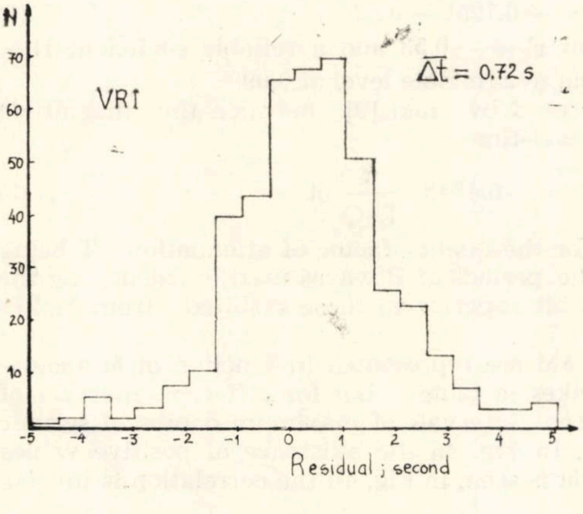

*Fig. 2*

enough and the PKR residuals are inverse and represent smaller differences. As the PKP waves come to stations under small angles made with the vertical line, the respective seismic rays penetrating the upper mantle and the crust beneath stations nearly perpendicular while the rays of P waves cross the crust under variable angles towards the vertical line some of them penetrating but very little into the mantle, it results that these differences of the mean residuals are mainly caused by the crust and uppermost mantle differences.

There exist some seismological stations presenting near P mean residuals, but having different PKP mean residuals, that fact leads to the conclusion of some differences in the upper mantle structure. But the number of PKP data is small yet as well as that of P data for some stations and this imposes the extension of the observation interval as well as the separation of the P residuals in function of epicentral distance, that is in function of the maximum depth the seismic rays penetrated into the interior of the earth.

The CFR seismical station, probably placed on the descended tectonic subplate, presents a pronounced negative P mean residual. This fact can't be explained by the variation of the crust or lithosphere depth. but more likely by the temperature variation of the medium beneath the station.

## 4. Lateral nonhomogeneities of the upper mantle in the Vrancea zone.

The graph of the magnitude residual $\delta M$ limited to $|\delta M| \leqslant 0.5$ in function of the travel-time residual $\delta t$ limited at $|\delta t| \leqslant 2{,}5$ seconds led some regressive equation under the form of:

$$\delta M = a\delta t + b \qquad (1)$$

in which the free terms b are negative and very small, they can even be neglected, and the coeficient a being negative too, but sensible different from an earthquake to another.

An exemple is shown in Fig. 3 for the earthquake in 1980 I 14, the resulted relation between $\delta M$ and $\delta t$ being

$$M = -0.12\delta t - 0.02 \qquad (2)$$

having a corelation coeficient $r' = -0.53$ and a reliable coeficient $H = |r|\sqrt{n-1} = 2.49$ coresponding to a reliable level of 0.99.

Supposing the relation used by Maki [9] between the magnitude anomalies and those of the travel-time

$$\delta M = -0.4343 \, \frac{\pi}{T \cdot Q} \, \partial t \qquad (3)$$

a value of $Q \approx 11$ resulted for the quality factor of attenuation : T being considered the mean of all the periods of P waves used in calculating the relation (2). This value is a bit superior to those resulted from Maki's graph [9].

In Figs 4 the anomalies $\delta M$ are represented in function of $\delta t$ anomalies for all the four earthquakes in table 2, but for different intervals of epicentral distance, for different intervals of maximum depths of seismic ray penetration respectively. In Fig. 4a the existence of positive values $\delta M$ correlated with negative $\delta t$ is seen, in Fig. 4b the correlation is inverse

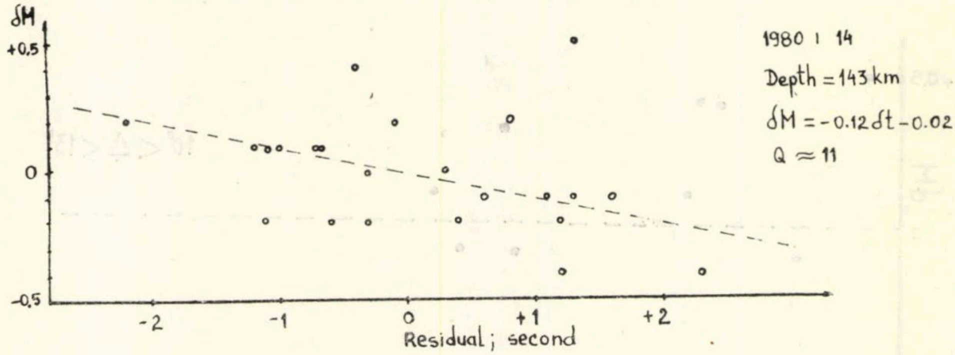

*Fig. 3*

and in Fig. 4c the negative values δM are prominent, but the correlation with δt is not evident. The regression straight lines give values between the limits 13 to 25 for Q, in accordance with the relation found by Okubo [11], Q $\approx 2.1\ Q_m$, and $50 < Q_w < 100$. These values for Q for different layer of the upper mantle point out the vertical nonhomogeneities of the mantle, as they were seen in [3] too.

For pointing out the lateral nonuniformities of the upper mantle in Figs 5 we present the anomalies distributions M in function of $i_f$ angle under which the seismic ray started from the hypocenter of the earthquakes, for the four earthquakes in table 2, too. In Fig. 5a these ones are represented only for the earthquake in 1981 V 31, having its depth of 120 km and for an interval limited by azymuth, it is seen from the figure. In Fig. 5b and 5c the same anomalies δM are presented in function of $i_f$ for the other three earthquakes having depth near to 150 km and for two azymuthal intervals. In Fig. 5a the existence of an interval of negative δM anomalies is seen, this interval become larger in Fig. 5b but the negative values lower, whereas for other azymuths, in Fig. 5c, the positive δM values are pronunced without being able to point out clear maximums and minimums.

The dependence of the magnitude upon the azymuth noticed by Gutenberg too [1] for the earthquakes of America is evident, it explaining the existence of the variation of upper mantle structure beneath the Vrancea zone on the horizontal including, not only on the vertical.

## 5. Conclusion

The difference between the P and PKP mean travel-time residuals at the seismological stations of Romania lead to the conclusion of the existence of a difference of the uppermost mantle and crust structure beneath Romania's territory.

The magnitudes residuals of the earthquakes in Vrancea present Azymuthal anomalies, that can be explained by the inclination of the lithospheric subplate which is subdued.

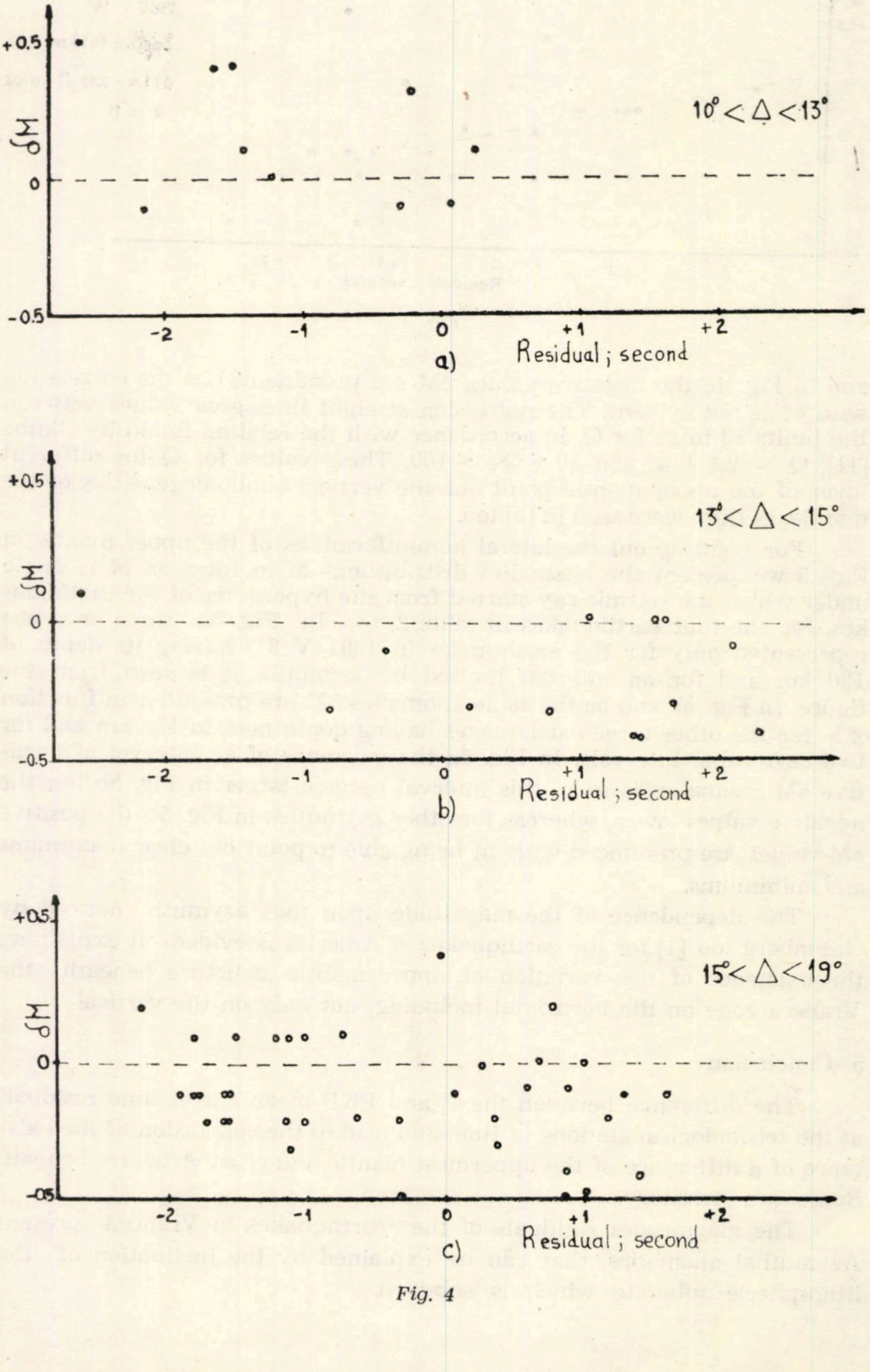
+0.5
$\delta M$
0
-0.5
$10^\circ < \Delta < 13^\circ$
-2
-1
0
+1
+2
Residual ; second
a)
+0.5
$\delta M$
0
-0.5
$13^\circ < \Delta < 15^\circ$
-2
-1
0
+1
+2
Residual ; second
b)
+0.5
$\delta M$
0
-0.5
$15^\circ < \Delta < 19^\circ$
-2
-1
0
+1
+2
Residual ; second
c)

*Fig. 4*

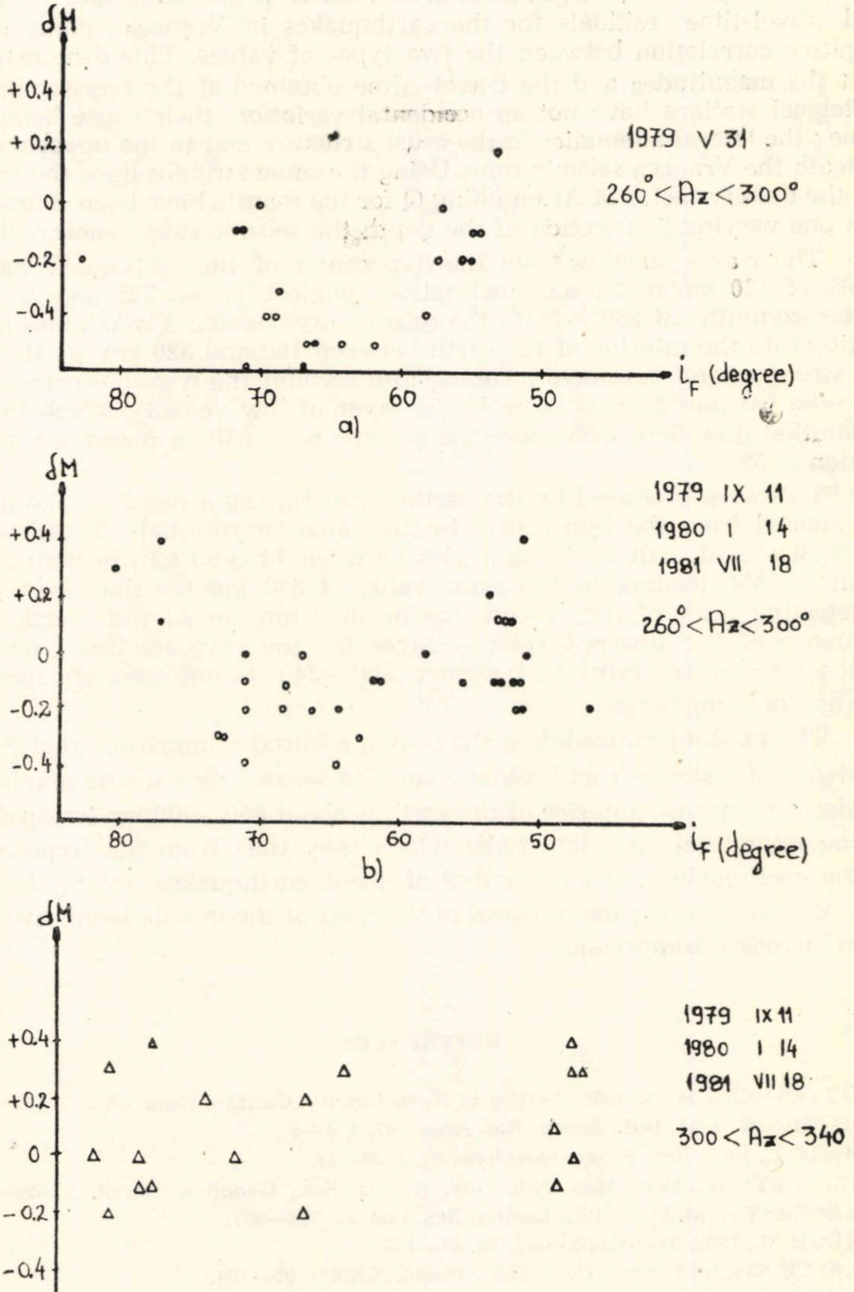
δM
+0.4
+0.2
0
-0.2
-0.4
80
70
60
50
$i_F$ (degree)
1979 V 31
260° < Az < 300°
a)
δM
+0.4
+0.2
0
-0.2
-0.4
80
70
60
50
$i_F$ (degree)
1979 IX 11
1980 I 14
1981 VII 18
260° < Az < 300°
b)
δM
+0.4
+0.2
0
-0.2
-0.4
80
70
60
50
$i_F$ (degree)
1979 IX 11
1980 I 14
1981 VII 18
300 < Az < 340
c)

Fig. 5

The regression straight lines drawn between the magnitude residuals and travel-time residuals for the earthquakes in Vrancea point out a negative correlation between the two types of values. This demonstrated that the magnitudes and the travel- time obtained at the registered seismological stations have not an accidental variation, their cause being the same ; the lateral anomalies in the crust structure and in the upper mantle beneath the Vrancea seismic zone. Using the same straight lines the values for the quality factor of Attenuating Q for the mantle have been estimated, this one varying in function of the depth the seismic rays penetrated.

The waves starting from the hypocenter of the earthquake have a depth of 120 km under an inclination angle between 72° and 56° and under azymuths of 260°—300°, the seismic rays having a maximum penetration into the interior of the earth between 180 and 320 km, go through the strong attenuating layer. Taking into account the negative correlation between $\delta M$ and $\delta t$, this layer is the layer of low velocity which in this azymuthal direction, influences the seismic rays with a maximum penetration of 320 km.

The waves produced by the earthquakes having a depth of about 150 km started from the hypocenter in the same azymuthal direction of 260°—300° and with inclining angles between 74° and 62°, present minimum for $\delta M$, leading to the same value of 320 km for the maximum penetrating limit of the seismic ray in the interior of the earth. The influence of the lowered velocity layer for the rays starting from the hypocenter under azymuths between 300°—340° is not seen, irrespective of the inclining angle.

The existent noticed data show us a reduced attenuation, that is the existence of a stronger and colder zone. The seismic rays whose maximum penetration into the interior of the earth is about 350—400 km irrespective of the azymuthal direction under which they start from the hypocenter of the earthquake and irrespective of these earthquakes depth, show, a reduced attenuation ; the material of this part of the mantle being subdued to an increased compression.

## REFERENCES

1. GUTENBERG B. B., 1955, *Earthq in Kern County*, Calif., during 1952, 2, 171—175.
2. HERRIN E., 1957, Bull. Seism. Soc. Amer. 47, 1, 1—5.
3. IOSIF T., 1966, Rev. Roum. Geophys., 10, 1, 33—41.
4. JEFFREYS H., 1936, Mon. Not. Roy. Astron. Soc., Geophys. Suppl. 3, 423—443.
5. KEBEASY R, M. 1970, Bull. Earthq. Res. Inst 48, 381—397.
6. KOCH M., 1982, Tectonophysics, 90, 91—115.
7. LASCU ST., 1983, Anal. Univ. Buc., Fizică, XXXII, 95—104.
8. MAKI T., 1981, Bull. Earthq. Res Inst., 56, 309—346.
9. MAKI T., 1982, Bull. Earthq. Res. Inst., 57, 151—192.
10. MITRONOVAS W., ISACKS B. L., 1971. Journ. Geophys. Res., 76. 7154—7180.
11. OKUB S., 1982, Bull. Earthq. Res. Inst., 57, 1—47.
12. UTSU T., 1971, Rev. Geophys. Space Phys., 9, 839—890.

ANALELE UNIVERSITĂȚII BUCUREȘTI, FIZICĂ, XXXIII, 1984, pag. 93—104

# THE STUDY OF NATURAL REMANENT MAGNETIZATION OF SOME NEOGENE VOLCANIC ROCKS FROM THE OAȘ—GUTÎI—ȚIBLEȘ MOUNTAINS, ROMANIA

ȘT. PĂTRAȘCU

University of Bucharest, Faculty of Physics *

*Summary*. The paper presents the results of the NRM study of some neogene volcanic rocks from 199 collecting site from the Oaș—Gutîi—Țibleș mountains. It was determined the structure of the NRM vector of 417 pilot specimens by using the gradual demagnetization in alternating magnetic fields. The rezults of the demagnetization were graphed and analysed after the method suggested by Zijderveld J.D.A. (1967). Structures with one, two or three components of various hardness were found. Primary-characteristic magnetizations of various zones in the investigated area were identified.

## 1. Introduction

650 oriented samples were collected from 199 sites from the Oaș—Gutîi—Țibleș mountains. The density of the sites varied with the number of outcroppings and their quality. Four oriented cubic specimens were made up from each rock sample. A pilot specimen was selected from two or three rock samples of each site for the study of the natural remanent magnetization (NRM). It was studied in particular the structure of the NRM vector in order to separate the components of magnetization and to identify the primary-characteristic magnetization.

The structure of the NRM vector was studied by demagnetization in alternating magnetic fields of the pilot specimens. The treatment resulted in the gradual destruction of the NRM vector beginning with the soft components and ending with the hard ones. The results of the gradual demagnetization were graphed and analysed after a method suggested by Zijderveld J.D.A. (1967) and used by Zijderveld J.D.A. and As J.A. (as shown by As J.A. in 1960), Wilson R.L. (1961) and Pătrașcu Șt. (1972, 1976).

## 2. Research method

The gradual demagnetization of a pilot specimen and the measurement of the magnetization vector after each step of demagnetization make it possible to find the remaining magnetization vectors in respect to the maximum initial intensity of the demagnetizing field. These data serve for plotting the curve of the path of the end of the remaining magnetization. This curve can be studied by its projections on horizontal and vertical planes. S—N and W—E directions are chosen in the horizontal plane as reference axis. The vertical plane is chosen to contain the S—N direction and the vertical of the site as reference axis, or the W—E direction and the vertical of the site, depending on the shape of the curve. Since either curve may be plotted on the same graph, the axes can have a double meaning and therefore the signs must be well precised. For instance, solid points are used for the horizontal projection and open circles for the vertical projection.

---

* National Center of Physics, Bucharest—Măgurele, S. 5, P.O.B. 5211, România

The shape of the curve may differ much with pilot specimen. In general, a curve may continue one or several rectilinear parts representing the directions of the remanent magnetization components of the respective NRM, which can be calculated from the graph. When the end of the remaining magnetization vector moves along a rectilinear part it is very likely that only a magnetization has been affected during the corresponding demagnetization interval. However, it is possible that the rock has two remanent magnetizations in that direction. If the two magnetizations have the same orientation, they cannot be separated with this method. It must be underlines that in reality it is very difficult to meet such a situation. The nonexistance of such situations constitutes a work hypothesis.

Besides determining the number of the component remanent magnetizations of a NRM, the method permits to separate the remanent magnetizations according to the hardness of magnetization and, at the same time it makes possible to obtain the demagnetization curves of each structural component.

In conclusion, the method permits to separate the remanent magnetizations of a rock according to their directions and hardness and by comparing the structure of the NRM of the rocks of a certain area it makes possible to identify the characteristic magnetization.

## 3. Results and discussion

In 377 pilot specimens out of the 417 pilot specimens investigated, the demagnetization response was clear, namely, the end of the remaining magnetization vector slowly moved along a curve on which at a certain moment it superposed tending to zero.

In most cases, the curves had two rectilinear parts, at the beginning and at the end, which served for determining the remanent magnetizations, components of the NRM. Figures 1—8 present examples of such structures, each figure having two diagrams. The diagram "a" present the projections of the curve described by the end of the remaining magnetization vector. For the projection of the curve on the vertical plane ox was chosen as axis for S—N and oz as axis for the vertical of the site. The diagram "b" presents the demagnetization curves of each structural component of the specimen. The demagnetization curve of the hardest component was marked with X and the other curves were marked with S or $S_1$ $S_2$ in the order of the hardness of the components.

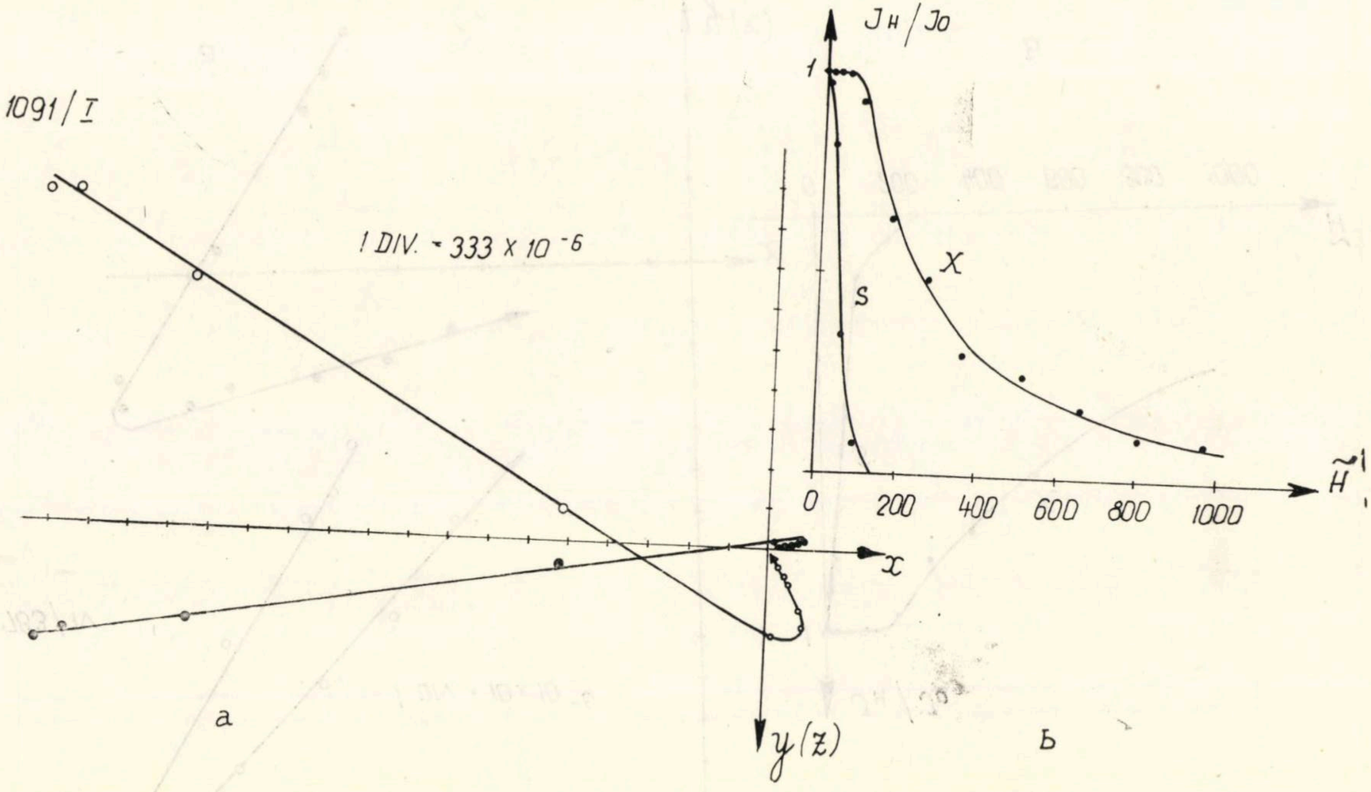

*Fig.* 1 — NRM structure and demagnetization curves for the specimen number 1091/I (biotite-quartz-pyroxenes andesite).

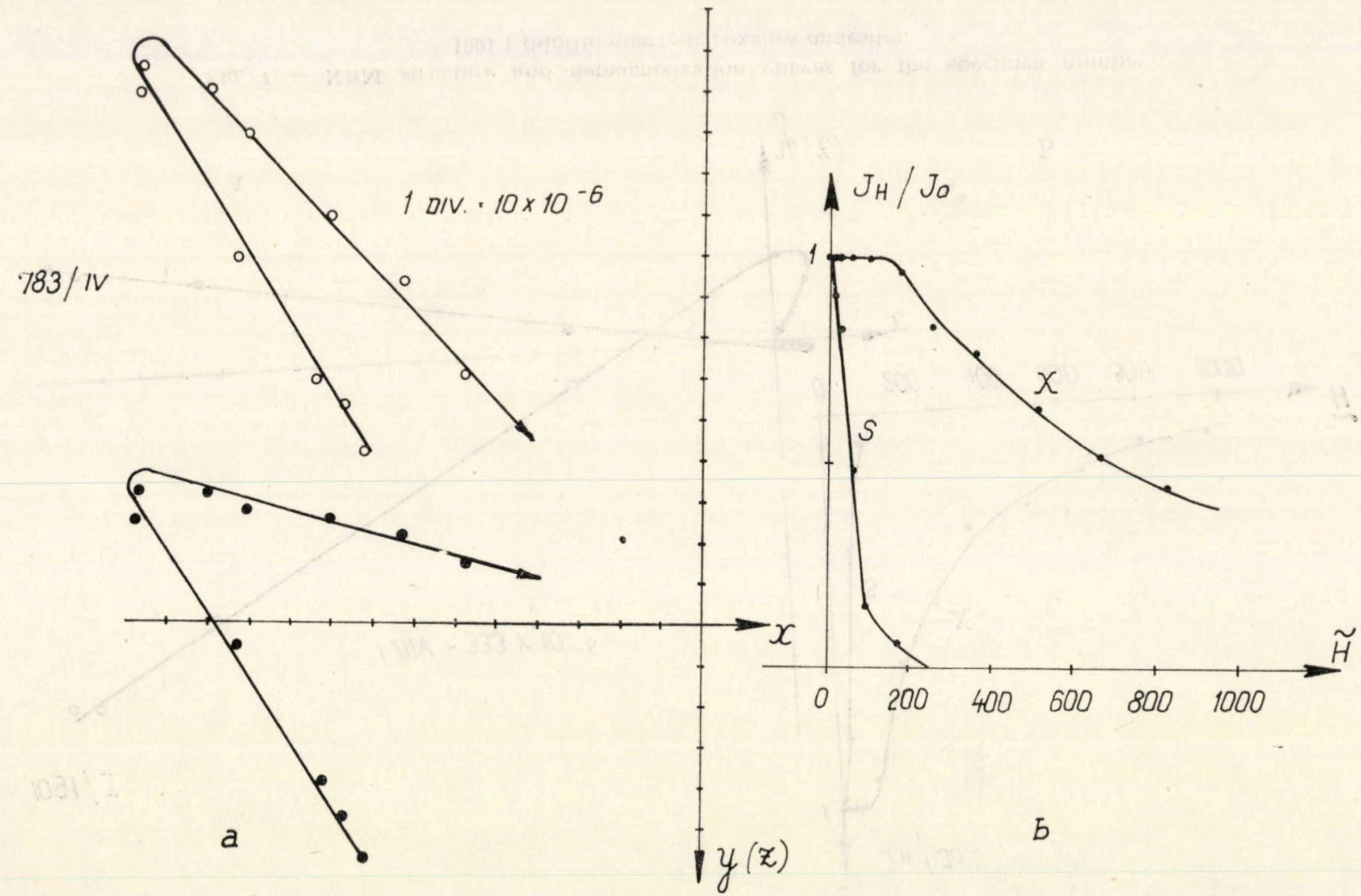

*Fig.* 2 — NRM structure and demagnetization curves for the specimen number 783/IV (pyroxenes andesite)

The analysis of the NRM structures of the 377 pilot specimens showed the following :

— Three structural types were found depending on the number of the rectilinear parts of the curves in the diagram "a" of each pilot specimen. In most cases (267), only two distinct rectilinear parts were found. In these circumstances it is possible to admit the existance of two remanent magnetizations if we suppose that only one magnetization exists on each rectilinear part. Figures 1 and 2 present two different examples of the orientation of the hardiest magnetization, the former normal and the latter reversed. In 96 cases a single rectilinear part was found and two examples are given in figures 3 and 4. Three rectilinear parts were found in 14 cases ; figures 5 and 6 present two examples of these.

— The resistance to the demagnetization in alternating magnetic fields of the structural components differs from specimen to specimen and in the same specimen irrespective of the number of rectilinear parts. As shown in diagrams "b" of any figure, when a specimen has at least two magnetizations, one of them is hardier and is not completely destroyed in 1000 Oe magnetic fields. The second structural component is soft and completely disappears in 200—400 Oe magnetic fields. The magnetization of the specimens whose curves have only rectilinear part is not totally destroyed in 1000 Oe magnetic fields.

— The comparison of the demagnetization curves of the hardiest components noted with X in diagrams "b" indicate that : — the shape of the demagnetization curve differs with each specimen and this is explained by the different hardness spectrum of each rock ; — the remaining magnetization after demagnetization in 1000 Oe magnetic fields is different in each sample ; this can be seen of two extreem situations in figures 3 and 7, the remaining magnetization being more than 50 % of the initial value and below 10%, respectively.

— The soft magnetizations of the specimens whose curves present two or three rectilinear parts have a different response either in the same specimen or in various specimens. Some of them disappear in magnetic field of maximum 200 Oe and others in magnetic fields of 400 Oe. In both cases, secondary remanent magnetizations of various types probably viscous (VRM) or anhysteretic (ARM) are concerned.

— Figure 8 presents an interesting case from the point of view of the method used. The curve of the specimen has two rectilinear parts in the same direction. However,it was possible to separate the two magnetizations because they orientations differed. The NRM of that specimen was roughly null as the two structural components had the same module.

## 4. **Conclusions**

The comparison of the hard magnetizations of the each pilot specimen, irrespective of the structural type, showed that their directions were not randomly oriented. They were grouped around two axes, one in the proximity of the vector of the actual geomagnetic field of the site (normal magnetizations) and the other in the opposite direction (reverse magnetizations).

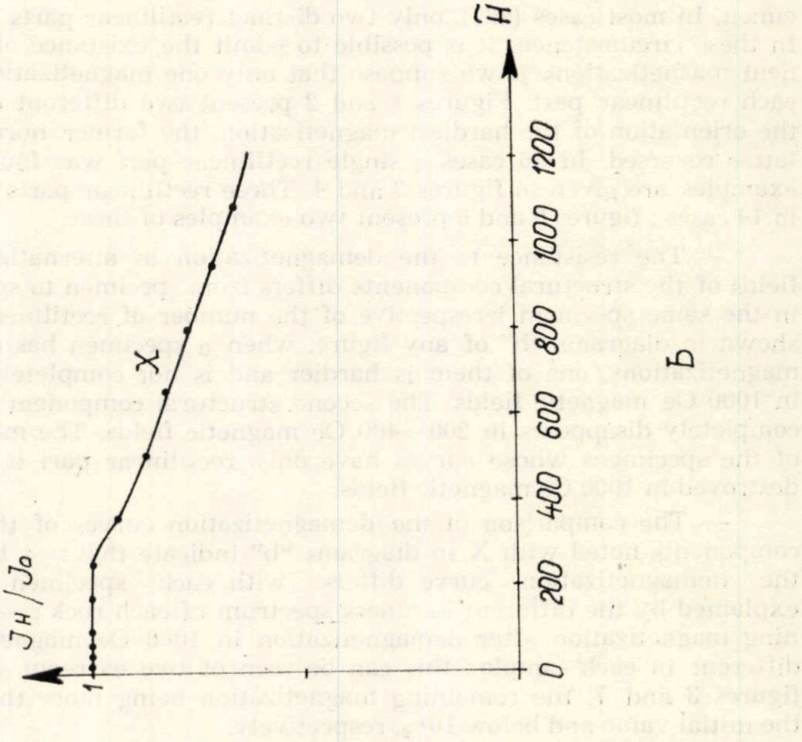

*Fig. 3* — **NRM structure and demagnetization curve for the specimen number 963 I (pyroxenes andesite of Seini)**

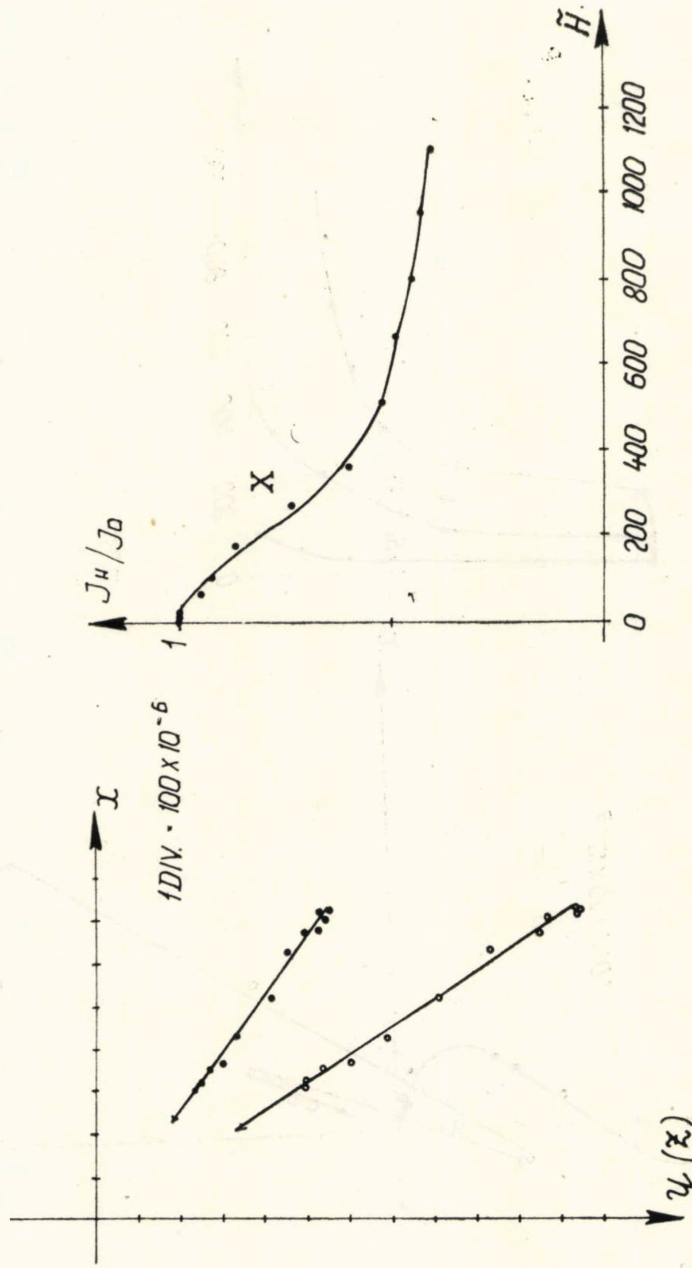

*Fig. 4* — NRM structure and demagnetization curve for the specimen number 1024/I (pyroxenes andesite of Socea)

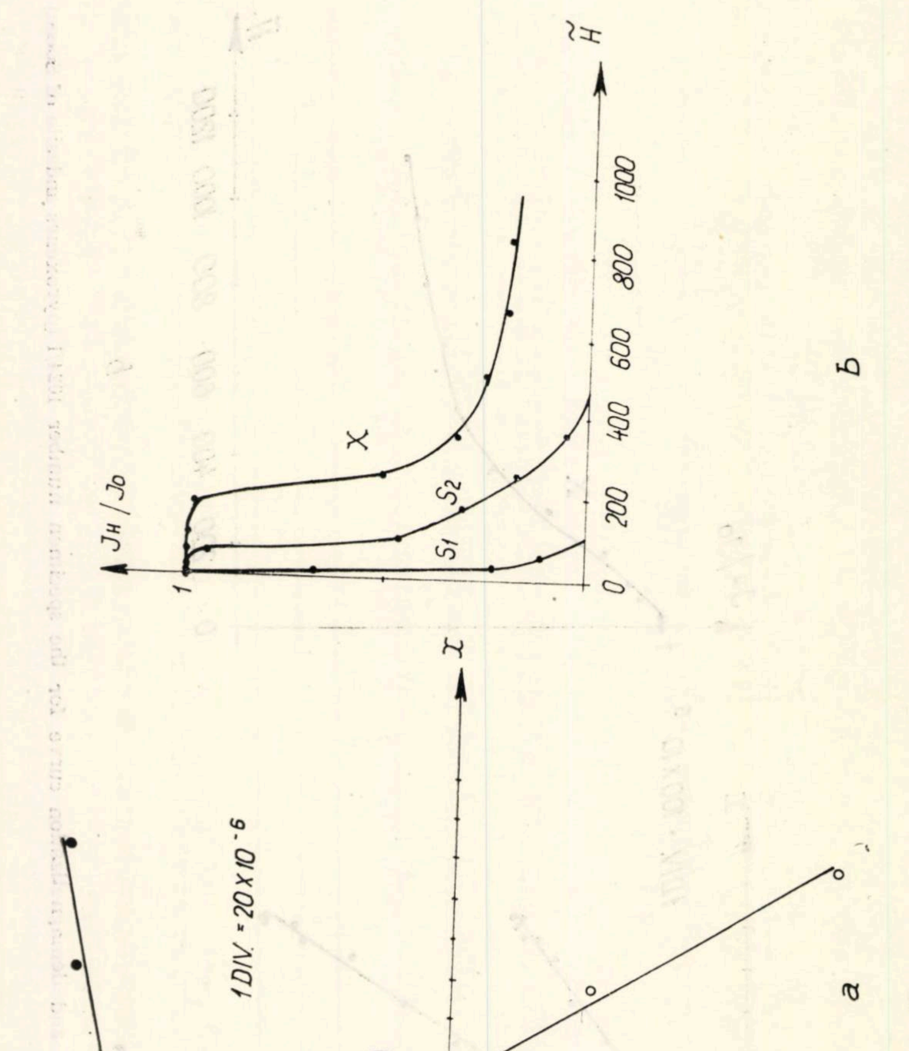

*Fig. 5* — NRM structure and demagnetization curves for the specimen number 1231/I (pyroxenes andesite of Igniş)

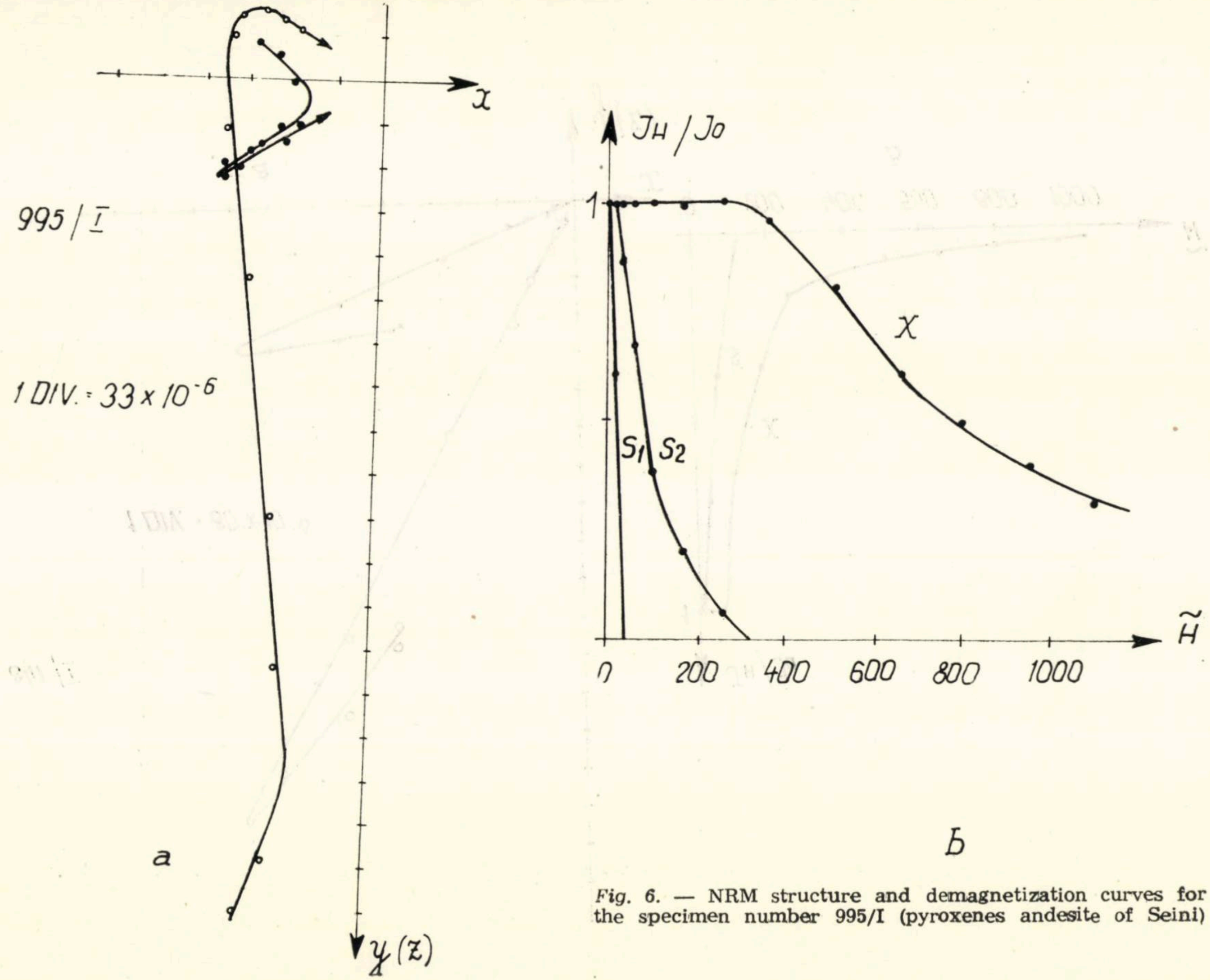

*Fig. 6.* — NRM structure and demagnetization curves for the specimen number 995/I (pyroxenes andesite of Seini)

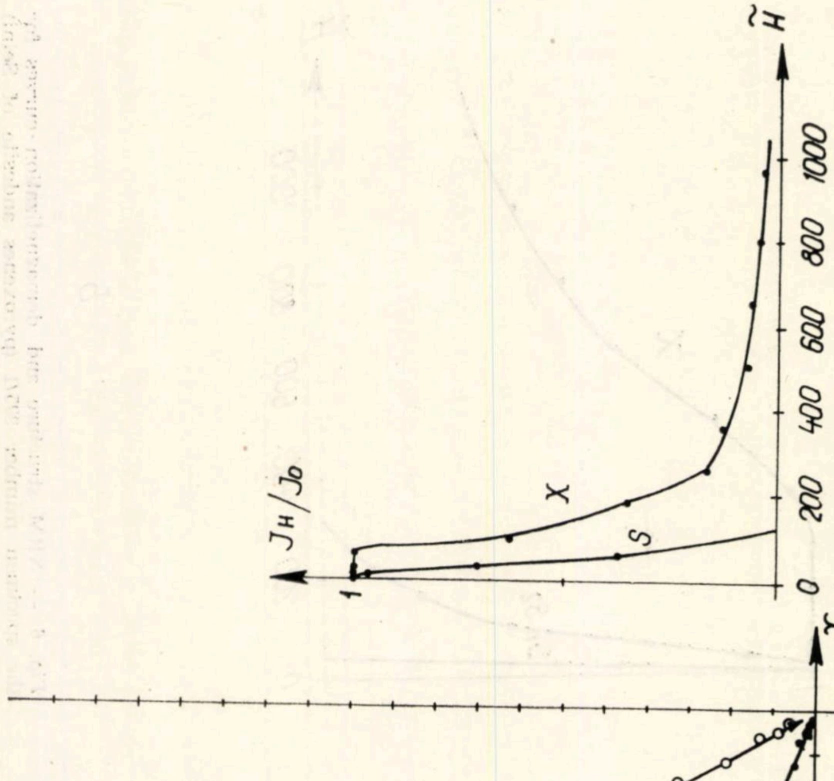

*Fig.* 7 — NRM structure and demagnetization curves for the specimen number 841 I (amphybole-biotite-pyroxenes andesite)

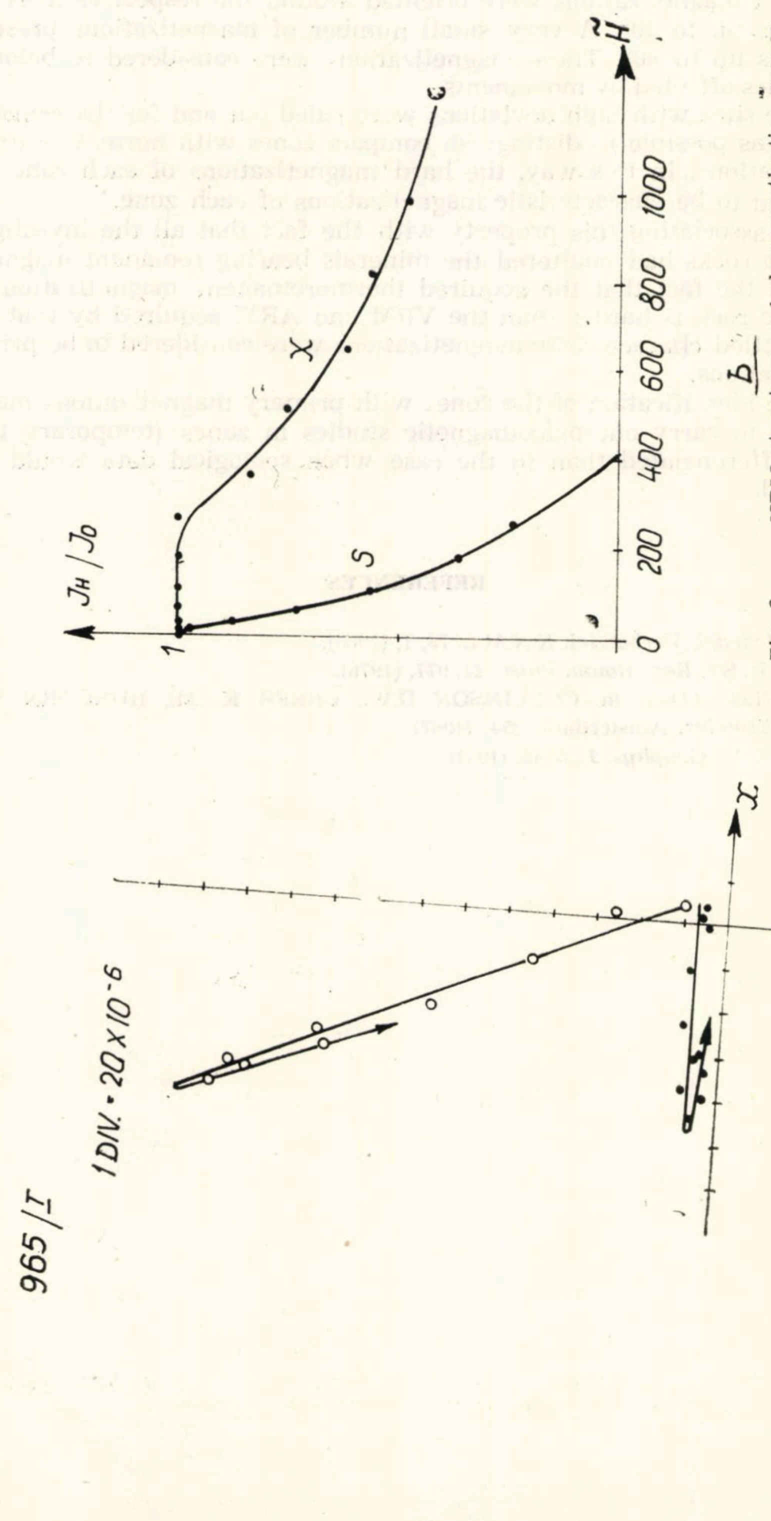

*Fig.* 8 — NRM structure and demagnetization curves for the specimen number 965/I (pyroxenes andesite of Seini)

Most magnetizations were oriented around the respective axes with deviations up to 40°. A very small number of magnetizations presented deviations up to 90°. These magnetizations were considered to belong to small zones affected by movements.

The sites with high deviations were ruled out and for the remaining sites it was possible to distinguish compact zones with normal or reverse magnetizations. In this way, the hard magnetizations of each zone were considered to be characteristic magnetizations of each zone.

By associating this property with the fact that all the investigated magmatic rocks had unaltered the minerals bearing remanent magnetism and with the fact that the acquired thermoremanent magnetization of a magmatic rock is harder than the VRM and ARM acquired by that rock, the identified characteristic magnetizations were considered to be primary magnetizations.

The identification of the zones with primary magnetizations made it possible to carry out paleomagnetic studies in zones (temporary units) better differenciated than in the case when geological data would have been used.

## REFERENCES

AS, J.A. *Mededel. Verhandel. K.N.M.I.*, *78*, 1, (1960).

PĂTRAŞCU, ŞT. *Rev. Roum. Phys.*, *21*, 977, (1976).

ZIJDERVELD, J.D.A. in COLLINSON D.W., CREER K. M., RUNCORN S. K., *Elsevier*, Amsterdam, 254, (1967).

WILSON, R. L., *Geophys. J.*, 5, 45, (1961).

## Le professeur dr. ION C. PETREA
## 1924—1983

Le 20 novembre 1983 est parti d'entre nous, après une longue et dure souffrance, le professeur universitaire dr. Ion C. Petrea, le chef de la chaire de Mécanique, Physique Moléculaire et Physique des Polymères.

Né à Galați le 19 juin 1924 il suit les cours du gymnase et commence les cours du lycée dans la ville natale, pour les continuer et terminer au lycée „Petru et Pavel" de Ploiești. Il fréquente les cours de la Faculté de Mathématique et Physique de l'Université de Bucarest, obtenant en 1951, à base de brillants résultats, le diplôme de licence ès-sciences physiques.

Entre 1951—1959 il fonctionne comme maître assistant, ensuite chargé de cours à l'Institut de Mines de Petroșani. Depuis 1959 il a enseigné à la Faculté de Physique de l'Université de Bucarest à la chaire de Physique Moléculaire. Entre février 1960 et juin 1963 il prépare sa thèse de doctorat à la Faculté de Physique de l'Université de Moscou, obtenant le titre de Docteur ès-Sciences Physiques. De retour à Bucarest, il passe par les degrés de l'hiérarchie universitaire : maître de conférences, professeur, pour qu'en 1978 il devienne le chef de la chaire de Mécanique, Physique Moléculaire et Physique des Polymères. A ce titre, le professeur Ion C. Petrea a développé une fructueuse activité ayant pour but l'organisation du procès d'enseignement, intégré à la recherche et à l'industrie. Par son dévouement, par l'implication de tous les jours dans les diverses formes d'activité de la faculté, par la générosité et la chaleur dont il s'est approché des jeunes studieux, le professeur Ion Petrea reste un exemple digne pour nous tous.

Son activité d'enseignement a été orientée vers les disciplines de base de la chaire, notamment dans le domaine de la Physique des polymères, le professeur Ion Petrea étant considéré l'organisateur et l'animateur de cette discipline de la physique chez nous. Il a fait des cours d'une haute tenue universitaire sur la structure des polymères et la physique de l'état mésomorphe. Seul, ou en collaboration, il a élaboré et publié un grand nombre de manuels, de cours, de recueils de problèmes, de monographies ainsi que d'autres travaux de spécialité d'une réelle utilité pour l'enseignement de la physique des polymères. Ses études monoyraphiques "Thermodynamique des macromolécules" et "Structure des polymères" peuvent être considérées comme travaux de référence dans ce domaine.

En même temps le professeur Ion Petrea a développé une remarquable activité de recherche scientifique, orientée prépondérément sur la physique des polymères, direction de recherche aux amples implications tant dans la physique fondamentale, que dans l'industrie.

Le professeur Ion Petrea est sans doute le promoteur de l'école roumaine de la physique des polymères. Il a publié, avec ses collaborateurs, de nombreux travaux scientifiques de spécialité et communications scientifiques. Assurant la direction de nombreuses thèses de doctorat dans le domaine de la physique des polymères, il a formé un grand nombre de spécialistes.

Remarquable est également l'activité du professeur Ion Petrea à la revue „Analele Universităţii Bucureşti, Fizică", dont il a été de nombreuses années le rédacteur en chef.

Maître d'école et prodigieux chercheur scientifique, le professeur Ion Petrea a été en même temps un fervent activiste dans le domaine social-politique. Remplissant avec passion et dévouement toutes ses responsabilités, le professeur Ion Petrea a apporté une contribution directe à la réalisation de la politique du Parti dans le domaine de l'enseignement, de l'éducation et de la recherche, des idéaux de progrès et prospérité de notre peuple.

Pour ses mérites il a été distingué avec des médailles du Parti et d'état telles que : la Médaille du Travail, le Mérite scientifique.

Par toute sa prestigieuse activité didactique, scientifique et sociale-politique, le professeur Ion Petrea a été une présence active, remarquable dans l'activité permanente de notre Faculté.

Les collègues, les collaborateurs et les étudiants du professeur Ion Petrea garderont toujours vif son souvenir dans leurs coeurs.

*Le Comité de rédaction*

**Lei 35**